

**STRUCTURAL ANALYSIS OF THE MECHANISM OF  
SUGAR BINDING AND HYDROLYSIS BY RICE  
OS7BGLU26  $\beta$ -MANNOSIDASE**

**Anupong Tankrathok**



**A Thesis Submitted in Partial Fulfillment of the Requirements for the  
Degree of Doctor of Philosophy in Biochemistry  
Suranaree University of Technology  
Academic Year 2013**

การวิเคราะห์โครงสร้างของกลไกการจับและการย่อยน้ำตาลโดยเอนไซม์  
บีตาแมนโนซิเดส OS7BGLU26 จากข้าว



วิทยานิพนธ์นี้เป็นส่วนหนึ่งของการศึกษาตามหลักสูตรปริญญาวิทยาศาสตรดุษฎีบัณฑิต  
สาขาวิชาชีวเคมี  
มหาวิทยาลัยเทคโนโลยีสุรนารี  
ปีการศึกษา 2556

**STRUCTURAL ANALYSIS OF THE MECHANISM OF SUGAR  
BINDING AND HYDROLYSIS BY RICE  
OS7BGLU26  $\beta$ -MANNOSIDASE**

Suranaree University of Technology has approved this thesis submitted in partial fulfillment of the requirements for the Degree of Doctor of Philosophy.

Thesis Examining Committee

---

(Assoc. Prof. Dr. Jatuporn Wittayakun)

Chairperson

---

(Prof. Dr. James R. Ketudat-Cairns)

Member (Thesis Advisor)

---

(Assoc. Prof. Dr. Mariena Ketudat-Cairns)

Member

---

(Assoc. Prof. Dr. Jaruwan Siritapetawee)

Member

---

(Asst. Prof. Dr. Prachumporn Kongsaree)

Member

---

(Dr. Chomphunuch Songsiriritthigul)

Member

---

(Prof. Dr. Sukit Limpijumnong)

Vice Rector for Academic Affairs  
and Innovation

---

(Assoc. Prof. Dr. Prapun Manyum)

Dean of Institute of Science

อนุพงษ์ ทานกระโทก : การวิเคราะห์โครงสร้างของกลไกการจับและการย่อยน้ำตาลโดย เอนไซม์ บีตาแมนโนซิเดส OS7BGLU26 จากข้าว (STRUCTURAL ANALYSIS OF THE MECHANISM OF SUGAR BINDING AND HYDROLYSIS BY RICE OS7BGLU26  $\beta$ -MANNOSIDASE) อาจารย์ที่ปรึกษา : ศาสตราจารย์ ดร.เจมส์ เกตุทัต-คาร์นีส, 119 หน้า.

เอนไซม์ Os7BGlu26 เป็นเอนไซม์ของข้าว (*Oryza sativa*) ซึ่งจัดอยู่ในตระกูล glycoside hydrolase family 1 (GH1) สามารถใช้ 4-nitrophenyl- $\beta$ -D-mannopyranoside เป็นสับสเตรทได้ดีกว่า 4-nitrophenyl- $\beta$ -D-glucopyranoside เพื่อที่จะเข้าใจความจำเพาะต่อสับสเตรทและกลไกการเร่งปฏิกิริยาของเอนไซม์ชนิดนี้ จึงทำการดักผลึกเอนไซม์ Os7BGlu26 นี้ร่วมกับลิแกนด์ต่างๆ เช่น น้ำตาลแมนโนส ตัวยับยั้ง 2,4-dinitrophenyl-2-deoxy-2-fluoroglucoside (dNPG2F) ตัวยับยั้ง isofagomine ตัวยับยั้ง mannoimidazole และตัวยับยั้ง glucoimidazole เอนไซม์ Os7BGlu26 มีโครงสร้างโดยทั่วไปเป็นแบบคลาสสิก TIM-barrel เหมือนกับโครงสร้างของโปรตีนอื่นๆ ในตระกูลนี้ โครงสร้างเชิงซ้อนของ Os7BGlu26 กับน้ำตาลแมนโนสหรือโครงสร้างของเอนไซม์กับผลิตภัณฑ์ พบว่าโครงรูปของน้ำตาลแมนโนสเป็นแบบเรือเอียง  ${}^1S_5$  เมื่อนำโครงรูป  ${}^1S_5$ ,  ${}^1S_5$ ,  ${}^2S_0$ , และ  ${}^3S_1$  ของสับสเตรท 4NPMAN และ 4NPGlc เข้าไปอยู่ในบริเวณเร่งของ Os7BGlu26 พบว่า โครงรูปแบบ  ${}^1S_5$  และ  ${}^1S_5$  มีค่าพลังงานต่ำสุด เมื่อเปรียบเทียบกับ docked conformers กับโครงสร้างของเอนไซม์ GH1 อื่นจากข้าว พบมีความแตกต่างของ กรดอะมิโนที่มีอันตรกิริยากับกรดอะมิโนตัวเร่งปฏิกิริยากรด/เบสระหว่างเอนไซม์ที่มี และไม่มีกิจกรรมของเอนไซม์บีตาแมนโนซิเดส การกลายพันธุ์ของ Tyr134 ไปเป็น Trp ของ Os7BGlu26 เป็นผลให้อัตราส่วนของค่า  $k_{cat}/K_m$  ระหว่าง 4NPMAN ต่อ 4NPGlc ลดต่ำลง ในขณะที่เอนไซม์กลายพันธุ์ที่ตำแหน่ง Tyr134 ไปเป็น Phe อัตราส่วนนี้เพิ่มขึ้น 13 เท่า การกลายพันธุ์ของเอนไซม์ที่ตำแหน่ง Cys182 เป็น Thr กิจกรรมของเอนไซม์ทั้งสองแบบลดลง และลดความจำเพาะต่อแมนโนส สรุปได้ว่าอันตรกิริยากับกรดอะมิโนตัวเร่งตัวเร่งปฏิกิริยากรด/เบสมิบบทบาทสำคัญต่อความจำเพาะกับน้ำตาล โครงสร้างเชิงซ้อนของ Os7BGlu26 กับตัวยับยั้ง dNPG2F แสดงการจับกันของลิแกนด์นี้ที่ตำแหน่งจับ +1 ถึง +2 และร่องที่สันนิษฐานว่าจับกับสับสเตรท แทนที่จะเป็นตำแหน่งจับ -1 ถึง +1 ในทางกลับกันผลึกเอนไซม์กลายพันธุ์ที่กรดอะมิโนตัวเร่งที่ทำหน้าที่ให้และรับโปรตรอน E179Q ที่แช่ด้วยตัวยับยั้งเดียวกันนี้ แสดงให้เห็นถึงโครงสร้างมัธยันต์แบบโควาเลนต์กับ G2F ที่มีโครงรูปเป็นแบบเก้าอี้  ${}^4C_1$  โครงสร้างของ Os7BGlu26 ร่วมกับตัวยับยั้งเอนไซม์ไกลโคซิเดส isofagomine และตัวยับยั้งที่คล้ายกับช่วง

ทรานซิชันที่เป็นอีพิเมอร์กัน mannoimidazole และ glucoimidazole ได้ทำการตรวจสอบพบว่า โครงสร้างเชิงซ้อนกับตัวยับยั้ง isofagomine มีลักษณะวงแหวนใกล้เคียงกับโครงสร้างเก้าอี้  ${}^4C_1$  ซึ่งเป็นโครงสร้างที่ผ่อนคลายของไกลโคไซด์ และตัวยับยั้งนี้มีค่าคงที่การยับยั้งแบบแข่งขัน ( $K_i$ ) เท่ากับ  $2.97 \times 10^{-6}$  โมลาร์ โครงสร้างของตัวยับยั้ง mannoimidazole แสดงการบิดของวงแหวนระหว่างรูปเรือบิด  ${}^1S_5$  และรูป  $B_{2,5}$  ซึ่งสอดคล้องกับโครงสร้างของน้ำตาลแมนโนสที่สภาวะทรานซิชันตัวยับยั้งนี้มีค่าคงที่การยับยั้งเท่ากับ  $13.2 \times 10^{-6}$  โมลาร์ ตัวยับยั้ง glucoimidazole มีการบิดตัวเป็นรูปของจดหมาย  ${}^4E$  ซึ่งมีลักษณะใกล้เคียงกับโครงสร้าง  ${}^4H_3$  half chair สภาวะทรานซิชันของน้ำตาลกลูโคส และตัวยับยั้งนี้มีค่าคงที่การยับยั้งแบบแข่งขัน เท่ากับ  $54.2 \times 10^{-9}$  โมลาร์ มากไปกว่านั้น ความก้าวหน้าของปฏิกิริยา (progress curves) การยับยั้งของตัวยับยั้ง isofagomine mannoimidazole และ glucoimidazole แสดงถึงการยับยั้งเอนไซม์ Os7BGlu26 แบบ slow onset ซึ่งจะพบได้ในการศึกษาการยับยั้งของตัวยับยั้งที่มีลักษณะคล้ายกับสภาวะทรานซิชันของสับสเตรท การศึกษานี้ได้ยืนยันว่า มีเส้นทางการบิดที่แตกต่างกัน 2 เส้นทาง ของน้ำตาลแมนโนส และน้ำตาลกลูโคสระหว่างการเร่งปฏิกิริยาไฮโดรไลซิสของเอนไซม์ Os7BGlu26

ANUPONG TANKRATHOK : STRUCTURAL ANALYSIS OF THE  
MECHANISM OF SUGAR BINDING AND HYDROLYSIS BY RICE  
OS7BGLU26  $\beta$ -MANNOSIDASE. THESIS ADVISOR :  
PROF. JAMES R. KETUDAT-CAIRNS, Ph.D. 119 PP.

### $\beta$ -MANNOSIDASE/ $\beta$ -GLUCOSIDASE/TRANSITION STATE ANALOGUE

Rice Os7BGlu26 is one member of glycoside hydrolase family 1 (GH1) which prefers to use 4-nitrophenyl- $\beta$ -D-mannopyranoside (4NPMan) as a substrate over 4NP- $\beta$ -D-glucopyranoside (4NPGlc). In order to understand its glycon specificity and catalytic mechanism, Os7BGlu26 is being investigated at the molecular level. The Os7BGlu26 protein was crystallized and soaked with or without ligands (mannose, 2,4-dinitrophenyl-2-deoxy-2-fluoroglucoside (dNPG2F), isofagomine, mannoimidazole and glucoimidazole). The overall structure of native Os7BGlu26 had the classic TIM-barrel, which is similar to other GH1 enzymes. The Os7BGlu26 structure with D-mannose corresponds to a product complex, with  $\beta$ -D-mannose in the  ${}^1S_5$  skew boat conformation. Docking of the  ${}^1S_3$ ,  ${}^1S_5$ ,  ${}^2S_0$ , and  ${}^3S_1$  pyranose ring conformations of 4NPMan and 4NPGlc substrates into the active site of Os7BGlu26 indicated lowest energies in  ${}^1S_5$  and  ${}^1S_3$  skew boat conformations. Comparison of these docked conformers with other rice GH1 structures revealed differences in the residues interacting with the catalytic acid/base between enzymes with and without significant  $\beta$ -D-mannosidase activities. Mutation of Tyr134 to Trp in Os7BGlu26 resulted in a lower ratio of  $k_{\text{cat}}/K_m$  for 4NPMan to that for 4NPGlc, while mutation of Tyr134 to Phe increased this ratio 13-fold. Mutation of Cys182 to Thr decreased both

activity and selectivity for  $\beta$ -D-mannoside. We conclude that interactions with the catalytic acid/base play a significant role in glycon selection. The structure of the Os7BGlu26 complex with dNPG2F showed that one ligand bound at the +1 to +2 subsites and another at a position further out in the putative substrate binding cleft, rather than at the expected subsite -1 to +1 position. In contrast, the E179Q Os7BGlu26 acid/base mutant soaked with this inhibitor yielded the structure of a covalent intermediate with G2F, which was found in a  ${}^4C_1$  chair conformation. The structures of the Os7BGlu26 with the glycosidase inhibitor isofagomine and the epimeric putative transition state mimic inhibitors mannoimidazole and glucoimidazole were also determined. The crystal structure of the complex with isofagomine showed a ring close to a  ${}^4C_1$  chair form, which is proposed to be the relaxed state conformation of glycosides, and this inhibitor had a competitive  $K_i$  constant of  $2.97 \times 10^{-6}$  M. The crystal structure of mannoimidazole showed a distorted ring between a  ${}^1S_5$  skew boat and a  $B_{2,5}$  boat, which is proposed to be the transition state conformation of mannosides, and this inhibitor had a competitive  $K_i$  constant of  $13.2 \times 10^{-6}$  M. Glucoimidazole also had distortion to a  ${}^4E$  envelope conformation, which is close to the  ${}^4H_3$  half chair transition state proposed for glucosides, and this inhibitor had a competitive  $K_i$  constant of  $54.2 \times 10^{-9}$  M. Moreover, the progress curves found that isofagomine, mannoimidazole and glucoimidazole show slow onset inhibition of Os7BGlu26, as seen in other transition state analogue studies. This study supports the use of two different distortion pathways for D-mannosides and D-glucosides during hydrolysis by Os7BGlu26.

School of Biochemistry

Student's Signature \_\_\_\_\_

Academic Year 2013

Advisor's Signature \_\_\_\_\_

## ACKNOWLEDGEMENTS

First, I would like to express my sincere gratitude to my thesis advisor, Prof. Dr. James R. Ketudat-Cairns for providing me the opportunity to study towards my Ph.D. degree in Biochemistry and his excellent guidance, caring, patience and encouragement.

I am very grateful to Prof. Dr. Maria Hrmova for her valuable guidance, advice on plant  $\beta$ -mannosidase work. I am also deeply grateful to Prof. Dr. Robert C. Robinson for providing me a chance to do some part of my research at Institute of Molecular and Cell Biology, Singapore, and his advice on the structural analysis. I express my thankfulness to Prof. Dr. Atsuo Kimura for giving me an opportunity for short-term research experience at Hokkaido University, Japan. Special thanks are extended to Zalihe Hakki, RohanWilliams and Assoc. Prof. Dr. Spencer J. Williams, University of Melbourne for providing transition state mimic inhibitors. I also thank Javier Iglesias-Fernández and Prof. Dr. Carme Rovira, Institut de Química Teòrica i Computacional for the computational docking study.

I would like to thank Dr. Sukanya Luang for cloning and construction of pET32a/*Os7BGlu26* and I also thank Dr. Salila Pengthaisong and Dr. Sompong Sansanya for the guidance on the crystallization techniques and data processing.

I would like to thank Prof. Dr. Chun-Jung Chen, Dr. Phimonphan Chuankhayan and the BL13B1 beamline staff at the National Synchrotron Radiation Research Center (NSRRC), Taiwan for their kind help in solving problems during X-ray diffraction data collection.

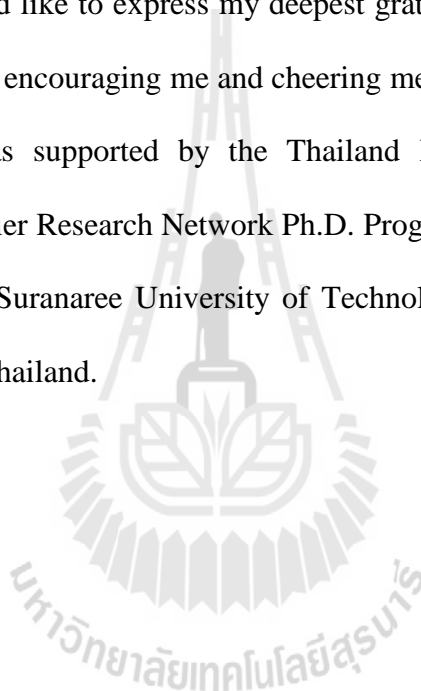
I sincerely thank Assoc. Prof. Dr. Jatuporn Wittayakun, Assoc. Prof. Dr. Mariena Ketudat-Cairns, Assoc. Prof. Dr. Jaruan Siritapetawee, Asst. Prof. Dr. Prachumporn Kongsaree and Dr. Chomphunuch Songsiriritthigul for patiently reading this dissertation and providing helpful comments.

Special thanks are extended to all my friends in the School of Biochemistry and School of Chemistry, Suranaree University of Technology for their help.

Finally, I would like to express my deepest gratitude to my family. They were always supporting me, encouraging me and cheering me up with their best wishes.

This work was supported by the Thailand Research Fund, the Strategic Scholarships for Frontier Research Network Ph.D. Program and the National Research University Project to Suranaree University of Technology from the Commission on Higher Education of Thailand.

Anupong Tankrathok



# CONTENTS

	<b>Page</b>
ABSTRACT IN THAI .....	I
ABSTRACT IN ENGLISH .....	III
ACKNOWLEDGEMENTS .....	V
CONTENTS .....	VII
LIST OF TABLES .....	XI
LIST OF FIGURES .....	XII
LIST OF ABBREVIATIONS AND SYMBOLS .....	XVI
<b>CHAPTER</b>	
<b>I INTRODUCTION .....</b>	<b>1</b>
1.1 General introduction.....	1
1.2 Research objectives .....	3
1.3 Research scope .....	4
<b>II LITERATURE REVIEW .....</b>	<b>6</b>
2.1 Glycoside hydrolases.....	6
2.2 $\beta$ -mannosidases .....	7
2.3 $\beta$ -glucosidases .....	9
2.4 Glycosidase mechanism.....	10
2.5 Nucleophile and acid/base mutants with rescued activity .....	14
2.6 Transition state mimicry of $\beta$ -D-mannosidases and $\beta$ -D-glucosidases .....	19

## CONTENTS (Continued)

	<b>Page</b>
2.7 Glycoside hydrolase family 1 crystal structures .....	25
2.8 Rice $\beta$ -mannosidases/ $\beta$ -glucosidases .....	30
2.9 Rice Os7BGlu26 $\beta$ -mannosidase .....	32
<b>III MATERIALS AND METHODS</b> .....	<b>34</b>
3.1 Materials.....	34
3.1.1 Plasmid and bacterial strain.....	34
3.1.2 Oligonucleotide and mutagenesis primers.....	35
3.2 General methods.....	37
3.2.1 Competent cell preparation.....	37
3.2.2 Bacterial transformation .....	37
3.2.3 Site-directed mutagenesis .....	37
3.2.4 Plasmid extraction by alkaline lysis .....	38
3.2.5 SDS-PAGE .....	39
3.3 Optimization of conditions for protein expression.....	40
3.4 Protein purification.....	41
3.5 Protein crystallization.....	42
3.5.1 Screening and optimization of Os7BGlu26 crystallization .....	42
3.5.2 Os7BGlu26 crystallization by hanging drop vapor diffusion.....	42
3.6 Data collection and processing.....	43
3.7 Structure refinement.....	44
3.8 Docking analysis .....	44

## CONTENTS (Continued)

	<b>Page</b>
3.9 Enzyme kinetics .....	45
3.9.1 Kinetic parameter analysis .....	45
3.9.2 HEPES inhibition .....	46
3.9.3 Time course of 2,4-dNP release from covalent inhibitors.....	46
3.9.4 Profile of activity versus pH.....	46
3.9.5 Effect of anionic nucleophiles in rescue of acid/base mutant activity .....	47
3.9.6 Effect of azide concentration on the activity of the Os7BGlu26 E179Q mutant.....	47
3.10 Transition state studies .....	47
3.10.1 Transition state analogue inhibition .....	47
3.10.2 Slow onset inhibition.....	48
<b>IV RESULTS AND DISCUSSION.....</b>	<b>49</b>
4.1 Os7BGlu26 expression and purification .....	49
4.2 Os7BGlu26 crystallization .....	52
4.3 Os7BGlu26 structure and model quality .....	53
4.4 Structural comparison of Os7BGlu26 with other rice GH1 structures .....	61
4.5 Os7BGlu26 in complex with the D-mannose hydrolysis product .....	63

## CONTENTS (Continued)

	<b>Page</b>
4.6 Docking studies of the Michaelis complex .....	66
4.7 Comparison of Os7BGlu26 with covalent intermediate complexes of other GH1 enzymes .....	69
4.8 Kinetic studies of glycon specificity mutants of Os7BGlu26 .....	74
4.9 Os7BGlu26 complex with dNPG2F.....	78
4.10 Characterization of Os7BGlu26 E179Q acid/base mutant activity and its rescue .....	84
4.11 The Os7BGlu26 E179Q covalent complex with G2F.....	87
4.12 Os7BGlu26 complexes with putative transition state analogues .....	91
<b>V CONCLUSION</b> .....	100
<b>REFERENCES</b> .....	103
<b>APPENDIX</b> .....	117
<b>CURRICULUM VITAE</b> .....	119

## LIST OF TABLES

<b>Table</b>	<b>Page</b>
2.1 Glycoside hydrolase family 1 structures from archaea .....	27
2.2 Glycoside hydrolase family 1 structures from bacteria.....	27
2.3 Glycoside hydrolase family 1 structures from eukaryotes.....	28
2.4 Relative rates of hydrolysis of natural and synthetic substrates by rice Os7BGlu26.....	33
3.1 Oligonucleotide primers for site-directed mutagenesis .....	35
4.1 Data-collection statistics of native Os7BGlu26 and its mannose complex .....	56
4.2 Refinement statistics of native Os7BGlu26 and its mannose complex .....	57
4.3 Kinetic parameters of wild type Os7BGlu26 and its mutants for 4NPMAN and 4NPGlc substrates.....	77
4.4 Data-collection statistics of complexes of Os7BGlu26with dNPG2F and Os7BGlu26 E179Q with G2F .....	79
4.5 Refinement statistics of complexes of Os7BGlu26with dNPG2F and Os7BGlu26 E179Q with G2F .....	80
4.6 Kinetics of inhibition of GH1 Os7BGlu26, Os3BGlu7 and rHvBII by putative transition state analogues .....	92
4.7 Data-collection statistics of Os7BGlu26 complexes with mannoimidazole, glucoimidazole and isofagomine.....	96
4.8 Refinement statistics of native Os7BGlu26 and with mannoimidazole, glucoimidazole and isofagomine.....	97

## LIST OF FIGURES

Figure	Page
2.1 Glycoside hydrolase activity .....	6
2.2 Endo/exo-acting glycoside hydrolases .....	6
2.3 Retaining and inverting glycoside hydrolase mechanisms .....	7
2.4 $\beta$ -Mannosidase structures from GH2 and GH5 families.....	8
2.5 $\beta$ -Glucosidase structures from various GH families .....	10
2.6 Glycosidase mechanisms for hydrolysis .....	12
2.7 Unusual glycosidase mechanisms for hydrolysis.....	14
2.8 Rescue of catalytic activity in the nucleophile and acid/base mutant by azide .....	16
2.9 Mechanism of transglycosylation with a glycosynthase .....	17
2.10 Rescue of catalytic activity in the nucleophile mutant of <i>Sulfolobus</i> <i>solfataricus</i> $\beta$ -glucosidase by formate .....	17
2.11 Rescue of catalytic activity in the acid/base mutant of <i>Agrobacterium</i> sp. $\beta$ -glucosidase by substrate-assisted protonation .....	18
2.12 A natural version of chemical rescue with <i>Sinapis alba</i> myrosinase utilizes ascorbate as a general base catalyst .....	18
2.13 Partial itinerary of pyranoside ring interconversions from various families of glycoside hydrolases .....	20

## LIST OF FIGURES (Continued)

Figure	Page
2.14 Schematic diagram of the proposed conformational itinerary for the glycosylation step of the retaining mechanism derived from three-dimensional structures .....	23
2.15 Structures of the transition state mimic inhibitors in the active site .....	24
2.16 Secondary structure diagram of white clover cyanogenic $\beta$ -glucosidase showing the eight parallel $\beta$ -strands that form the barrel core.....	26
2.17 Rice $\beta$ -glucosidase structures.....	29
2.18 Relationship between rice and other plant GH1 $\beta$ -mannosidase/ $\beta$ -glucosidase enzymes.....	32
3.1 Construct of the protein-coding sequence of recombinant pET32a(+) with the <i>Os7bglu26</i> cDNA inserted after the enterokinase cleavage site .....	34
4.1 SDS-PAGE of Os7BGlu26 expressed in different conditions .....	50
4.2 The $\beta$ -glucosidase activity of expressed protein in crude <i>E. coli</i> strain Rosetta-gami(DE3) extracts after induction with different concentrations of IPTG .....	50
4.3 SDS-PAGE of Os7BGlu26 throughout purification .....	51
4.4 The initial Os7BGlu26 crystals.....	52
4.5 Structure of rice Os7BGlu26 $\beta$ -D-mannosidase. ....	58
4.6 Multiple sequence alignment of rice Os7BGlu26, HvBII, LeMside, AtBGlu44, Os3BGlu7, Os3BGlu6 and Os4BGlu12.....	59
4.7 Noncompetitive inhibition of Os7BGlu26 by HEPES.....	60

## LIST OF FIGURES (Continued)

<b>Figure</b>	<b>Page</b>
4.8	Comparison of the active site clefts of the rice GH1 structures..... 62
4.9	Chemical structures of natural substrates hydrolyzed by Os7BGlu26..... 63
4.10	The structure of rice Os7BGlu26 in complex with $\beta$ -D-mannose ..... 65
4.11	Structures of Os7BGlu26 in complex with 4NPGlc and 4NPMan obtained by computational docking. .... 68
4.12	DNP release from 2,4-dinitrophenyl 2-deoxy-2-fluoromannoside ..... 72
4.13	Comparison of the active sites of the rice Os7BGlu26 $\beta$ -D-mannosidase and other rice GH1 $\beta$ -D-glucosidases with bound 2-deoxy-2-fluoroglucoside moieties. .... 73
4.14	The electrostatic surface structure of rice Os7BGlu26 in complex with 2,4 dinitrophenyl 2-deoxy-2-fluoroglucoside ..... 81
4.15	Electron density map of 2,4-dinitrophenyl 2-deoxy-2-fluoroglucoside molecules in the Os7BGlu26 active site ..... 82
4.16	Amino acid residues interacting with 2,4 dinitrophenyl 2-deoxy-2- fluoroglucosides ..... 83
4.17	The activities of the acid–base mutant forms of Os7BGlu26 in the presence and absence of nucleophiles..... 85
4.18	The azide concentration dependence of 4NPMan hydrolysis by the Os7BGlu26 E179Q mutant ..... 86
4.19	Activity versus pH profiles of the Os7BGlu26 E179Q mutant and wild type Os7BGlu26 in universal buffer ..... 86

## LIST OF FIGURES (Continued)

<b>Figure</b>	<b>Page</b>
4.20 The structure of rice Os7BGlu26 E179Q in a covalent complex with a 2-deoxy-2-fluoroglucoside (G2F) moiety .....	89
4.21 Hydrogen bonding in the active site of the structure of rice Os7BGlu26 E179Q in complex with 2-deoxy-2-fluoroglucoside.....	90
4.22 The slow onset inhibition of Os7BGlu26 with putative transition state mimic inhibitors.....	93
4.23 The structures of rice Os7BGlu26 in complexes with mannoimidazole, glucoimidazole and isofagomine. ....	98
4.24 Polar interactions of rice Os7BGlu26 with putative transition state mimics. .	99

## LIST OF ABBREVIATIONS AND SYMBOLS

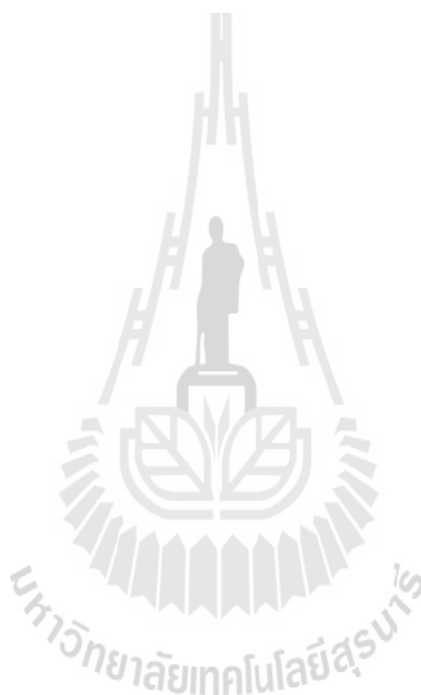
ASU	Asymmetric unit
bp	Base pair, (s)
BSA	Bovine serum albumin
CV	Column volume, (s)
DNA	Deoxyribonucleic acid
DNase	Deoxyribonuclease
DNP	2,4-Dinitrophenol
DNP2FG	2,4-Dinitrophenyl 2-deoxy-2-fluoro- $\beta$ -D-glucopyranoside
DNP2FM	2,4-Dinitrophenyl 2-deoxy-2-fluoro- $\beta$ -D-mannopyranoside
EDTA	Ethylenediaminetetraacetate
(m, $\mu$ )g	(milli, micro) Gram
GH	Glycoside hydrolase
GH1	Glycoside hydrolase family 1
h	Hour
HEPES	Hydroxyethyl piperazineethanesulfonic acid
IMAC	Immobilized metal affinity chromatography
IPTG	Isopropyl thio- $\beta$ -D-galactoside
KF	Potassium fluoride
kDa	Kilo Dalton

**LIST OF ABBREVIATIONS AND SYMBOLS (Continued)**

(m, $\mu$ )l	(milli, micro) Liter
(m, $\mu$ )M	(milli, micro) Molar
MES	2-Morpholinoethanesulfonic acid
min	Minute
MWCO	Molecular weight cut off
NaCl	Sodium chloride
NaCO <sub>3</sub>	Sodium carbonate
(NH <sub>4</sub> ) <sub>2</sub> SO <sub>4</sub>	Ammonium sulphate
nm	Nanometer
OD	Optical density
PCR	Polymerase chain reaction
PEG	Polyethylene glycol
PMSF	Phenyl methylsulfonyl fluoride
4NP	4-Nitrophenyl
4NPGlc	4-Nitrophenyl- $\beta$ -D-glucopyranoside
4NPMAN	4-Nitrophenyl- $\beta$ -D-mannopyranoside
rpm	Revolutions per minute
SDS	Sodium dodecyl sulfate
SDS-PAGE	Polyacrylamide gel electrophoresis with SDS
TE	Tris-EDTA
TEMED	Tetramethylenediamine
TFA	Trifluoroacetic acid

**LIST OF ABBREVIATIONS AND SYMBOLS (Continued)**

$T_m$	Melting temperature
Tris	Tris-(hydroxymethyl)-aminoethane
v/v	Volume per volume
w/v	Weight per volume



# CHAPTER I

## INTRODUCTION

### 1.1 General introduction

$\beta$ -D-Mannosidases ( $\beta$ -D-mannopyranoside mannohydrolase, E.C. 3.2.1.25) hydrolyze  $\beta$ -glycosidic linkages between non-reducing  $\beta$ -D-mannosyl residues and the neighboring aglycons or oligosaccharides.  $\beta$ -D-Mannosidases are found in a variety of organisms, including archaea, bacteria, animals, fungi, and plants (Cantarel *et al.*, 2009). In plants, these enzymes are present during and following seed germination in legumes (McCleary and Matheson, 1975), lettuce (*Lactuca sativa* L.) (Ouellette and Bewley, 1986) and tomato (*Lycopersicon esculentum* Mill.) (Mo and Bewley, 2002). Hrmova and colleagues (2006) showed that a barley (*Hordeum vulgare* L.)  $\beta$ -mannosidase, HvMannos appears to work in concert with  $\beta$ -mannanase to hydrolyze barley seed  $\beta$ -D-mannans.

$\beta$ -Mannosidases belong to glycoside hydrolase (GH) families GH1, GH2 and GH5 in the Carbohydrate-Active enZYme Database (CAZy, <http://www.cazy.org>; Cantarel *et al.*, 2009). These families fall within the GH-A clan, members of which adopt a  $(\beta/\alpha)_8$  barrel structure with two catalytic glutamic acid residues, the acid/base and the nucleophile, located at the C-terminal ends of  $\beta$ -strands 4 and 7, respectively. Currently, only two  $\beta$ -mannosidase structures have been reported, both from bacteria, GH2 Man2A from *Bacteroides thetaiotaomicron* VPI-5482 (Tailford *et al.*, 2008) and

GH5 Man5A from *Cellvibrio mixtus* NCIMB 8633 (Dias *et al.*, 2004). No GH1  $\beta$ -mannosidase structure had yet been reported prior to the work in this thesis.

It is believed that  $\beta$ -D-mannosides and  $\beta$ -D-glucosides are hydrolyzed *via* different conformational trajectories, based on X-ray crystallographic (Vocadlo and Davies, 2008) and conformational free energy landscape analysis (Biarnés *et al.*, 2007; Adrèvol *et al.*, 2010) data. During hydrolysis,  $\beta$ -D-glucopyranosyl rings are thought to undergo a conformational change via a  ${}^4H_3$  half-chair near or at the transition state. The ring appears to be primed to form this half-chair by its distortion to a  ${}^1S_3$  skew boat upon binding the enzyme and upon completing the glycosylation step of hydrolysis, and the glucose in the covalent glycosyl-enzyme intermediate is found in a relaxed  ${}^4C_1$  conformation (Davies *et al.*, 1998; 2012). In contrast, crystal structures of the  $\beta$ -D-mannosidase complexes with substrate and transition-state-based inhibitors reveal a  ${}^1S_5$  skew boat in the Michaelis complex, which proceeds through a  $B_{2,5}$  boat near the transition state to a  ${}^0S_2$  skew boat in the covalent complex (Ducros *et al.*, 2002; Tailford *et al.*, 2008).

Plant  $\beta$ -D-mannosidases fall in a single amino acid sequence-based phylogenetic cluster of GH1, which also contains  $\beta$ -D-glucosidases with  $\beta$ -D-mannosidase activity (Opassiri *et al.*, 2006; Kuntothom *et al.*, 2009). The amino acid sequence of rice Os7BGlu26 and three closely related rice  $\beta$ -D-glycosidase isoenzymes (Os3BGlu7, Os1BGlu1 and Os3BGlu8) are grouped in the same phylogenetic cluster with barley HvBII (Leah *et al.*, 1995; Hrmova *et al.*, 1996; 1998), Arabidopsis BGLU44 (Xu *et al.*, 2004) and tomato LeMside (Mo and Bewley, 2002)  $\beta$ -D-mannosidases. Within this group, only Os3BGlu7 has an elucidated structure, but

Os3BGlu7 hydrolyzes 4NPGlc with a 34-fold higher  $k_{\text{cat}}/K_{\text{m}}$  value than 4NPMan (Opassiri *et al.*, 2004). In contrast, rice Os7BGlu26 and barley HvBII, which have closely related amino acid sequences, hydrolyze 4NPMan with 3-fold and 12-fold higher  $k_{\text{cat}}/K_{\text{m}}$  values than 4NPGlc, respectively (Kuntothom *et al.*, 2009).

Given the difference seen in hydrolysis of the glucoside and mannoside substrates, it is of interest to understand the basis for  $\beta$ -D-mannosidase catalysis in GH1 enzymes that have both  $\beta$ -D-mannosidase and  $\beta$ -D-glucosidase activities, and their preference for  $\beta$ -D-mannoside *versus*  $\beta$ -D-glucoside substrates. To investigate the molecular mechanism for  $\beta$ -D-mannosidase specificity in plant GH1  $\beta$ -D-mannosidases, we determined the Os7BGlu26  $\beta$ -D-mannosidase crystal structure with and without mannose and putative transition state analogues and probed the residues involved by computational docking and mutagenesis.

## 1.2 Research objectives

- 1.2.1 To produce, crystallize and determine the structure of rice Os7BGlu26  $\beta$ -mannosidase/ $\beta$ -glucosidase.
- 1.2.2 To investigate the inhibition of rice Os7BGlu26  $\beta$ -mannosidase/ $\beta$ -glucosidase by covalent and noncovalent substrate-based and mechanism-based inhibitors.
- 1.2.3 To determine the inhibition constants of transition state analogues.
- 1.2.4 To crystallize and determine the structure of rice Os7BGlu26  $\beta$ -mannosidase/ $\beta$ -glucosidase with transition state analogues.

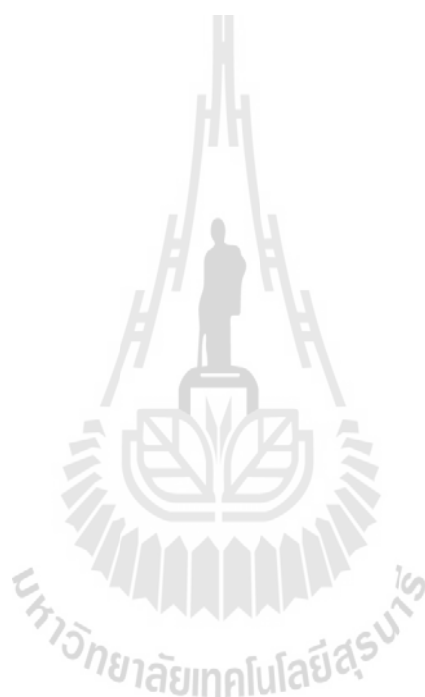
- 1.2.5 To explore amino acids responsible for  $\beta$ -D-mannoside or  $\beta$ -D-glucoside substrate preference of plant  $\beta$ -mannosidase/ $\beta$ -glucosidases by site-directed mutagenesis and kinetic studies.

### 1.3 Research scope

The scope of this project is to investigate the rice GH1 Os7BGlu26  $\beta$ -mannosidases at the molecular level. This includes improving the production of rice Os7BGlu26  $\beta$ -mannosidase/ $\beta$ -glucosidase, developing the purification process for adequate purity and recovery, screening for crystallization conditions for this enzyme, optimizing the crystal growth, diffraction of crystals at a synchrotron, such as the National Synchrotron Radiation Research Center (NSRRC, Hsinchu, Taiwan), and solving the structure by molecular replacement (MR). The goal was to crystallize Os7BGlu26  $\beta$ -mannosidase/ $\beta$ -glucosidase and solve its structure. Moreover, this work tried to elucidate what putative transition state analogues were closest to true transition state mimics by determination of inhibition constants and Os7BGlu26 was crystallized with transition state analogues, in order to determine the true shape of the transition state. The rice Os7BGlu26  $\beta$ -mannosidase/ $\beta$ -glucosidase acid/base mutant E179Q was characterized with 4NPGlc, and 4NPMAN in the presence and absence of nucleophiles, such as azide and the pH profile with the nucleophile azide was also determined. This mutant was produced to study the structure of the manno- and/or gluco-oligosaccharide complexes, in order to see the shape of the nonreducing sugar residue in the Michaelis complex.

Finally, this project explored amino acids responsible for  $\beta$ -mannosidase or  $\beta$ -glucosidase activity of plant  $\beta$ -mannosidase/ $\beta$ -glucosidases by site-directed

mutagenesis of rice Os7BGlu26 and kinetic studies of the mutated enzymes to see whether a difference in the active site amino acids between the  $\beta$ -mannosidase cluster and other GH1 enzymes determines the presence of significant  $\beta$ -mannosidase activity.

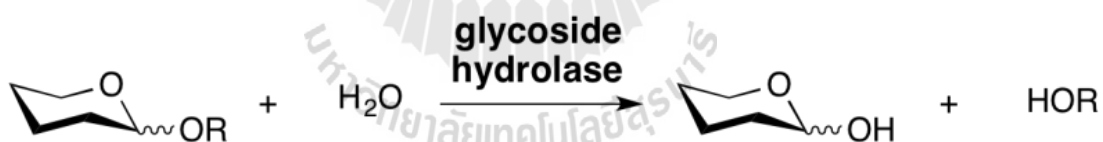


## CHAPTER II

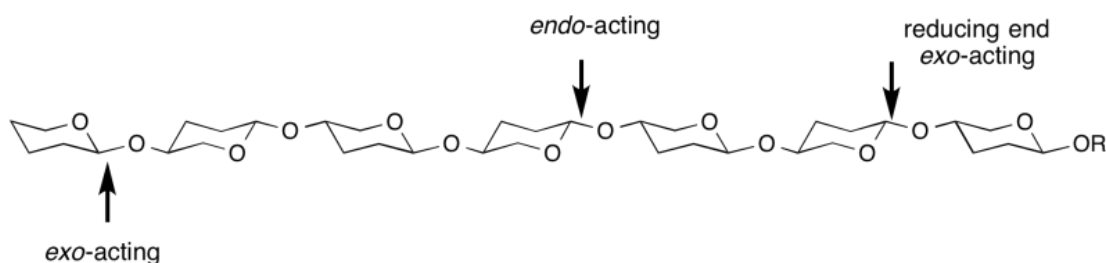
### LITERATURE REVIEW

#### 2.1 Glycoside Hydrolases

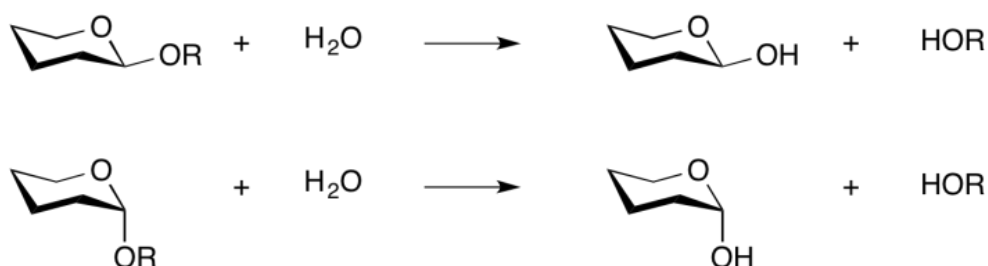
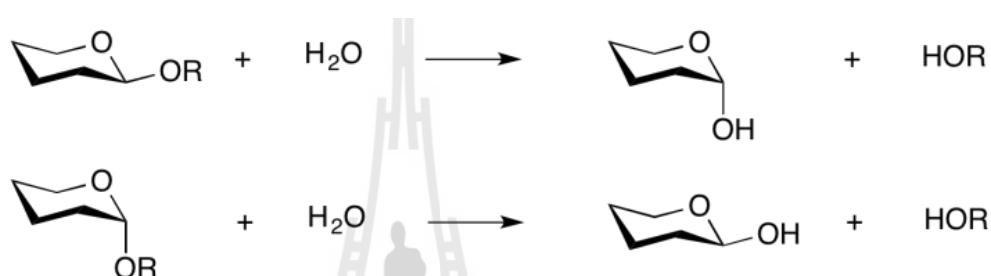
Glycoside hydrolases (GH) are enzymes that breakdown the glycosidic linkages of saccharide molecules (Figure 2.1). Glycoside hydrolases are also referred to as glycosidases, and sometimes also as glycosyl hydrolases. Glycoside hydrolases can be classified in many different ways, such as endo/exo acting (Figure 2.2), enzyme commission (EC) number, mechanistic classification (Figure 2.3) and sequence-based classification. From amino acid sequence similarity, these enzymes have so far been classified into 132 glycoside hydrolase families, which show varieties of substrate specificities and structural models ([www.cazy.org](http://www.cazy.org)).



**Figure 2.1** Glycoside hydrolase activity ([www.cazypedia.org](http://www.cazypedia.org)).



**Figure 2.2** Endo/exo-acting glycoside hydrolases ([www.cazypedia.org](http://www.cazypedia.org)).

**Retaining glycoside hydrolases:****Inverting glycoside hydrolases:**

**Figure 2.3** Retaining and inverting glycoside hydrolase mechanisms (www.cazypedia.org).

## 2.2 $\beta$ -Mannosidases

Beta-mannosidases ( $\beta$ -D-mannopyranoside mannohydrolases, E.C. 3.2.1.25) are enzymes that hydrolyze the glycosidic bond between the reducing side of a nonreducing terminal  $\beta$ -D-mannosyl residue and an aglycon or oligosaccharide.  $\beta$ -Mannosidases are members of GH families GH1, GH2 and GH5, which are in glycoside hydrolase clan GH-A ( $(\beta/\alpha)_8$  barrel structure) (Henrissat *et al.*, 1995; Jenkin *et al.*, 1995). Currently, only two  $\beta$ -mannosidase structures have been reported, both from bacteria, the GH2 Man2A from *Bacteroides thetaiotaomicron* VPI-5482 (Tailford *et al.*, 2007) and GH5 Man5A from *Cellvibrio mixtus* NCIMB 8633 (Dias *et al.*, 2004), which are shown in Figure 2.4.

There is little information about  $\beta$ -mannosidases in plants. This enzyme activity is present during flowering in *Onchidium* orchid (Wang *et al.*, 2008) and during and following seed germination in tomato (Mo and Bewley, 2002), lettuce (Ouellette and Bewley, 1986) and legumes (McCleary and Matheson, 1975). Hrmova and colleagues (2006) showed that a barley GH1 isoenzyme, HvMannos, appears to work in concert with  $\beta$ -mannanase to hydrolyze barley seed  $\beta$ -mannans. An *Arabidopsis* GH1 enzyme with a sequence similar to tomato and barley  $\beta$ -mannosidases was also shown to be a  $\beta$ -mannosidase that could hydrolyze mannoooligosaccharides (Xu *et al.*, 2004).

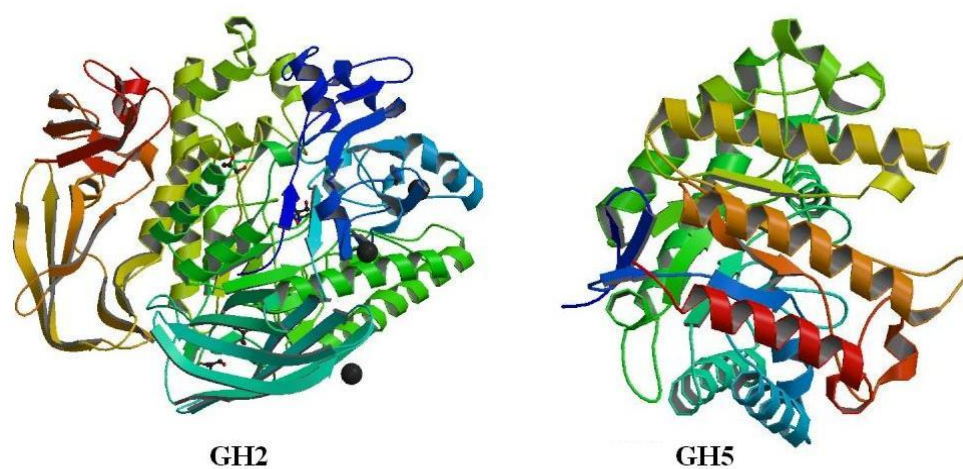


**Figure 2.4**  $\beta$ -Mannosidase structures from GH2 and GH5 families. GH2, BtMan2A from *Bacteroides thetaiotaomicron* (2JE8), and GH5, CmMan5A from *Cellvibrio mixtus* (1UUQ).

## 2.3 $\beta$ -Glucosidases

Beta-glucosidases ( $\beta$ -D-glucopyranoside glucohydrolases, E.C. 3.2.1.21) are enzymes that catalyze the hydrolysis of the beta-glycosidic bond between the reducing side of a terminal  $\beta$ -D-glucosyl residue and an aryl or alkyl aglycon or oligosaccharide.  $\beta$ -Glucosidases are found in at least 6 families of GH and show different structures depending on of which GH family they are a member (www.cazy.org). The GH1, GH5 and GH30 families belong to Clan GH-A, the members of which have  $(\beta/\alpha)_8$  barrel domains that contain their active sites. In contrast, family GH 9 enzymes have  $(\alpha/\alpha)_6$  structures, while GH3 enzymes use the cooperation of two domains, one  $(\beta/\alpha)_8$  barrel and one  $(\beta/\alpha)_6$  sandwich domain, for their active sites (Figure 2.5). No structure of a GH116  $\beta$ -glucosidase is currently available, but GH116 enzymes show distant homology to families with  $(\alpha/\alpha)_6$  structures.

In plants,  $\beta$ -glucosidases play essential roles in many biological processes, such as chemical defense against pathogens and herbivores (Morant *et al.*, 2008), lignification (Escamilla-Trevino *et al.*, 2006), cell wall modification (Hrmova and Fincher, 2001) and phytohormone activation (Schroeder and Nambara, 2006). Based on amino acid sequence similarities, plant beta-glucosidase can be classified in GH families GH1, GH3 (Henrissat, 1991) and GH5 (Opassiri *et al.*, 2007), while plants also have uncharacterized GH116 genes that are likely to encode beta-glucosidases.

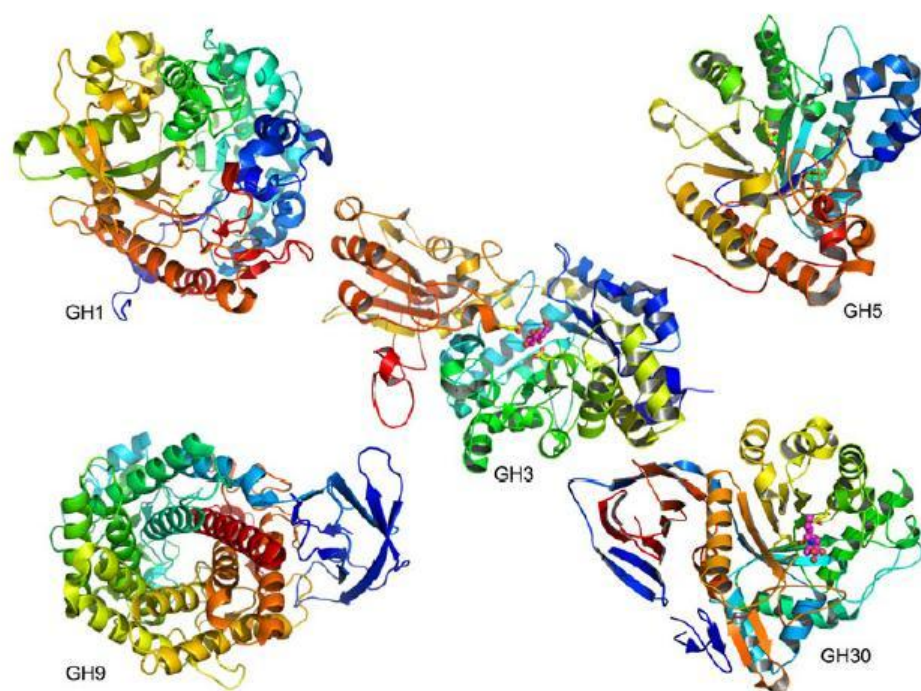


**Figure 2.5**  $\beta$ -Glucosidase structures from various GH families (Ketudat Cairns and Esen, 2010).

## 2.4 Glycosidase mechanism

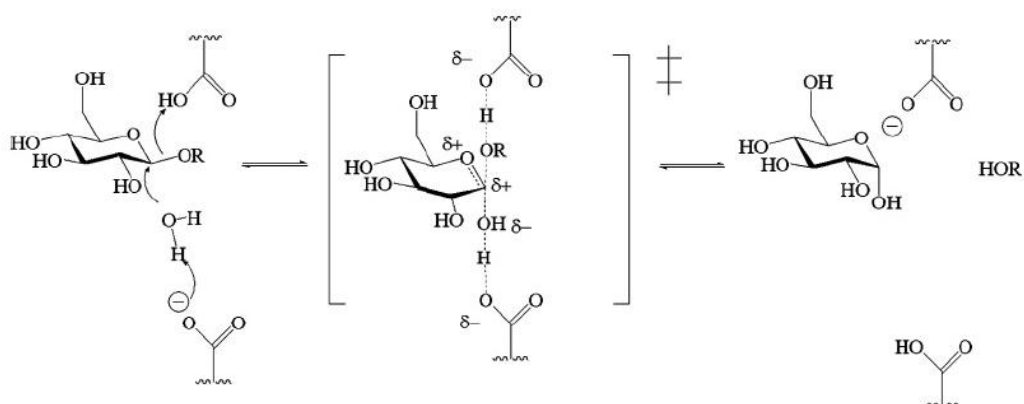
The hydrolysis of glycosidic bonds usually proceeds via one of two mechanisms, which are classically defined as those with inversion and retention of anomeric configuration (Figure 1.3; Sinnott, 1990; McCarter and Withers, 1994; Ly and Withers, 1999). Traditionally, GH enzymes are thought to use general acid catalysis, which involves two acidic catalytic residues in the active site that act as a general acid or proton donor and a general base or nucleophile, for hydrolysis (Koshland, 1953).

Inversion of stereochemistry occurs in a single step mechanism (Davies *et al.*, 1998; Sinnott, 1990), which allows both the substrate and a water molecule to be bound concurrently (Figure 2.6). The inverting mechanism effects bond cleavage

through the action of two carboxylic acid amino acids (Asp or Glu) that are located on opposite sides of the active site. One of the catalytic amino acids acts as a general acid residue and the other as a general base residue. The water is deprotonated by the general base residue and then acts as nucleophilic molecule to attack at the anomeric carbon of the sugar next to the bond being hydrolyzed. Then, a general acid residue donates a proton to the glycosidic oxygen to aid in bond cleavage and departure of the aglycon.

Retention of stereochemistry occurs via a double displacement mechanism, consisting of two steps (Figure 2.6). The retaining mechanism also uses a pair of essential carboxylic acid residues (generally Asp or Glu) located on opposite sides of the enzyme active site, but they are normally closer together than those in the inverting mechanism. One of the catalytic residues acts as the acid/base residue and the other as a nucleophile. A deprotonated carboxylate acts as a nucleophile, attacking at the anomeric carbon and the acid/base protonates the glycosidic oxygen to aid in release of the aglycon at the same step. This step is referred to as the glycosylation step because the enzyme forms a covalent glycosyl-enzyme intermediate. In the second step, which is the deglycosylation step, the acid/base residue deprotonates a water molecule, which provides a nucleophilic species to attack at the anomeric carbon and displace the enzyme from the glycosyl group. The glycon is released as a free sugar with the same anomeric configuration as the substrate.

**Inverting mechanism for a  $\beta$ -glucosidase:**



**Retaining mechanism for a  $\beta$ -glucosidase:**

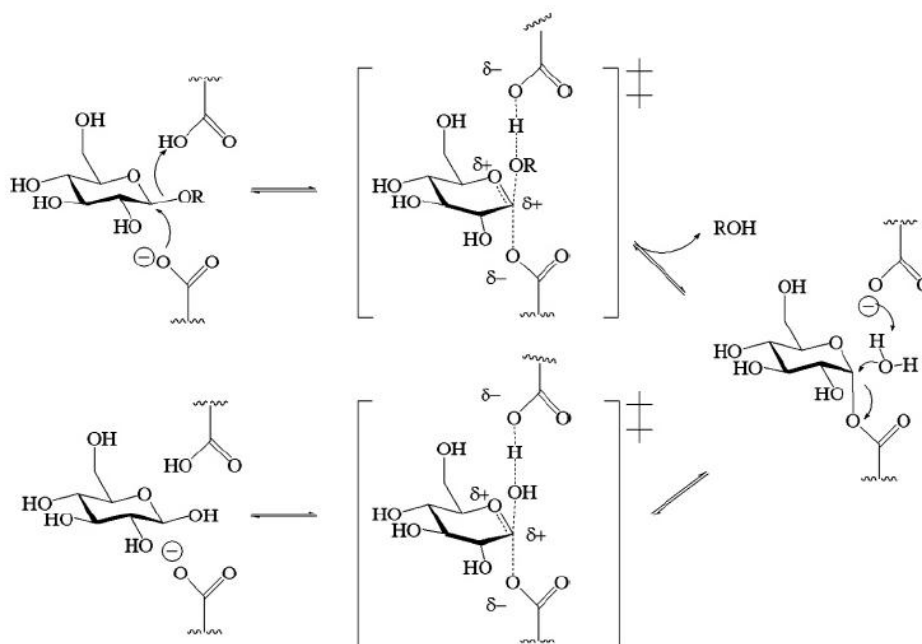


**Figure 2.6** Glycosidase mechanisms for hydrolysis. Classical mechanism for inversion of stereochemistry and classical mechanism for retention of stereochemistry (Rempel and Withers, 2008).

Gloster and Davies (2010) reviewed the other mechanisms that have been proposed for small sets of families of glycoside hydrolases. A substrate-assisted catalytic mechanism (Figure 2.7A) has been proposed for glycoside hydrolases which catalyse hydrolysis of substrates containing *N*-acetylhexosamine with retention of the configuration, despite the absence of a conventional nucleophile. These enzymes are grouped into families GH18, GH20, GH25, GH56, GH84, and GH85. The catalytic nucleophile is not derived from the enzyme, but instead is from the acetamido group at the C2 position of the substrate. The *N*-acetyl carbonyl group of the substrate acts as a nucleophile to attack the anomeric carbon to create a covalent oxazoline intermediate. The breakdown of this intermediate is achieved by the attack by a water molecule, which is activated by a general base residue. A second carboxylate-containing residue mostly orients and polarizes the *N*-acetyl carbonyl group to increase its nucleophilicity. In GH33 and GH34, some sialidases and neuraminidases hydrolyze sialic acid-containing substrates in an *exo* fashion with retention of configuration, using a tyrosine residue to act as the catalytic nucleophile (Figure 2.7B). A Tyr/Glu couple is invoked to relay the charge from a close glutamate residue to provide a nucleophilic oxygen atom carrying some negative charge; it is proposed that not using a glutamate residue in this position avoids electrostatic repulsions with the sialic acid carboxylate group.

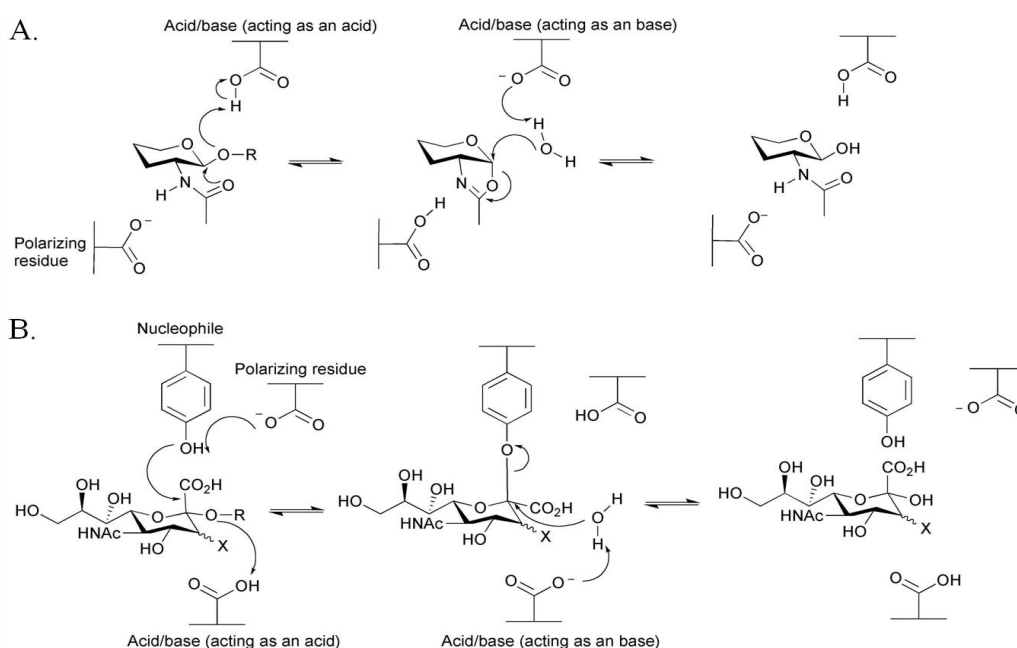


**Figure 2.7** Unusual glycosidase mechanisms for hydrolysis (Gloster and Davies, 2010). (A) Substrate-assisted mechanism. (B) Mechanism using a tyrosine residue as the nucleophile.

## 2.5 Nucleophile and acid/base mutants with rescued activity

Rescue of the activity of mutants by azide may be used to identify the catalytic acid/base and nucleophile residues (MacLeod *et al.*, 1996). The Ala mutant of the nucleophile of *Agrobacterium*  $\beta$ -glucosidase (Abg) enzyme (Figure 2.8A), which completely lacks activity, can be reactivated for hydrolysis of 2,4-dinitrophenyl glycoside by azide, formate, or acetate. With azide, this rescue results in the formation of glycoside with the inverted anomeric configuration, e.g.  $\alpha$ -glucosyl azide is obtained from the rescue of the activity of Abg nucleophile mutant (Figure 2.8A) (Wang *et al.*, 1994). Moreover, the nucleophile mutants of glycosidases can be used for synthesis of specific oligosaccharides in appropriate quantities for many desired applications. These mutants cannot form a reactive  $\alpha$ -glycosyl-enzyme intermediate

for transglycosylation. However, when an  $\alpha$ -glycosyl fluoride is present as a glycosyl donor, the mutant enzymes can transfer the glycosyl moiety to acceptor alcohols without hydrolysis of the products, as shown in Figure 2.9 (Shaikh and Withers, 2008). In contrast, the glycine nucleophile mutant of a *Sulfolobus solfataricus*  $\beta$ -glucosidase was shown to act as a retaining glycosidase in the presence of formate (Figure 2.10).

On the other hand, azide rescue of the Abg acid/base mutant cleavage of 2,4-dinitrophenyl  $\beta$ -D-glucoside results in the formation of glycoside with the retained anomeric configuration as the substrate, to yield  $\beta$ -glucosyl azide (Figure 2.8B) (Wang *et al.*, 1995). In this case, the good leaving group has a low  $pK_a$  and therefore does not require protonation, which eliminates the requirement for the acid catalyst in the glycosylation step whereas the azide does not require basic assistance in the deglycosylation step. The catalytic activity can be restored to the acid/base mutant of *Agrobacterium* sp.  $\beta$ -glucosidase (E170G) by the inclusion of a suitably positioned carboxyl group into the substrate without an external nucleophile (Figure 2.11) (Zechel and Withers, 2000). The carboxyl groups of such substrates may function as the general acid catalyst when bound to the mutant enzyme, but cannot act in the active site of the wild-type (WT) enzyme. Such “substrate-assisted catalysis” was suggested to be important for the thioglycosidases of family GH1, such as *Sinapis alba* myrosinase, which has a Gln residue at this position. This enzyme can hydrolyze its highly reactive substrate sinigrin and other glucosinolate substrates to perform the glycosylation step without an acid catalyst, while ascorbate acts as a base catalyst in the deglycosylation step after departure of the aglycon (Burmeister *et al.*, 2000) (Figure 2.12).

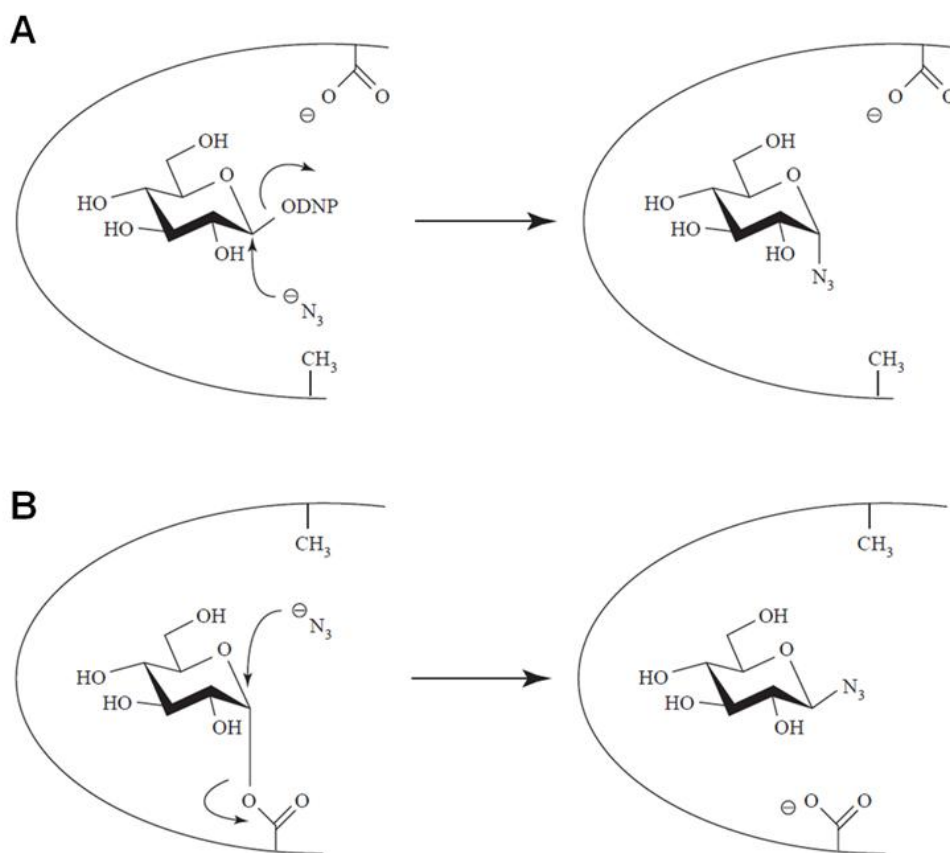


**Figure 2.8** Rescue of catalytic activity in the nucleophile and acid/base mutant by azide (Ly and Withers, 1999).

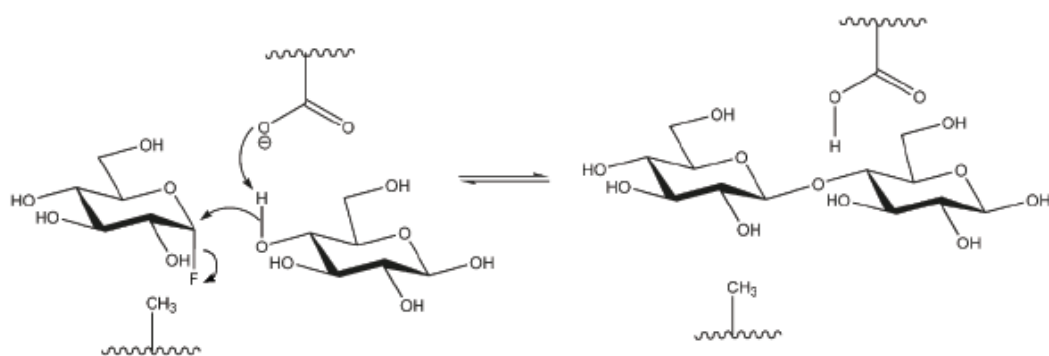


**Figure 2.9** Mechanism of transglycosylation with a glycosynthase (Shaikh and Withers, 2008).

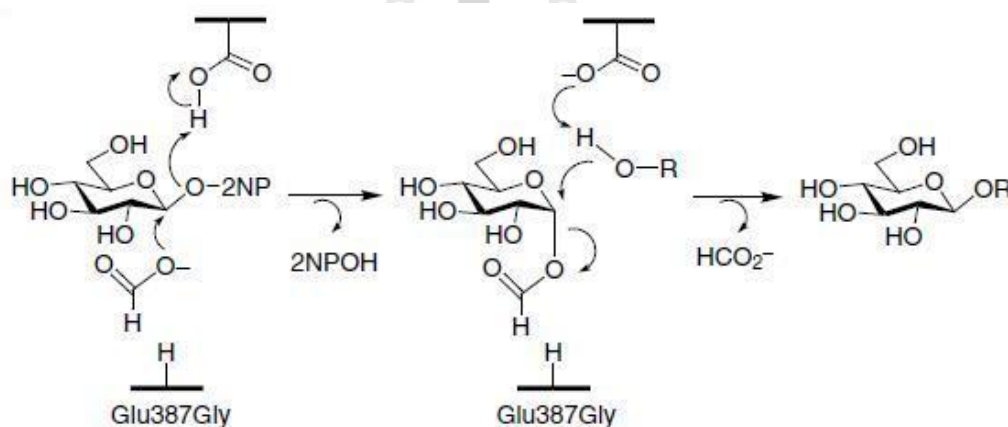


**Figure 2.10** Rescue of catalytic activity in the nucleophile mutant of *Sulfolobus solfataricus*  $\beta$ -glucosidase by formate (Zechel and Withers, 2001).

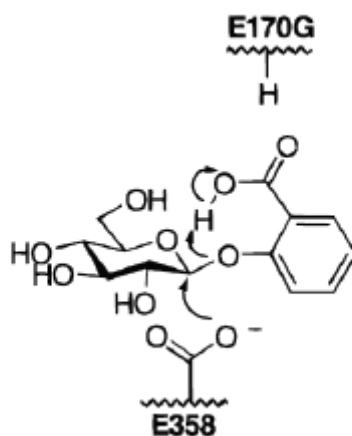


**Figure 2.11** Rescue of catalytic activity in the acid/base mutant of *Agrobacterium* sp.  $\beta$ -glucosidase by substrate-assisted protonation (Zechel and Withers, 2000).

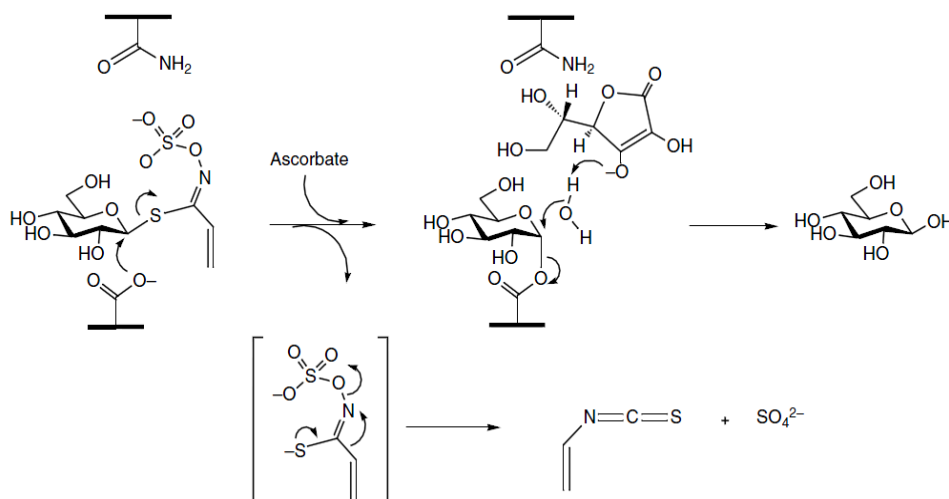


**Figure 2.12** A natural version of chemical rescue with *Sinapis alba* myrosinase utilizes ascorbate as a general base catalyst (Burmeister *et al.*, 2000; Zechel and Withers, 2001).

## 2.6 Transition state mimicry of $\beta$ -mannosidases and $\beta$ -glucosidases

More than four decades ago, Stoddard (1971) proposed the conformational itinerary of pyranosides. This scheme shows the range of substrate distortion that might occur during the enzymatic hydrolysis of glycosides (Figure 2.13). Transition states occur at the anomeric center of the bond that is cut in either the inverting or retaining mechanism of hydrolysis. The transition state conformation of the glycoside during enzymatic hydrolysis from both mechanisms is thought to have an oxocarbenium ion-like character, in which the anomeric center has greater planar-trigonal  $sp^2$ -hybridization than in the intermediate. These transition states are stabilized by delocalization of electrons across the C1-O5 bond. The partial double bond character between the anomeric carbon and the endocyclic oxygen demands that near the transition state C5, O5, C1 and C2 must be coplanar. Therefore, the pyranoside ring conformation must place these 4 atoms in the same plane, a trait seen only in two half-chair ( ${}^4H_3$  and  ${}^3H_4$ ) and two classical boat ( $B_{2,5}$  and  ${}^{2,5}B$ ) conformations, as observed by Sinnott (1990).

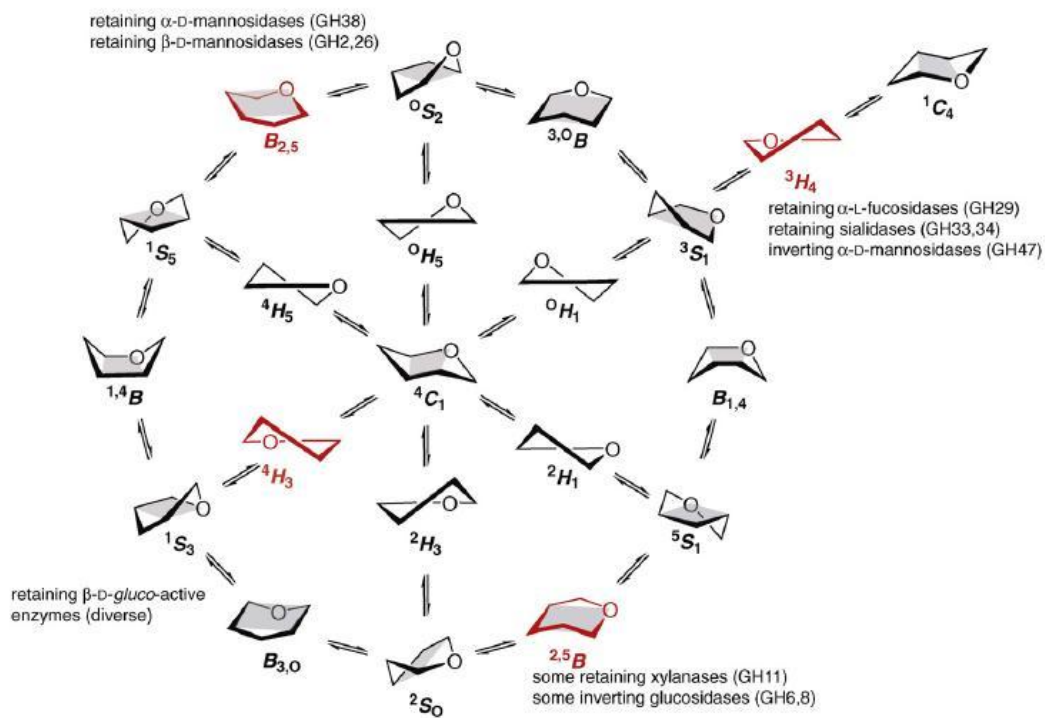
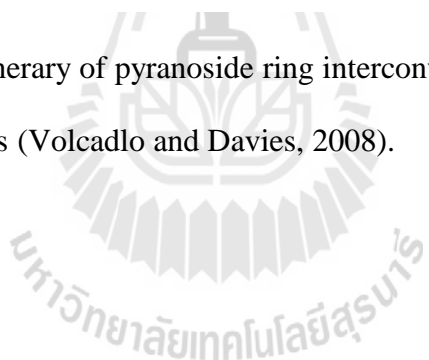


**Figure 2.13** Partial itinerary of pyranoside ring interconversions from various families of glycoside hydrolases (Volcardo and Davies, 2008).



Although the conformation of a pyranose ring has four possible forms that can fit the above mentioned requirements for coplanarity of the atoms, initially, only for  $B_{2,5}$  and  ${}^4H_3$  was strong evidence observed by X-ray crystallography (Davies *et al.*, 2003). Retaining  $\beta$ -D-glucosyl-enzymes from various GHs are thought to pass through a  ${}^4H_3$  half-chair in the transition state, which is preceded by a  ${}^1S_3$  skew boat (Michaelis complex). The structure of Cel5A from *Bacillus agaradhaerens* with 2,4-dinitrophenyl-2-deoxy-2-fluoro- $\beta$ -D-cellobioside showed a  ${}^1S_3$  Michaelis complex and that of the covalent glycosyl-enzyme intermediate had the 2-deoxy-2-fluoroglucosyl residue in a relaxed  ${}^4C_1$  conformation (Davies *et al.*, 1998). This evidence suggests that the  ${}^4H_3$  conformation is used for the oxocarbenium-ion-like transition state in what may be described as a  ${}^1S_3 \rightarrow {}^4H_3 \rightarrow {}^4C_1$  pathway for the glycosylation step of the reaction (Figure 2.14A). The  ${}^1S_3$  skew boat conformation of  $\beta$ -D-glucoside substrates has been published in several enzymes, including the GH1 sorghum dhurrinase (PDB entry 1V03, Verdoucq *et al.*, 2004), rice (*Oryza sativa*) Os3BGlu6 (3GNP, Seshadri *et al.*, 2009), termite (*Neotermes koshunensis*)  $\beta$ -D-glucosidase NKBgl (3AI0, Jeng *et al.*, 2011), and rice Os4BGlu12 (3PTQ, Sansenya *et al.*, 2011). In the case of rice BGlu1 (designated here as Os3BGlu7), the nonreducing  $\beta$ -D-glucopyranosyl ring in the oligosaccharide complexes with catalytic mutants was reported to be between the  ${}^1S_3$  and  ${}^4H_3$  or closely related  ${}^4E$  conformations, again supporting the trajectory of  ${}^1S_3$  to  ${}^4H_3$  (Chuenchor *et al.*, 2011). Strong evidence was found in the structure of the family GH1 *S. alba* myrosinase with glucotetrazole, in which this inhibitor distorted to the  ${}^4H_3$  conformation (PDB entry: 1C6Q) (Figure 2.15B) (Burmiester *et al.*, 2000). Such observations were also made in *Thermotoga maritima*  $\beta$ -glucosidase and *Sulfolobus solfataricus*  $\beta$ -glycosidase complexes with glycosidase inhibitors (Zechel *et al.*, 2003,

Gloster *et al.*, 2006, 2007). Moreover, in the family GH3 barley  $\beta$ -D-glucan glucohydrolase complex with glucophenylimidazole, the strong inhibitor distorted to the  ${}^4E$  envelope conformation, which is closely related to the  ${}^4H_3$  conformation (Hrmova *et al.*, 2004, 2005). Enzymatic mannoside hydrolysis appears to use a different conformational pathway. The structure of a GH26 endo- $\beta$ -mannanase from *Cellvibrio japonicus* in complex with 2-fluoro-2-deoxy- $\beta$ -D-mannobioside revealed a  ${}^1S_5$  conformation for the unhydrolysed Michaelis complex (Ducros *et al.*, 2002). More recent work on family GH2 *Bacteroides thetaiotaomicron*  $\beta$ -mannosidase BtMan2A with 2,4-dinitrophenyl 2-deoxy-2-fluoro- $\beta$ -D-mannoside revealed a  ${}^1S_5$  conformation for its Michaelis complex (Offen *et al.*, 2009). Moreover, this enzyme presented a  $B_{2,5}$  boat transition state conformation when the complexes with putative  $\beta$ -mannosidase transition state mimic inhibitors were analyzed (Figure 2.15A) (Tailford *et al.*, 2008). This strong evidence implies that the retaining  $\beta$ -mannosidase used the  ${}^1S_5 \rightarrow B_{2,5} \rightarrow {}^oS_2$  pathway for the glycosylation step (Figure 2.14B). In contrast, the GH1 cytosolic  $\beta$ -glucosidase acid/base mutant E165Q had a  ${}^4C_1$  chair conformation of mannoside in its covalent complex (PDB entry: 3VKK) (Noguchi *et al.*, unpublished). However, computational modeling analysis of the conformation free energy landscape of  $\beta$ -glucoside and  $\beta$ -mannoside also support the itinerary of the  ${}^1S_3 \rightarrow {}^4H_3 \rightarrow {}^4C_1$  glucoside (Biarnés *et al.*, 2007) and the  ${}^1S_5 \rightarrow B_{2,5} \rightarrow {}^oS_2$  mannoside pathway (Adrèvol *et al.*, 2010).

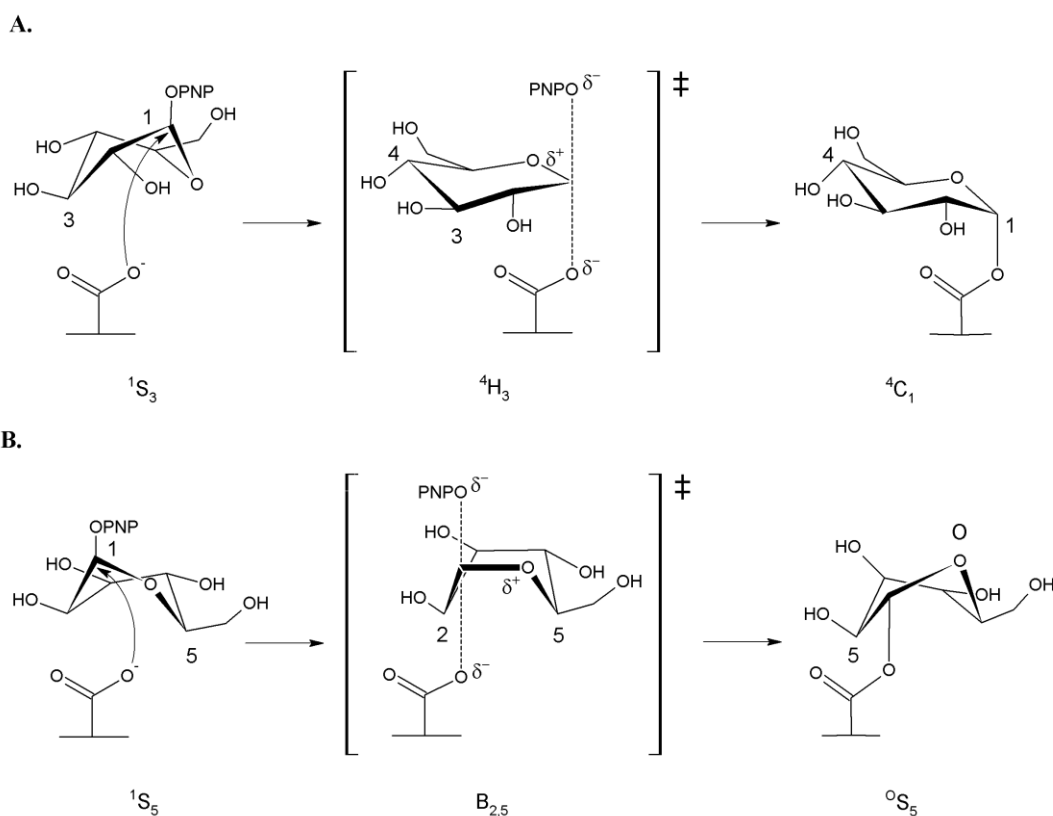


**Figure 2.14** Schematic diagram of the proposed conformational itinerary for the glycosylation step of the retaining mechanism derived from three-dimensional structures. (A.) The *gluco*-derived substrates model, based on structures of trapped intermediates of hydrolysis by Cel5A. (B.) The *manno*-configured model based on structures of substrates trapped in the process of hydrolysis by Man26A (Davies *et al.*, 2003).

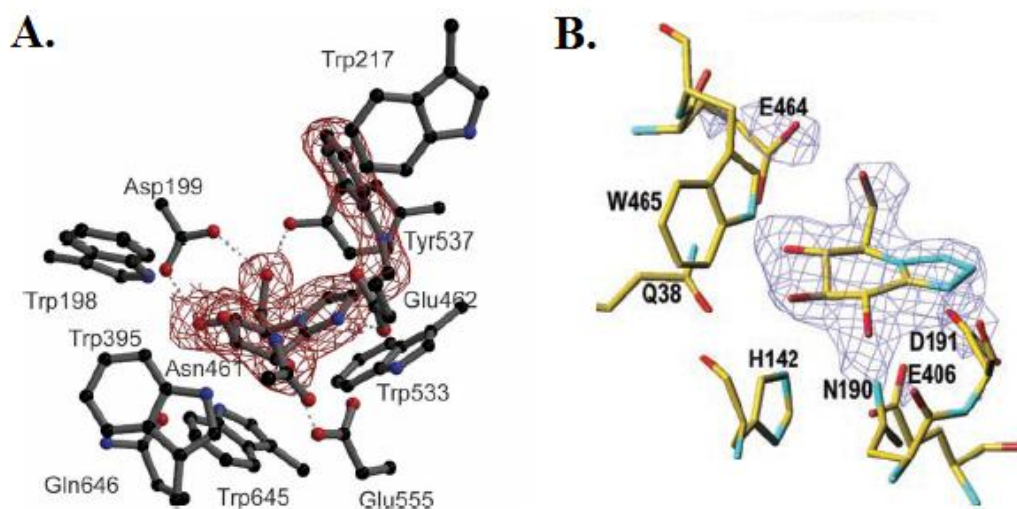
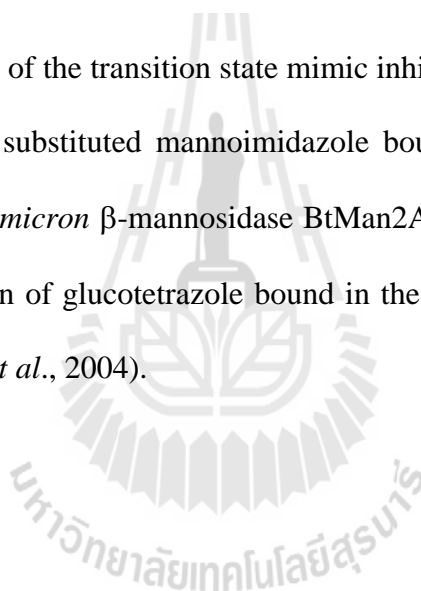


**Figure 2.15** Structures of the transition state mimic inhibitors in the active site. A.  $B_{2,5}$  boat conformation of substituted mannoimidazole bound in the active site of GH2 *Bacteroides thetaiotaomicron*  $\beta$ -mannosidase BtMan2A (Tailford *et al.*, 2008). B.  $^4H_3$  half chair conformation of glucotetrazole bound in the active site of a GH1 sorghum dhurinase (Verdoucq *et al.*, 2004).



## 2.7 Glycoside hydrolase family 1 crystal structures

Most plant beta-glucosidases that have been characterized belong to GH1, which also contains a wide range of other  $\beta$ -glycosidases, including  $\beta$ -galactosidases,  $\beta$ -mannosidases,  $\beta$ -fucosidases, phospho- $\beta$ -galactosidases, phospho- $\beta$ -glucosidases, and thioglucosidases ([www.cazy.org](http://www.cazy.org)). Moreover, plant GH1 enzymes may be highly specific for their aglycons, as has been seen for strictosidine  $\beta$ -glucosidase, amygdalin  $\beta$ -glucosidase, prunasin  $\beta$ -glucosidase, raucaffricine  $\beta$ -glucosidase, dhurrinase, and isoflavonoid 7-O- $\beta$ -apiosyl- $\beta$ -glucosidase ([www.cazy.org](http://www.cazy.org)).

The first GH 1 structure published was from the white cover cyanogenic  $\beta$ -glucosidase (PDB entry: 1CBG), which has a  $(\beta/\alpha)_8$  or TIM barrel conformation, consisting of a core of eight twisted parallel  $\beta$ -strands and eight  $\alpha$ -helices that form the outer layer of the core structure connected by long loops (Barrett *et al.*, 1995). The conserved catalytic acid/base and nucleophile are located at the ends of  $\beta$ -strands 4 and 7 on opposite sides of a cleft at the bottom of the active site (Figure 2.16). Currently, structures of 39 GH1 hydrolases are available, including 5 from archaea, (Table 2.1) 17 from bacteria (Table 2.2), and 17 from eukaryotes (Table 2.3), most of which represent  $\beta$ -D-glucosidases (E.C. 3.2.1.21). A few other GH1 structures represent bacterial  $\beta$ -D-glycosidases with broad substrate specificity, two are thioglucosidases (E.C. 3.2.1.147), five are 6-phospho- $\beta$ -glucosidases (E.C. 3.2.1.86), and one is a 6-phospho- $\beta$ -galactosidase (E.C. 3.2.1.85). From rice, 3 published structures are available, those of the rice BGlu1 or Os3BGlu7, Os3BGlu6 and Os4BGlu12 (Figure 2.17).

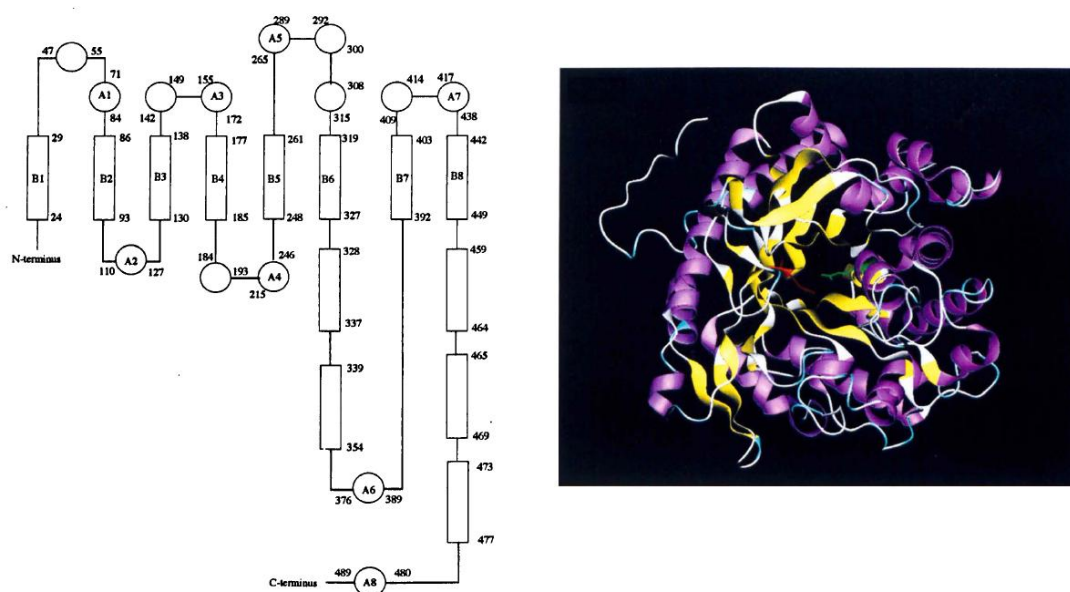


**Figure 2.16** Secondary structure diagram of white clover cyanogenic  $\beta$ -glucosidase showing the eight parallel  $\beta$ -strands that form the barrel core. The  $\beta$ -strands are represented by rectangles and the  $\alpha$  helices by circles. The eight  $\beta$ -strands forming the barrel are labeled B1-B8 and the eight peripheral helices A1-A8 (left panel). The three-dimensional structure of white clover cyanogenic  $\beta$ -glucosidase (right panel) (Barrett *et al.*, 1995).

**Table 2.1** Glycoside hydrolase family 1 structures from archaea.

<b>Protein Name</b>	<b>Organism</b>	<b>PDB</b>
$\beta$ -glycosidase	<i>Acidilobus saccharovorans</i> 345-15	4HA3
$\beta$ -glucosidase / $\beta$ -glycosidase / $\beta$ -rutinosidase	<i>Pyrococcus furiosus</i> DSM 3638	3APG
alkyl $\beta$ -glucosidase	<i>Pyrococcus horikoshii</i> OT3	1VFF
$\beta$ -glycosidase S	<i>Sulfolobus solfataricus</i> P2	1GOW
$\beta$ -glycosidase	<i>Thermosphaera aggregans</i> M11TL	1QVB

**Table 2.2** Glycoside hydrolase family 1 structures from bacteria.

<b>Protein Name</b>	<b>Organism</b>	<b>PDB</b>
$\beta$ -glucosidase (BglA)	<i>Bacillus circulans</i> subsp. alkalophilus	1QOX
$\beta$ -glucosidase A (BglA;BG)	<i>Clostridium cellulovorans</i>	3AHX
6-P- $\beta$ -glucosidase A	<i>Escherichia coli</i> K-12 MG1655	2XHY
$\beta$ -glucosidase A	<i>Halothermothrix orenii</i> H 168 H 168; DSM 9562	3TA9
6-P- $\beta$ -glucosidase	<i>Lactobacillus plantarum</i> WCFS1	3QOM
6-P- $\beta$ -galactosidase (LacG)	<i>Lactococcus lactis</i> Z268	1PBG
$\beta$ -glucosidase A (BglA)	<i>Paenibacillus polymyxa</i>	1BGA
$\beta$ -glucosidase B (BglB)	<i>Paenibacillus polymyxa</i>	2JIE
6-P- $\beta$ -glucosidase	<i>Streptococcus mutans</i> UA159	3PN8
6-P- $\beta$ -glucosidase	<i>Streptococcus pneumoniae</i> TIGR4	4IPL
6-phospho- $\beta$ -glucosidase	<i>Streptococcus pyogenes</i> M1 GAS SF370	4B3K
$\beta$ -glucosidase (Bgl3)	<i>Streptomyces</i> sp. QM-B814	1GNX
$\beta$ -glucosidase A	<i>Thermotoga maritima</i> MSB8	1OD0
$\beta$ -glycosidase	<i>Thermus nonproteolyticus</i> HG102	1NP2
$\beta$ -glycosidase / $\beta$ -glucosidase	<i>Thermus thermophilus</i> HB8	1UG6
$\beta$ -glycosidase	<i>Thermus thermophilus</i> TH125	3ZJK
$\beta$ -glycosidase / $\beta$ -glucosidase	uncultured bacterium	3CMJ

**Table 2.3** Glycoside hydrolase family 1 structures from eukaryotes.

<b>Protein Name</b>	<b>Organism</b>	<b>PDB</b>
myrosinase	<i>Brevicoryne brassicae</i>	1WCG
cytoplasmic $\beta$ -glucosidase	<i>Homo sapiens</i>	2E9L
$\beta$ -glucosidase	<i>Neotermes koshunensis</i>	3AHZ
$\beta$ -glucosidase (BGlu1; Os3BGlu7)	<i>Oryza sativa</i> Japonica Group	2RGL
$\beta$ -glucosidase (Os3BGlu6)	<i>Oryza sativa</i> Japonica Group	3GNO
$\beta$ -glucosidase (Os4BGlu12; OsTAGG2)	<i>Oryza sativa</i> Japonica Group	3PTK
$\beta$ -glucosidase (Bgl1A)	<i>Phanerochaete chrysosporium</i> K-3	2E3Z
strictosidine $\beta$ -glucosidase	<i>Rauwolfia serpentina</i>	2JF6
raucaffricine $\beta$ -glucosidase	<i>Rauwolfia serpentina</i>	3U57
$\beta$ -glucosidase (ScGlu)	<i>Secale cereale</i>	3AIU
myrosinase	<i>Sinapis alba</i>	1DWA
cyanogenic $\beta$ -glucosidase (dhurrinase 1)	<i>Sorghum bicolor</i> P721N	1V02
$\beta$ -glucosidase 2 (Ce11A)	<i>Trichoderma reesei</i> QM9414	3AHY
$\beta$ -glucosidase 2 (cyanogenic)	<i>Trifolium repens</i>	1CBG
$\beta$ -glucosidase (Glu1B;TaGlu1b)	<i>Triticum aestivum</i>	2DGA
zeatin $\beta$ -glucosidase (Glu1;p60.1;Zm-p60.1)	<i>Zea mays</i>	1HXJ
$\beta$ -glucosidase 1 (Glu1)	<i>Zea mays</i>	1E1E



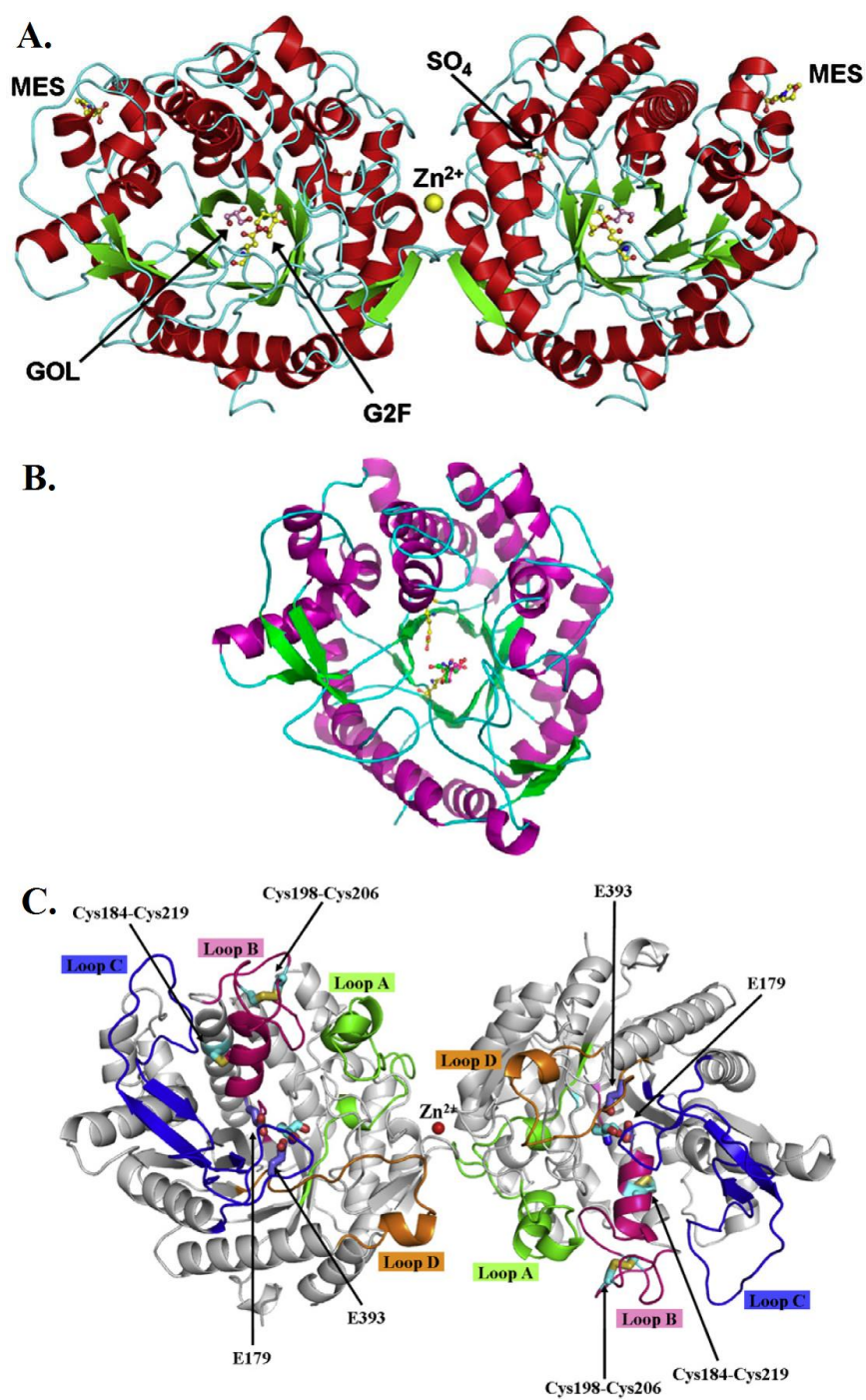


**Figure 2.17** Rice  $\beta$ -glucosidase structures. A. Os3BGlu7 (Chuenchor *et al.*, 2008); B. Os3BGlu6 (Seshadri *et al.*, 2009); and C. Os4BGlu12 (Sansenya *et al.*, 2011).

## 2.8 Rice $\beta$ -mannosidase/ $\beta$ -glucosidase

Forty GH1 genes from rice were identified and 34 of these were found to be likely to encode rice proteins that function as  $\beta$ -glycosidases (Opassiri *et al.*, 2006). The GH1  $\beta$ -glucosidase BGlu1 (systematically named Os3BGlu7) is highly expressed in rice (*Oryza sativa*) flower and germinating shoots (Opassiri *et al.*, 2003). Several rice GH1 enzymes, such as Os3BGlu7, Os4BGlu12 and Os3BGlu6, have been expressed in *Escherichia coli* and characterized, and found to have rather broad glycon specificity (Opassiri *et al.*, 2003, Opassiri *et al.*, 2006, Seshadri *et al.*, 2009). Analysis of the relationship between rice GH1 members and other plant GH1  $\beta$ -mannosidase/ $\beta$ -glucosidase enzymes found that four rice isoenzymes (Os3BGlu7, Os1BGlu1, Os3BGlu8, and Os7BGlu26) are grouped in the same phylogenetic cluster with barley HvBII (*Hordeum vulgare*) (Leah *et al.*, 1995; Hrmova *et al.*, 1996) *Arabidopsis thaliana* BGLU44 (Xu *et al.*, 2004) and tomato  $\beta$ -D-mannosidases (Mo and Bewley, 2002), with which Os7BGlu26 shares 82%, 66% and 66% amino acid sequence identity, respectively (Opassiri *et al.*, 2006; Kuntothom *et al.*, 2009) (Figure 2.18). Recently, rice Os3BGlu8 and Os7BGlu26 were expressed and characterized, and were found to exhibit both  $\beta$ -D-mannosidase and  $\beta$ -D-glucosidase activities at different rates (Kuntothom *et al.*, 2009). The Os3BGlu8 amino acid sequence is most similar to Os3BGlu7, and it hydrolysed 4-nitrophenyl- $\beta$ -D-glucopyranoside (4NPGlc) faster than 4-nitrophenyl- $\beta$ -D-mannopyranoside (4NPMan). On the other hand, the Os7BGlu26 amino acid sequence is very close to that of HvBII, and it hydrolysed 4NPMan faster than 4NPGlc. In the group of plant GH1  $\beta$ -mannosidase/ $\beta$ -glucosidases, only Os3BGlu7 has a known structure. Therefore, the reason why Os3BGlu7 and Os7BGlu26 can catalyze hydrolysis of both mannosides and

glucosides, despite the fact that these sugars have been proposed to go through different shaped transition states, has yet to be explored at the structural level.

Saturation transfer difference nuclear magnetic resonance (STD-NMR) studies showed that HvBII  $\beta$ -D-mannosidase bound 4NP  $\beta$ -D-thiogluco-  
 $^1S_3$  or  $^3S_5$  conformation and 4NP- $\beta$ -D-thiomannoside in a relaxed  $^4C_1$  chair (Kuntothom *et al.*, 2010). Quantum mechanics/molecular mechanics (QM/MM) simulations for Os3BGlu7  $\beta$ -D-glucosidase and HvBII  $\beta$ -D-mannosidase binding indicated their preference to bind  $^1S_3$  skew boat conformations of 4NPGlc, 4NPMAN and 4-nitrophenyl  $\beta$ -D-thiomannoside, and the  $^4C_1$  chair conformation of  $\beta$ -D-thiogluco-  
 in the Michaelis complex. Notably, Kuntothom and colleagues (2010) used a homology model of the HvBII  $\beta$ -D-mannosidase for the QM/MM simulations, due to lack of a GH1  $\beta$ -D-mannosidase structure.

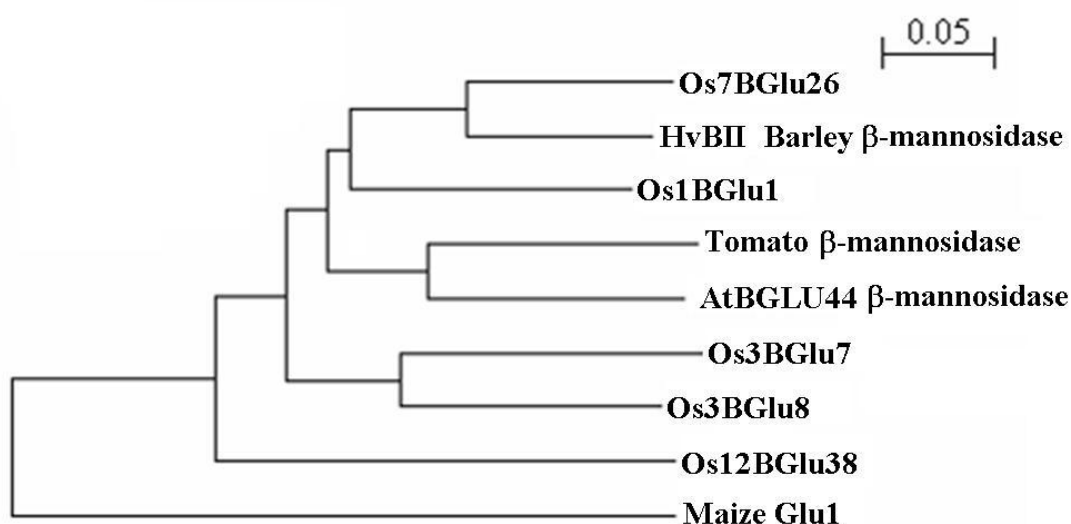


**Figure 2.18** Relationship between rice and other plant GH1  $\beta$ -mannosidase/ $\beta$ -glucosidase enzymes. Maize Glu1 is included as an out group.

## 2.9 Rice Os7BGlu26 $\beta$ -mannosidase

Os7BGlu26 is a member of GH family 1 which is a  $\beta$ -mannosidase/ $\beta$ -glucosidase. Kuntothom and colleagues (2009) characterized the activities of this enzyme, which had the substrate preferences indicated by the relative activities in Table 2.4. Os7BGlu26 prefers to hydrolyze 4NP- $\beta$ -D-mannopyranoside approximately 3-fold more than 4NP- $\beta$ -D-glucopyranoside and is also able to hydrolyze mannooligosaccharides and cellooligosaccharides. For the natural substrate, the Os7BGlu26 also hydrolyzes natural glycoside substrates, such as dhurrin, sambunigrin, D-amgdalin, prunasin, 4-coumaryl alcohol glucoside and quercetin-3-glucoside. From these results, Os7BGlu26 might be involved in cell wall degradation, lignification, secondary metabolite hydrolysis and chemical defense.

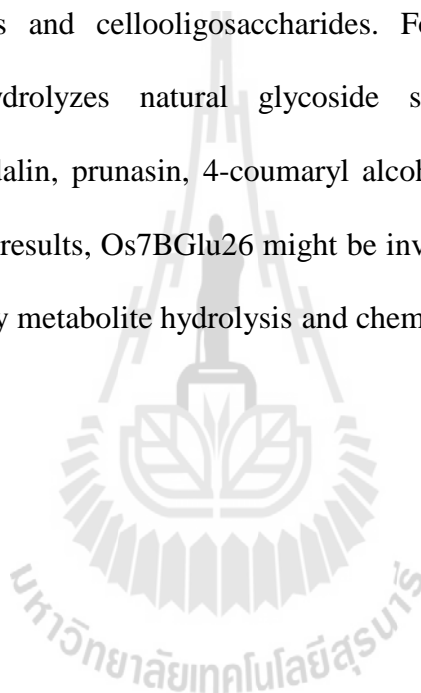


**Table 2.4** Relative rates of hydrolysis of natural and synthetic substrates by rice Os7BGlu26 (Kuntothom *et al.*, 2009).

Substrate	Relative activity percent
4NP- $\beta$ -D-glucopyranoside	100 $\pm$ 4
4NP- $\beta$ -D-mannopyranoside	302 $\pm$ 4
4NP- $\beta$ -D-galactopyranoside	12.6 $\pm$ 1.7
4NP- $\beta$ -D-xylopyranoside	6.4 $\pm$ 1.5
4NP- $\beta$ -D-fucopyranoside	128 $\pm$ 8
4NP- $\beta$ -L-arabinopyranoside	9 $\pm$ 3
Oligosaccharides	
Sophorose [ $\beta$ -(1,2)-linked]	25 $\pm$ 4
Laminaribiose [ $\beta$ -(1,3)]	158 $\pm$ 13
Laminaritriose	23 $\pm$ 5
Cellobiose [ $\beta$ -(1,4)]	21 $\pm$ 5
Cellotriose	124 $\pm$ 18
Cellotetraose	194 $\pm$ 11
Cellopentaose	403 $\pm$ 17
Cellohexaose	472 $\pm$ 12
Mannobiose [ $\beta$ -(1,4)]	+
Mannotriose	+
Mannotetraose	+
Mannopentaose	+
Mannohexaose	+
Natural glucosides	
Dhurrin	+
D-Amygdalin	+
4-Coumaryl alcohol glucoside	+

# CHAPTER III

## MATERIALS AND METHODS

### 3.1 Materials

#### 3.1.1 Plasmid and bacterial strain

The *Os7bglu26* cDNA was previously cloned into the pET32a(+) expression vector to produce an N-terminally thioredoxin, His<sub>6</sub> and S-tagged Os7BGlu26 fusion protein with an enterokinase cleavage site between the fusion tags and Os7BGlu26, as shown in Figure 2.1 (Kuntothom *et al.*, 2009). The *Escherichia coli* strains XL-1 Blue and Rosetta-gami(DE3) were used as bacterial host cells for cloning and recombinant protein expression, respectively.

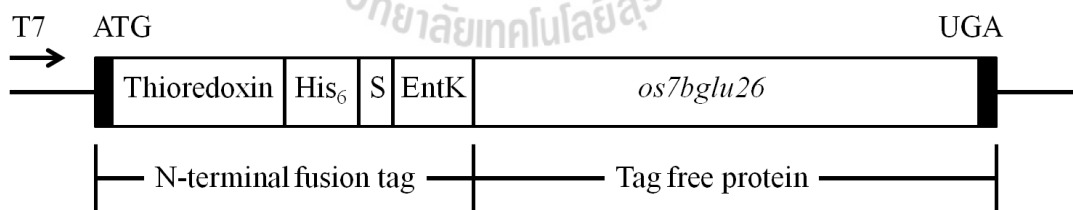


**Figure 3.1** Construct of the protein-coding sequence of recombinant pET32a(+) with the *Os7bglu26* cDNA inserted after the enterokinase cleavage site.

### 3.1.2 Oligonucleotide and mutagenesis primers

All primers used for site-directed mutagenesis are shown in Table 3.1 and were ordered from Bio Basic Inc. (Ontario, Canada), except the E179Q mutant primers and other rice GH1 isoenzyme mutants were ordered from BioDesign Co., Ltd (Pathumthani, Thailand).

**Table 3.1** Oligonucleotide primers for site-directed mutagenesis.

Mutant	Primer name	Sequence	Length (bp)	T <sub>m</sub> (°C)
Os7BGlu26 E179Q	E179Q_f	5'-GAC TGG TTT ACC TTC AAT <u>CAG</u> CCG AGA TGC GTT GCT G-3'	37	72.8
	E179Q_r	5'-CAG CAA CGC ATC TCG GCT GAT TGA AGG TAA ACC AGT C-3'	37	72.8
Os7BGlu26 Y134W	Y134W_f	5'-GCA AAC CTC TAC CAC <u>TGG</u> GAC CTA CCA TTA GCA C-3'	34	83.4
	Y134W_r	5'-GTG CTA ATG GTA GGT CCC AGT GGT AGA GGT TTG C-3'	34	83.4
Os7BGlu26 Y134F	Y134F_f	5'-CGC AAA CCT CTA CCA <u>CTT</u> TGA CCT ACC ATT AGC AC-3'	35	82.1
	Y134F_r	5'-GTG CTA ATG GTA GGT CAA AGT GGT AGA GGT TTG CG-3'	35	82.1
Os7BGlu26 C182T	C182T_f	5'-CTT CAA TGA GCC GAG <u>AAC</u> CGT TGC TGC TCT AGG-3'	33	83.4
	C182T_r	5'-CCT AGA GCA ACG GTT CTC GGC TCA TTG AAG-3'	33	83.4

**Table 3.1** Oligonucleotide primers for site-directed mutagenesis (Cont.).

Mutant	Primer name	Sequence	Length (bp)	T <sub>m</sub> (°C)
Os7BGlu26 E179D	E179D_f	5'-GGT TTA CCT TCA ATG ATC CGA GAT GCG TTG CTG-3'	33	81.0
	E179D_r	5'-CAG CAA CGCATC TCG GAT CAT TGA AGG TAA ACC-3'	33	81.0
Os7BGlu26 E389Q	E389Q_f	5'-CCC TAC AAT GAT CCT TTC TCA GAA TGG TAT GGA CCA ACC TGG-3'	42	85.0
	E389Q_r	5'-CCA GGT TGG TCC ATA CCA TTC TGA GAA AGG ATC ATT GTA GGG-3'	42	85.0
Os7BGlu26 C182A	C182A_f	5'-CTT CAA TGA GCC GAG AGC CGT TGC TGC TCT AGG-3'	33	84.7
	C182A_r	5'-CCT AGA GCA GCA ACG GCT CTC GGC TCA TTG AAG -3'	33	84.7
Os7BGlu26 E179A	E179A_f	5'-CTG GTT TAC CTT CAA TGC GCC GAG ATG CGT TGC TG-3'	35	84.5
	E179A_r	5'-CAG CAA CGC ATC TCG GCG CAT TGA AGG TAA ACC AG-3'	35	84.5

## 3.2 General methods

### 3.2.1 Competent cell preparation

The bacteria (*E. coli* strains XL-1 Blue and Rosetta-gami(DE3)) were grown in 3 ml Lennox broth (LB, 10 g/l peptone, 5 g/l yeast extract, 5 g/l sodium chloride) at 37 °C, 200 rpm for 16 – 18 h as starter, then 1 ml starter was inoculated to 100 ml LB and cultured at 37 °C, 200 rpm until the OD<sub>600</sub> reached 0.3 - 0.4. The cell pellet was collected by centrifugation at 2500 rpm, 10 min, 4 °C. The pellet was resuspended in 10 ml of cold 0.1 M CaCl<sub>2</sub>, gently mixed and stored on ice for 20 min. The cell suspension was centrifuged at 2500 rpm, 10 min, 4 °C, the supernatant discarded, and 2 ml of cold 0.1 M CaCl<sub>2</sub> added, after which the cells were kept on ice for 1 h. Then, 300 µl glycerol was added, and the cell suspension was mixed very well and aliquoted into microcentrifuge tubes with 50 µl per tube. The tubes of competent cells were used immediately or kept at -80 °C.

### 3.2.2 Bacterial transformation

Fifty nanograms plasmid DNA was added into 50 µl competent *E. coli* cells then gently mixed. The competent cells were incubated on ice for 30 min. The cells were heat shocked at 42 °C 45 s, then immediately incubated on ice for 2-3 min. Then, 500 µl LB was added to the cells and incubated at 37 °C for 1 h. The 100 µl cell mixture was spread on an LB agar plate containing appropriate antibiotics, depending on the bacterial host and plasmid, in incubated at 37 °C overnight.

### 3.2.3 Site-directed mutagenesis

The mutations E179Q, Y134W, Y134F, C182T, E179A, C182A, Y134W/C182T and Y134W/C182A of the rice *Os7bglu26* cDNA were constructed. The primers used are shown in Table 2.1 and the presence of all desired mutations and

lack of undesired mutations were confirmed by DNA sequencing (Macrogen, Seoul, Korea). The QuikChange® Site-Directed Mutagenesis Kit (Stratagene, La Jolla, CA, USA) was used to generate the Os7BGlu26 mutations. The pET32a/Os7bglu26 plasmid was used as a template for a full-length plasmid strand amplification from two complementary oligonucleotide primers containing the desired mutation point (Table 2.1). *Pfu* DNA polymerase (with proofreading activity) was used to synthesize the mutated plasmid DNA during the temperature cycling, which included step 1, 95 °C 30 s; step 2, 95 °C 30 s; step 3, 55 °C 1 min and step 4, 68 °C 15 min, with steps 2 to 4 repeated for 17 cycles. The PCR products were treated with *DpnI* endonuclease for 3 h at 37 °C to eliminate methylated and hemimethylated DNA of the parental DNA template. Repair of the nicked circular dsDNA products was accomplished by transforming the DNA into competent XL-1 Blue cells. The transformants were selected on agar plates containing ampicillin. All mutations were confirmed by DNA sequencing (Macrogen). The mutagenic oligonucleotide primers used for the kit were specifically designed according to the criteria of the QuikChange® manual to have lengths of 25-45 bases with  $T_m \geq 78$  °C. The  $T_m$  was calculated from following formula:  $T_m = 81.5 + 0.41 (\%GC) - 675/N - \% \text{ mismatch}$ , where N is the primer length in bases, and %GC and % mismatch are whole numbers

#### **3.2.4 Plasmid extraction by alkaline lysis**

The *E. coli* containing plasmid were grown on LB broth for 18 h at 37 °C. The cells were pelleted in sterile microcentrifuge tubes, and each pellet was resuspended with 100 µl of lysis buffer (0.05 M Tris-HCl, pH 8.0, 0.01 M EDTA, and 0.05 M glucose) by vortexing. Two hundred microliters of fresh 1% SDS/0.2 M NaOH solution were added into the resuspended solution and gently mixed by

inverting. Then, 150  $\mu$ l of cold 3 M potassium acetate, pH 4.8, was added and mixed in by inverting briefly. The cell lysate was incubated on ice for 3-5 min. The mixture was centrifuged at 12,000 rpm, 4 °C for 5 min. The supernatant was transferred into a new sterile microcentrifuge tube and 600  $\mu$ l absolute ethanol was added to precipitate the DNA at 4 °C for 10 min. The precipitated DNA was centrifuged at 12,000 rpm, 4 °C for 5 min. The DNA pellet was washed with 500  $\mu$ l of 70% ethanol and centrifuged at 12,000 rpm, 4 °C for 5 min. All the solution was removed by pipetting and the DNA was dried by incubating it at 37 °C for 10 min. The pellet was dissolved with 100  $\mu$ l of TE buffer (10 mM Tris-HCl, 1 mM EDTA, pH 8.0) containing 20  $\mu$ g/ml RNase A and incubated at 37 °C for 10 min. The plasmid DNA was precipitated with 70  $\mu$ l 20% (w/v) PEG 6000/2.5 M NaCl solution and incubated on ice for 1 h. Then, the precipitated plasmid was centrifuged at 12,000 rpm, 4 °C for 5 min. The pellet was washed with 500  $\mu$ l 70% ethanol and centrifuged at 12,000 rpm, 4 °C for 5 min. The DNA was dried as described above and dissolved with 20  $\mu$ l TE buffer.

### 3.2.5 SDS-PAGE

Polyacrylamide gel electrophoresis in the presence of sodium dodecyl sulfate (SDS-PAGE) was performed as described by Laemmli (1970) using 13% T polyacrylamide separating gels. The separating gel was prepared by mixing 3.3 ml distilled water, 2.5 ml 1.5 M Tris-HCl, pH 8.8, 4 ml 30% acrylamide /bisacrylamide solution, 100  $\mu$ l 10% (w/v) SDS, 100  $\mu$ l 10% (w/v) ammonium persulfate, and 4  $\mu$ l TEMED. The 5% stacking gel was prepared by mixing 3.4 ml distilled water, 0.63 ml 0.5 M Tris-HCl, pH 6.8, 0.83 ml 30% acrylamide /bisacrylamide solution, 50  $\mu$ l 10% (w/v) SDS, 50  $\mu$ l 10% (w/v) ammonium persulfate, and 5  $\mu$ l of TEMED. The protein sample was mixed with loading dye (2.5 M Tris-HCl, pH 6.8, 10% (w/v) SDS, 50%

(v/v) glycerol, 0.5% (w/v) bromophenol blue, 4% (v/v) 2-mercaptoethanol) and boiled at 100 °C for 5 min. The protein was loaded onto the gel under running buffer (25 mM Tris-HCl, 192 mM glycine, 0.1% SDS, pH 7.5) and placed in an electric field at 150 volts. The protein bands were detected by staining with Coomassie brilliant blue solution (0.1% (w/v) Coomassie brilliant blue R-250, 40% (v/v) methanol, 10% (v/v) glacial acetic acid, 50% (v/v) distilled water) and the blue background was washed out with destaining solution (40% (v/v) methanol, 10% (v/v) glacial acetic acid, 50% (v/v) distilled water). Phosphorylase B (97 kDa), bovine serum albumin (66 kDa), chicken ovalbumin (45 kDa), carbonic anhydrase (30 kDa), trypsin inhibitor (20 kDa), and  $\alpha$ -lactalbumin (14.4 kDa) were used as standard proteins.

### 3.3 Optimization of conditions for protein expression

The pET32a/Os7BGlu26 plasmid, which includes the *Os7BGlu26* cDNA in frame to produce an N-terminally thioredoxin and His-tagged Os7BGlu26 fusion protein (Kuntothom *et al.*, 2009), was transformed into *E. coli* strain Rosetta-gami(DE3) cells. The cells were cultured in low salt LB (Lennox) media containing 50  $\mu$ g/ml ampicillin, 15  $\mu$ g/ml kanamycin, 12.5  $\mu$ g/ml tetracyclin and 34  $\mu$ g/ml chloramphenicol at 37 °C. When the culture optical density at 600 nm reached 0.4-0.5, protein expression was induced by addition of IPTG. The concentration of IPTG and induction time were varied, and the induction temperature set at 20 °C. Cell pellets were collected by centrifugation and suspended in the extraction buffer (50 mM Tris-HCl, pH 8.0, 150 mM sodium chloride, 200  $\mu$ g/ml lysozyme, 1% (v/v) Triton-X 100 mM, 1 mM PMSF, 4  $\mu$ g/ml DNase I) at approximately 25 °C, 30 min. Centrifugation

removed insoluble debris, and the soluble protein was checked on SDS-PAGE and  $\beta$ -glucosidase activity measured.

### 3.4 Protein purification

The cell pellets were collected by centrifugation and suspended in the extraction buffer (50 mM Tris-HCl, pH 8.0, 150 mM sodium chloride, 200  $\mu$ g/ml lysozyme, 1% (v/v) Triton-X, 100 mM, 1 mM PMSF, 4  $\mu$ g/ml DNase I) at approximately 25 °C, 30 min. Centrifugation removed insoluble debris, and the protein was purified from the soluble extract by Immobilized Metal-Affinity Chromatography (IMAC) on cobalt-equilibrated IMAC resin (GE Healthcare, Uppsala, Sweden). The resin was washed with the equilibration buffer (150 mM NaCl, 50 mM Tris-HCl, pH 8.0), followed by 20 mM imidazole in the equilibration buffer, and eluted with 250 mM imidazole in the equilibration buffer. The fractions of Os7BGlu26 containing  $\beta$ -glucosidase activity, as judged by 4NPGlc hydrolysis, were pooled and imidazole removed by dialysis in 150 mM NaCl, 20 mM Tris-HCl buffer, pH 8.0. The dialyzed preparation was concentrated in a 30 kDa molecular mass cut off (MWCO) Centricon centrifugal filter (Millipore, Billerica, MA, USA). The N-terminal fusion tag was removed from the Os7BGlu26 fusion protein by cleavage with 2 ng enterokinase (New England Biolabs, Cambridge, MA, USA) per 1 mg of fusion protein at 23 °C for 18 h, followed by a second round of IMAC. The flow-through fractions containing  $\beta$ -glucosidase activity were pooled and the protein purity was analyzed by SDS-PAGE. The Os7BGlu26 was dialyzed and concentrated with a 30 kDa MWCO Centricon filter to obtain approximately 6 mg/ml of Os7BGlu26 protein in 150 mM NaCl, 20 mM Tris-HCl buffer, pH 8.0.

All the Os7BGlu26 mutants, E179Q, Y134W, Y134F, C182T, E179A, C182A, Y134W/C182T and Y134W/C182A, were expressed and purified in the same manner as the native protein.

## **3.5 Protein crystallization**

### **3.5.1 Screening and optimization of Os7BGlu26 crystallization**

Before crystallization, purified Os7BGlu26 was filtered through an Ultrafree-M 0.22  $\mu\text{m}$  filter (Millipore) (4,000 rpm, 4  $^{\circ}\text{C}$ , 5 min) and used to screen for crystallization conditions by the microbatch under the oil method at 15  $^{\circ}\text{C}$  with precipitants from the Crystals Screen HT screening kits (Hampton Research). The conditions for native crystals were optimized by varying the pH, salt concentration, buffer and protein concentration in hanging drop vapor diffusion trials. The crystals were soaked in the cryoprotectant for 5 min before flash freezing in liquid nitrogen.

### **3.5.2 Os7BGlu26 crystallization by hanging drop vapor diffusion**

The purified protein that was concentrated by Centricon centrifugal filter to 10 mg/mL, while changing the buffer to 20 mM Tris-HCl, pH 8.0, 150 mM NaCl. Before crystallization, the protein solution was filtered through an Ultrafree-M 0.22  $\mu\text{m}$  filter (Millipore) at 4,000 rpm for 5 min. The Os7BGlu26 protein was crystallized by the hanging drop vapor diffusion method with microseeding. The preliminary Os7BGlu26 crystals were broken and diluted with precipitant solution for use as seed stock. The Os7BGlu26 seeds were seeded into pre-equilibrated drops for 3 h at 15  $^{\circ}\text{C}$ . The crystallized plate was incubated at 15  $^{\circ}\text{C}$  and the development of the crystals was checked under a microscope. After screening of the crystallization conditions, the crystals were grown in 0.8 M K,Na tartrate, 0.1 M Na HEPES, pH 7.5. Conditions for

crystallization were optimized from the conditions identified from screening by varying the salt and protein concentration and buffer pH. A drop of 2  $\mu$ l of pure protein was mixed with 1  $\mu$ l of precipitant solution on a siliconized cover slip and the drop was equilibrated against a reservoir containing 0.5 ml of precipitant solution. Prior to data collection, the crystals were soaked in cryoprotectant containing glycerol with and without 400 mM D-mannose, 50 mM mannoimidazole, 50 mM glucoimidazole, or 50 mM isofagomine. The crystals were flash vitrified by putting them in a nylon loop and dipping them in liquid nitrogen, then the loop was put in a cryocap capsule (Hampton Research) and kept at liquid nitrogen temperature.

### 3.6 Data collection and processing

The X-ray data for Os7BGlu26 and Os3BGlu7 were collected at the BL13B1 beamline at the National Synchrotron Radiation Research Center (NSRRC), Hsinchu, Taiwan, with a 1.0 Å wavelength X-ray beam and an ADSC Quantum 315 CCD detector. The crystals were maintained at 110 K in a cold stream of nitrogen throughout data collection. The mounted crystal was translated and rotated using the goniometer head to center the crystal in the X-ray beam. During X-ray diffraction, data frames were collected over 0.5° oscillations, and an exposure time of 5-15 s per frame for 180° rotation or until the data collection were complete. The distance between the crystal and the detector was in the range of 160-300 mm, depending on the highest resolution of the data and spot overlap. All data sets were indexed, integrated, and scaled with the HKL-2000 package (Otwinowski and Minor, 1997). The maximum resolution for each data set was determined by choosing the outer shell that gave a ratio of measured intensity to its standard deviation ( $I/\sigma(I)$ ) >2-fold.

Moreover, the completeness, redundancy, and linear residual factor after merging (linear  $R_{\text{merge}}$ ) were considered for evaluating the resolution of the data set. The cut off for the linear  $R_{\text{merge}}$  was  $\leq 0.5$  in the outer shell, but was kept  $< 0.4$  if the redundancy was low.

### 3.7 Structure refinement

The native structure was solved by molecular replacement with the rice Os3BGlu7  $\beta$ -glucosidase structure (PDB code 2RGL) as a search model and the *MOLREP* program (Vagin and Teplyakov, 1997) in the *CCP4* suite of programs (Winn et al., 2011), followed by refinement with *REFMAC5* (Murshudov et al., 1999). For the complex structures, the structures were solved by rigid body refinement of the native structure in *REFMAC5*. Model building was performed with the *COOT* program (Emsley et al., 2004). The quality of the final model was assessed with *PROCHECK* (Laskowsky et al., 1993) and *MOLPROBITY* (Chen et al., 2010). Representation graphics of structures was generated in *PyMol* (Schrödinger LLC). Cremer–Pople analysis of sugar puckering to identify the ring form (Cremer and Pople, 1975) was done via the Cremer–Pople calculator website of Prof. Shinya Fushinobu (University of Tokyo, <http://www.ric.hi-ho.ne.jp/asfushi/>).

### 3.8 Docking analysis

The 4NPMAN and 4NPGlc ligands were docked into the active site of Os7Glu26 with a Lamarckian genetic search algorithm, as implemented in the *Autodock 4.2* program (Morris et al., 2009). The ligands were docked into four different conformations ( $^1S_3$ ,  $^1S_5$ ,  $^2S_0$ ,  $^3S_1$ ), which are representative of the different catalytic

itineraries followed by glycoside hydrolases (Vocadlo and Davies, 2008). Ligand conformations were constructed manually by adding the 4NP portion to the corresponding sugar conformation obtained from previous works (Biarnés *et al.*, 2007; Adrèvol *et al.*, 2010). All ligands were geometry optimized using Density Functional Theory and the *CPMD* software package (IBM Corporation). A restraint on the sugar ring was added to maintain the desired conformation. All calculations were performed on the Os7BGlu26 enzyme excluding all crystallographic water molecules. Protonation states for histidine residues were assigned based on the hydrogen bond environment and Glu179 was modeled as protonated because of its role as an acid/base residue. Gasteiger charges were assigned to the protein and ligand atoms using *AutoDock tools*. One hundred *AutoDock* runs were performed for each one of the substrates tested to calculate the binding energy, holding the enzyme but not the ligands fixed. A grid with dimensions 40 x 40 x 40 (Å)<sup>3</sup> centered on the catalytic residues acid/base (Glu179) and nucleophile (Glu389) was used.

### 3.9 Enzyme kinetics

#### 3.9.1 Kinetic parameter analysis

The kinetic parameters of the enzymes with the 4NPGlc and 4NPMan substrates were determined from triplicate assays containing 0.05 - 18.5 µg enzyme, substrates at concentrations from 0.01 to 30 mM, and 1 µg/µl BSA in 50 mM sodium acetate buffer, pH 5.0, in a total volume of 140 µl, at 30 °C for reaction intervals that had linear initial velocities (pseudo-first order rate or  $V_0$ ). The substrate concentration were varied over the range between 0.3 to  $3K_m$ . Reactions were stopped by alkalization with 70 µl of 0.4 M sodium carbonate and the absorbance at 405 nm

was read and compared to a 4-nitrophenolate standard curve in the same buffer. The kinetic parameters were calculated by nonlinear regression of the Michaelis-Menten plots with *GraFit 5.0* (Erithacus Software, Horley, Surrey, UK). The Gibbs free energy change for transition state binding was calculated as:

$$\Delta\Delta G_{S^*mut} = -RT[\ln(k_{cat}/K_m)_{mutant} - \ln(k_{cat}/K_m)_{wildtype}] \text{ (Fersht } et al., 1987).$$

### 3.9.2 HEPES inhibition

The inhibition constant ( $K_i$ ) of Os7BGlu26 for inhibition by HEPES was determined at 30 °C by incubating 2 µg enzyme in 50 mM sodium acetate buffer, pH 5.0, containing 1 µg/µl BSA, and with 0-300 mM HEPES for 10 minutes. The residual enzyme activities were monitored at 405 nm in assays of activity against 0.1, 0.5, 1.0 and 1.5 mM 4NPMAN. Inhibition constants,  $K_i$ , were calculated by linear regression of a plot of the apparent  $K_m/V_{max}$  values (slopes of Lineweaver-Burk plots) *versus* inhibitor concentrations.

### 3.9.3 Time course of 2,4-dNP (2,4-dinitrophenol) release from covalent inhibitors

The release of 2,4-dNP from 2,4-dNPM2F (2,4-dinitrophenyl 2-deoxy-2-fluoro-β-D-mannoside) or 2,4-dNPG2F (2,4-dinitrophenyl 2-deoxy-2-fluoro-β-D-glucoside) as the substrate for Os7BGlu26 was determined. Os7BGlu26 (10 µg) was mixed with 50 mM MES buffer, pH 5.0, 100 µg BSA and 1 mM 2,4-dNPM2F or 2,4-dNPG2F in 100 µl. The released 2,4-dNP was monitored at 405 nm every 30 s.

### 3.9.4 Profile of activity versus pH

The pH dependence of the enzyme activity was determined with 1 mM 4NPMAN as substrate. The pH profile was determined by incubating 0.5 µg enzyme in universal pH buffer (solution A: 0.2 M boric acid + 0.05 M citric acid, solution B:

0.05 M tri-sodium phosphate, with pH ranging from 3-9) and with 50 mM sodium azide in 140  $\mu$ l total volume at 30 °C for 30 min and the reactions were stopped by adding 70  $\mu$ l of 0.4 M NaCO<sub>3</sub>. The enzyme activity (4NP released) was monitored at 405 nm.

### **3.9.5 Effect of anionic nucleophiles in rescue of acid/base mutant activity**

Various anionic nucleophiles, including acetate, azide, ascorbate, formate, trifluoroacetate (TFA), and fluoride (KF), were tested for their effects on the enzyme activity of Os7BGlu26 E179Q. This mutant was assayed in 50 mM anionic nucleophile in 50 mM MES buffer, pH 5.0, and 1 mM 4NPGlc or 1 mM 4NPMAN as a substrate at 30 °C for 30 min and the reactions were stopped by adding 70  $\mu$ l of 0.4 M NaCO<sub>3</sub>. The enzyme activity (4NP released) was monitored at 405 nm.

### **3.9.6 Effect of azide concentration on the activity of the Os7BGlu26 E179Q mutant**

The dependence of Os7BGlu26 E179Q enzyme activity on azide concentration was determined with 4NPMAN and 4NPGlc. A concentration range of 25 - 1600 mM azide was tested for its effect on the activity of 0.5  $\mu$ g Os7BGlu26 E179Q hydrolysis of 1 mM 4NPMAN or 4NPGlc in 50 mM MES buffer, pH 5.0 at 30°C for 30 min and the reactions were stopped by adding 70  $\mu$ l of 0.4 M NaCO<sub>3</sub>. The enzyme activity (4NP released) was monitored at 405 nm.

## **3.10 Transition state studies**

### **3.10.1 Transition state analogue inhibition**

The constants for inhibition of Os7BGlu26, Os3BGlu7 and rHvBII by mannoimidazole, glucoimidazole, isofagomine, phenethylglucoimidazole,

glucotetrazole, deoxynojirimycin, deoxymannojirimycin and nojirimycin sulfate were determined. The inhibition constant ( $K_i$ ) of Os7BGlu26 was determined at 30 °C by incubating 0.5 µg enzyme in 50 mM sodium acetate buffer, pH 5.0, containing 1 µg/µl BSA, and with inhibitor for 10 minutes. The residual enzyme activities were monitored by assaying activity against 1.0 mM 4NPMAN at 30 °C for 25 min. For Os3BGlu7, 0.2 µg enzyme was used, and the residual enzyme activities were monitored by assaying activity against 0.2 mM 4NPGlc at 30 °C for 15 min. For rHvBII, 0.5 µg enzyme was used, and the residual enzyme activities were monitored by assaying activity against 0.5 mM 4NPMAN at 30 °C for 45 min. The residual activity of each enzyme was measured as 4NP released per min, monitored at 405 nm after alkalization of the assay solution with sodium carbonate. Each inhibitor was tested in triplicate, at least six concentrations that were 0.5 - 2 or 3 times the  $K_i$ . The inhibition constants,  $K_i$ , were determined by the Dixon plot of inhibitor concentrations *versus*  $1/V$  values (Dixon, 1953). Inhibition constants  $K_i$  were calculated by linear regression analysis with *GraFit* 5.0.

### 3.10.2 Slow onset inhibition

Slow onset inhibition was determined with 4NPMAN as the substrate for Os7BGlu26. Enzyme was incubated inhibitor with transition state analogue for 0 min, 10 min or 2 h in 50 mM acetate buffer pH 6.5 at 25 °C. Then, 4NPMAN was added to the enzyme/inhibitor solution to 1 mM final concentration. The released 4NP was monitored at 405 nm 30 s thereafter.

## CHAPTER IV

### RESULTS AND DISCUSSION

#### 4.1 Os7BGlu26 expression and purification

The *Os7bglu26* cDNA was previously cloned into the pET32a(+) expression vector to produce an N-terminally thioredoxin, His<sub>6</sub> and S-tagged Os7BGlu26 fusion protein with an enterokinase cleavage site before the start of the Os7BGlu26 sequence, as shown in Figure 2.1 (Kuntothom *et al.*, 2009). In that previous report, the protein was expressed in *Escherichia coli* strain Origami(DE3), which provided only low amounts of protein for enzymatic characterization. To improve protein expression in the current work, the *Escherichia coli* strain Rosetta-gami(DE3) was used as the bacterial host for recombinant protein expression, since this strain enhances expression of eukaryotic proteins from genes that contain codons rarely used in *E. coli*. The expression of Os7BGlu26 His-tagged fusion protein in *E. coli* strain Rosetta-gami(DE3) was optimized by varying the IPTG concentration and induction time. The fusion protein was highly expressed in the conditions of 0.3 mM IPTG and 24 h induction time, as shown in Figures 4.1 and 4.2.

Os7BGlu26 was purified by immobilized metal affinity chromatography (IMAC). The 66 kDa thioredoxin and His-tagged Os7BGlu26 fusion protein fractions contained many contaminant protein bands after the 1<sup>st</sup> IMAC column. It was then cleaved by enterokinase, and the 50 kDa tag-free protein was further purified by a 2<sup>nd</sup> round of IMAC. The purity of the protein increased to approximately 90% (Figure 4.3).

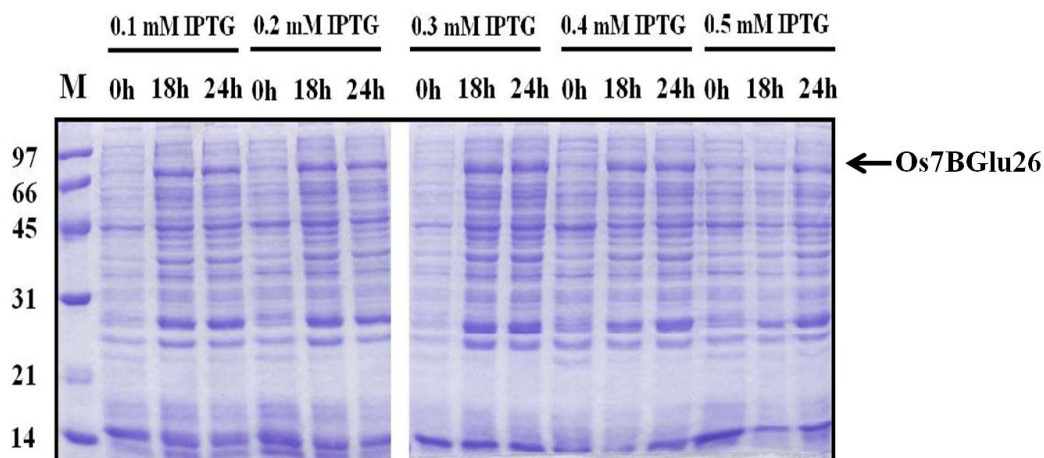


**Figure 4.1** SDS-PAGE of Os7BGlu26 expressed in different conditions. The pattern of protein expressed in *E. coli* strain Rosetta-gami(DE3) after induction with different concentrations of IPTG for 0, 18 or 24 h at 20 °C.

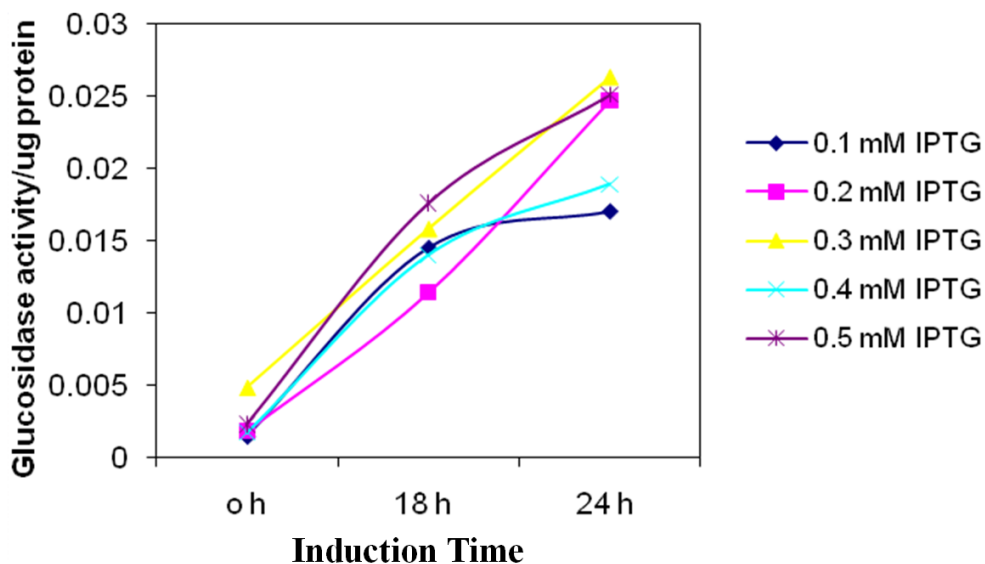


**Figure 4.2** The  $\beta$ -glucosidase activity of expressed protein in crude *E. coli* strain Rosetta-gami(DE3) extracts after induction with different concentrations of IPTG.

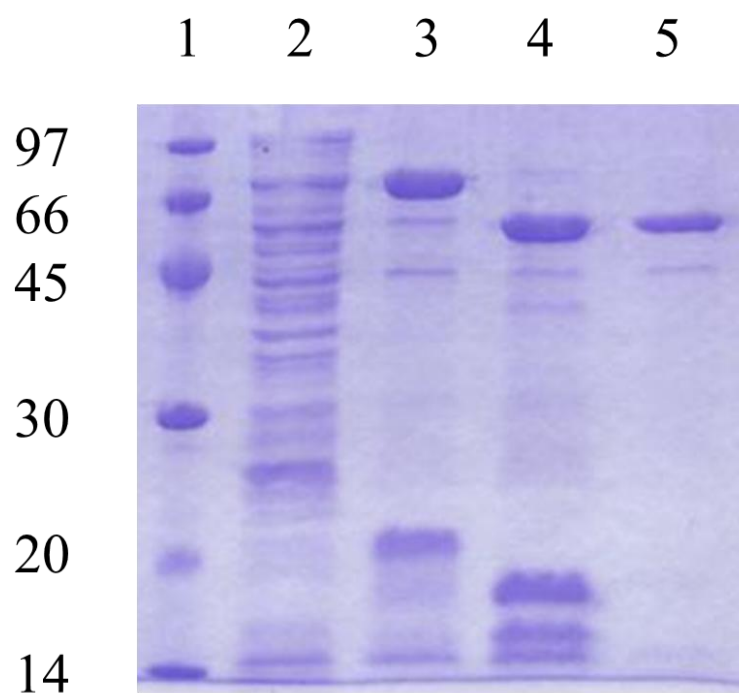


**Figure 4.3** SDS-PAGE of Os7BGlu26 throughout purification. Lane 1, Bio-Rad low molecular-mass markers (masses shown at left in kDa); Lane 2, crude extract of soluble proteins from *E. coli* strain Rosetta-gami(DE3); Lane 3, the N-terminal thioredoxin/His<sub>6</sub>-tagged Os7BGlu26 fusion protein after the first IMAC step; Lane 4, the products of digestion of the thioredoxin/His<sub>6</sub>-tagged Os7BGlu26 protein by enterokinase; Lane 5, purified Os7BGlu26 after the second IMAC step.

## 4.2 Os7BGlu26 crystallization

The purified Os7BGlu26 protein was screened for crystallization, and Os7BGlu26 crystals with dimensions of 90 x 20 x 20  $\mu\text{m}$  were observed within one week in microbatch with the Hampton Research Crystal Screen HT screening kit precipitant solution number C5 of 0.8 M K,Na tartrate, 0.1 M Na HEPES, pH 7.5. When the pH and salt concentrations of the precipitant were optimized in hanging-drop vapor diffusion, a single crystal with dimensions of 160 x 25 x 25  $\mu\text{m}$  was obtained within 5 days in 0.58 M K,Na tartrate, 0.1 M Na HEPES, pH 7.25 (Figure 4.4).

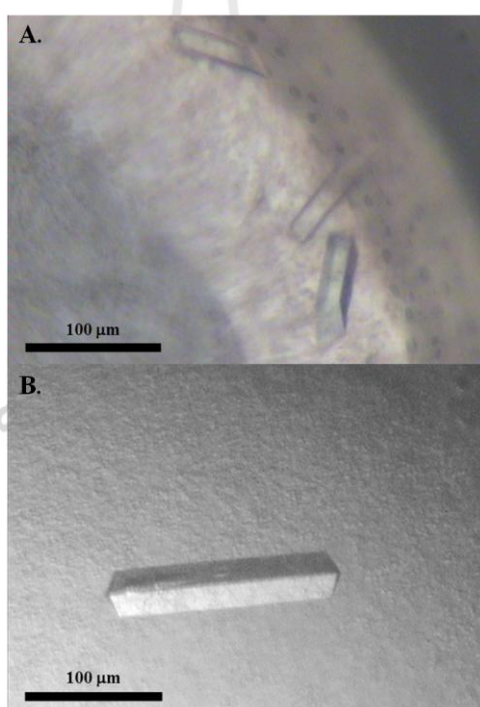


**Figure 4.4** The initial Os7BGlu26 crystals. (A), Crystals in 0.1 M sodium HEPES, pH 7.5, containing 0.8 M Na,K tartrate grown with the microbatch technique. (B.), A crystal grown after optimization in a hanging-drop with 0.1 M sodium HEPES, pH 7.25, containing 0.58 M Na,K tartrate.

### 4.3 Os7BGlu26 structure and model quality

The apo Os7BGlu26 crystal diffracted X-rays to 2.20 Å resolution, and belonged to the orthorhombic  $P2_12_12_1$  space group. Its unit-cell parameters were  $a = 68.1$  Å,  $b = 71.7$  Å,  $c = 136.7$  Å. Diffraction of the crystal soaked in D-mannose gave an isomorphous dataset that was processed to 2.45 Å resolution and had the unit cell parameters of  $a = 68.0$  Å,  $b = 73.6$  Å,  $c = 134.0$  Å. The data collection statistics for both crystals are summarized in Table 4.1. The asymmetric units of both crystals were estimated to contain one molecule, with a Matthews coefficient ( $V_M$ ) of  $3.03$  Å<sup>3</sup> Da<sup>-1</sup> (Matthews, 1968) and a solvent content of 59.5% for the apo Os7BGlu26 crystal, and a  $V_M$  of  $3.05$  Å<sup>3</sup> Da<sup>-1</sup> and a solvent content of 59.7% for the D-mannose-soaked crystal.

The structure of Os7BGlu26 is a classic TIM ( $\beta/\alpha$ )<sub>8</sub>-barrel fold, similar to other GH1 enzymes (Figure 4.5A). The structure placed the highly conserved E179 and E389 residues at the C-terminal ends of  $\beta$ -strands 4 and 7, respectively. These residues are positioned at the bottom of the active site cleft, as observed for the catalytic acid/base and nucleophile residues in other members of GH clan A (Jenkins *et al.*, 1995; Henrissat *et al.*, 1995). Furthermore, nucleophilic rescue of mutants of the corresponding residues confirmed they are the catalytic residues in the closely related Os3BGlu7  $\beta$ -D-glucosidase (Hommalai *et al.*, 2007; Chuenchor *et al.*, 2011). The four variable loops that have been reported to account for much of GH1 structural and functional diversity (Sanz-Aparicio *et al.*, 1998) connect the  $\beta$ -strands and  $\alpha$ -helices at the carboxy-terminal side of the core barrel structure. These loops are: loop A (A28-D68), loop B (E179-T209), loop C (H317-P366) and loop D (N390-D406) (Figure 4.5A and 4.6). Although, no electron density was observed for the 14-residues from

the N-terminal fusion tag (A-M-A-D-I-T-S-L-Y-K-K-A-G-S-A) and the five C-terminal residues (S-K-K-R-N), five amino acid residues of the fusion protein linker region (A-A-P-F-T) and residues 1-478 of the mature Os7BGlu26 gave clear electron density for the structure. Two cis-peptide bonds were found between A194 and P195, and between W436 and S437, as seen in other plant GH1 enzymes (Barrett *et al.*, 1995). The conserved disulfide bond found in nearly all plant GH1 enzymes was present on loop B between C198 and C201. The conserved active site W, W444, fell in the outlier region of the Ramachandran plot, while it is found in a similar outlier or borderline region in other GH1 enzymes (Czjzek *et al.*, 2000; Chuenchor *et al.*, 2008). Other Ramachandran statistics were similar to other plant GH1 structures, in that of the amino acid residues in this structure, 88.5% fell in the most favored region whereas 87.8%, 88.5%, 88.0% and 89.0% were found in this region in cyanogenic beta-glucosidase from white clover (1CBG), myrosinase (1MYR), wheat beta-glucosidase (2DGA) and rice BGlu1(2RGL), respectively.

Figure 4.5B shows that a glycerol molecule, originating from the cryoprotectant, was bound in the active site. This molecule hydrogen bonded to Q32, Y318, E389, E443 and two water molecules, which also interacted with H133, W444, and the catalytic residues E179 and E389. The distance between the C $\delta$  carbons of the catalytic acid/base, E179, and nucleophile, E389, was 4.9 Å, consistent with the distance expected for the retaining mechanism of glycoside hydrolases, although on the lower end of the range (Rye and Withers, 2000). The carboxyl oxygen of E179 acid/base residue had a close contact of 2.7 Å with the Y134 hydroxyl. In addition, the conserved W436 and F452 residues at the -1 subsite provided an aromatic platform for sugar binding and the additional hydrophobic interactions with the substrate,

respectively (Figure 4.5B and 4.5C), as noted for other GH1 enzymes (Czjzek *et al.*, 2000). A HEPES molecule from the crystallization buffer was found in the substrate binding cleft at the +1, +2 and +3 subsites, which were defined for binding of  $\beta$ -(1,4)-linked D-glucosyl residues in Os3BGlu7 (Chuenchor *et al.*, 2011). The HEPES molecule was most favorably modeled in two alternate conformations, both of which hydrogen bonded to E179 and Y360 (Figure 4.5C). HEPES was found to bind to Os7BGlu26 with a non-competitive inhibition constant  $K_i$  of 81.4 mM and  $\Delta G$  -6.3 kJ mol<sup>-1</sup> (Figure 4.7). The combined occupancy of the two alternate HEPES molecules was constrained to be 1.0 in the refinement. This artificial full occupancy is reflected by higher temperature factors ( $B = 28.9$  to 46.4 for the individual HEPES atoms) (Table 4.2).

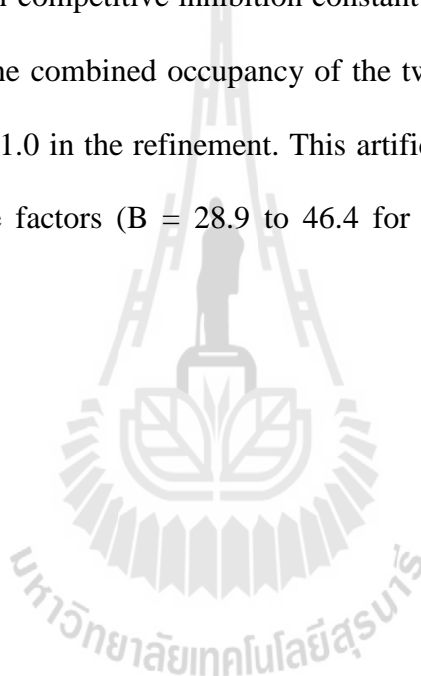


**Table 4.1** Data-collection statistics of native Os7BGlu26 and its mannose complex.

Values in parentheses are for the outer shell.

	Native Os7BGlu26	Os7BGlu26/mannose complex
PDB code	4JHO	4JIE
Wavelength (Å)	1.00	1.00
Resolution range (Å)	30 - 2.20 (2.28 - 2.20)	30 - 2.45 (2.54 - 2.45)
Completeness (%)	99.9 (99.9)	95.8 (79.9)
Average redundancy per shell	5.5 (5.5)	6.1 (4.4)
$R_{\text{merge}}^{\dagger}$ (%)	8.8 (49.4)	14.9 (45.6)
$\{I/\sigma(I)\}$	18.0 (3.2)	11.9 (3.2)
Space group	$P2_12_12_1$	$P2_12_12_1$
Unit cell parameters (Å)	$a = 68.1, b = 71.7, c = 136.7$	$a = 68.0, b = 73.6, c = 134.0$
No. of unique reflections	34370	24116
No. of observed reflections	188040	147585
No. of molecules per ASU	1	1

$$\dagger R_{\text{merge}} = \frac{\sum_{\text{hkl}} \sum_i |I_i(\text{hkl}) - \{I(\text{hkl})\}|}{\sum_{\text{hkl}} \sum_i I_i(\text{hkl})}$$

**Table 4.2** Refinement statistics of native Os7BGlu26 and its mannose complex.

Values in parentheses are for the outer shell.

	Native Os7BGlu26	Os7BGlu26/mannose complex
PDB code	4JHO	4JIE
$R_{\text{factor}}$ (%)	17.6	15.3
$R_{\text{free}}^{\dagger\dagger}$ (%)	21.9	19.5
No. of protein atoms	3955	3960
No. of water molecules	305	234
No. of ligand atoms	None	12
No. of non solvent hetero atoms	51	51
r.m.s.d. bonds (Å)	0.010	0.010
r.m.s.d. angles (°)	1.155	1.212
Mean $B$ -factor		
- Protein	22.9	23.7
- non solvent hetero atom	45.0	46.9
- solvent	32.8	30.8
- D-mannose	None	31.4
Ramachandran plot (%)		
Most favored	88.5	88.0
Allowed region	11.3	11.7
Outlier region	0.2	0.2

$R_{\text{free}}^{\dagger\dagger}$  represents the residual factor calculated from approximately 5% of the data that was not used in the refinement.

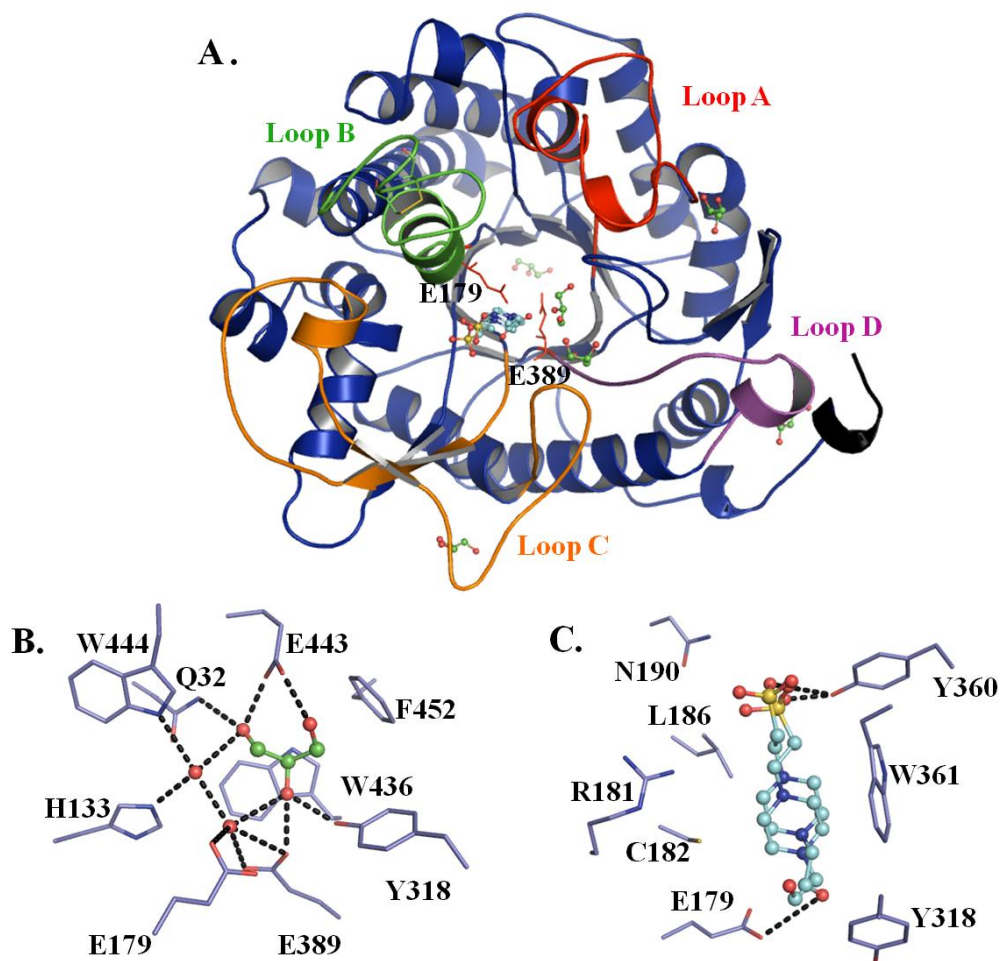


**Figure 4.5** Structure of rice Os7BGlu26  $\beta$ -D-mannosidase. (A) Cartoon of the overall structure of rice Os7BGlu26. The catalytic acid/base and nucleophile residues are represented as red sticks (Glu179 and Glu389), glycerol and HEPES are represented as green and cyan ball-and-sticks, respectively. Loops A, B, C and D are indicated in red, green, orange and magenta, respectively. The N-terminus is indicated in black. (B) Amino acid residues around the -1 subsite with contacts to glycerol and water mediated through hydrogen bonds. (C) Amino acid residues interacting with the HEPES molecule in the active site. The contacts through hydrogen bonds between the protein and HEPES are indicated as black dashed lines in B and C.

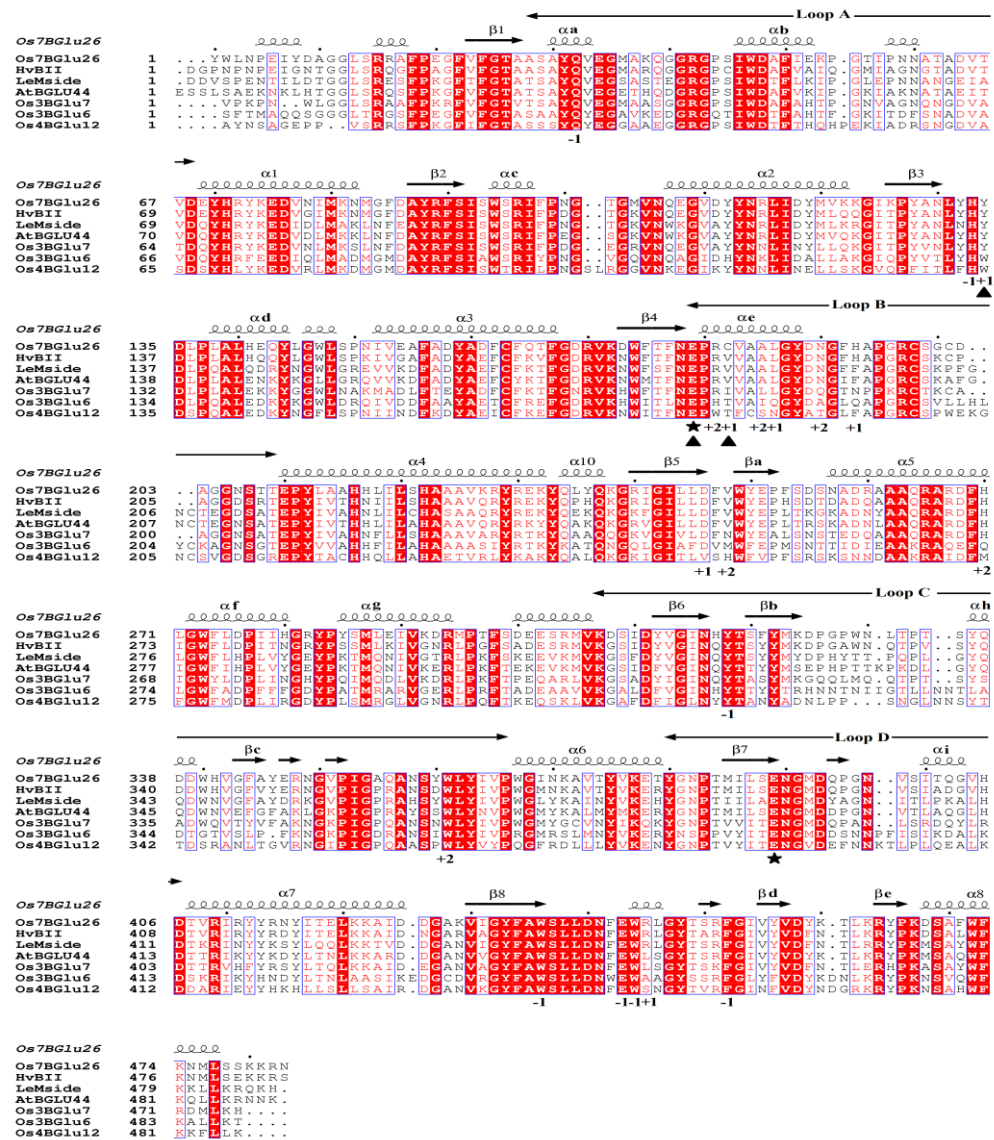


**Figure 4.6** Multiple sequence alignment of rice Os7BGlu26, HvBII, LeMside, AtBGLU44, Os3BGLu7, Os3BGLu6 and Os4BGLu12. Amino acid sequences were aligned with *ClustalW*, and the secondary structure of Os7BGlu26 was represented on the top of the Figure with the *ESPrpt* program (Gouet *et al.*, 2003). Stars indicate catalytic acid/base and nucleophilic residues, and black arrowheads mark the amino acid residues mutated in this study. The GenBank entry accessions are: Os7BGlu26, ACF35791; HvBII, AAA87339; LeMside, AAL37714; AtBGLU44, Q9LV33; Os3BGLu7, AC091670; Os3BGLu6, AC146619; and Os4BGLu12, AAAA02014151.

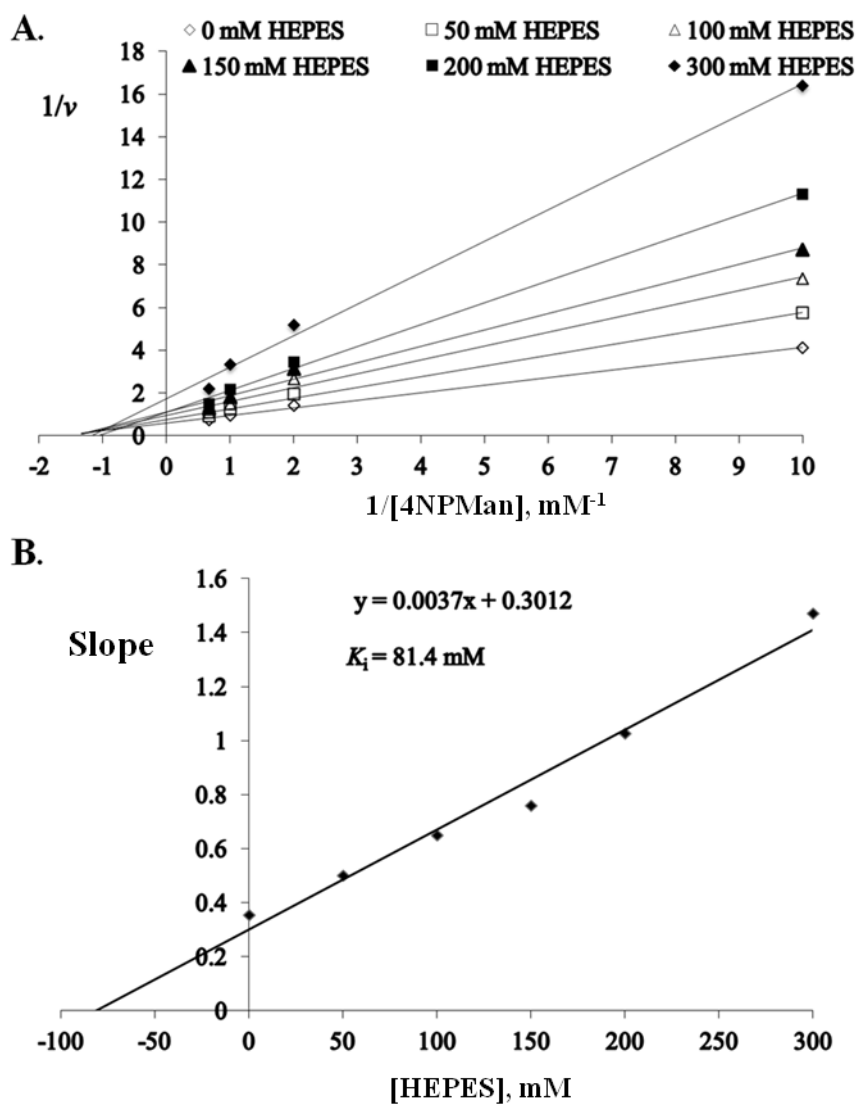


**Figure 4.7** Noncompetitive inhibition of Os7BGlu26 by HEPES. (A) The  $1/S$  vs  $1/v$  plots (Lineweaver-Burk plots). (B) To determine  $K_i$  values, the slopes of the Lineweaver-Burk plots were plotted against the HEPES concentration and the data were subjected to linear regression ( $R^2=0.979$ ).

#### 4.4 Structural comparison of Os7BGlu26 with other rice GH1 structures

In comparison to other rice GH1 structures, the active site of Os7BGlu26 has the narrowest shape, with a gate of 9.9 Å x 12.5 Å (from the atom centers of Q337 O $\epsilon$ 1 to Y360 O $\eta$  and from N190 N $\epsilon$ 2 to Y346 O $\eta$ , respectively), due to the presence of F192 on loop B and Y360 on loop C, which constrict the substrate route into the active site. In comparison, these parameters for the Os3BGlu7 (10.3 Å x 18.1 Å from Q187 C $\delta$  to W358 C $\beta$  and from Y341 C $\epsilon$ 2 to L442 C $\beta$ , respectively), Os3BGlu6 (12.1 Å x 20.8 Å from A189 C $\beta$  to W366 C $\beta$  and from L342 C $\delta$ 2 to A454 C $\alpha$ , respectively), and Os4BGlu12 (10.1 Å x 19.8 Å from K203 C $\epsilon$  to W365 C $\beta$  and from L348 C $\delta$ 1 to N452 C $\alpha$ )  $\beta$ -D-glucosidases indicate that these enzymes have broader substrate-binding clefts (Figure 4.8). This suggests that a preferred substrate for Os7BGlu26 should be the one with a small aglycon or a straight and narrow chain oligosaccharide, consistent with its hydrolysis of  $\beta$ -(1,4)-linked manno- and gluco-oligosaccharides, dhurrin, D-amygdalin, and *p*-coumaryl alcohol glucoside (Figure 4.9) (Kuntothom *et al.*, 2009).

Although the four rice GH1 enzymes have different substrate specificities, their overall structures are very similar. Upon superposition of these structures, Os7BGlu26 had the RMSD value of 0.576 Å over 437 C $\alpha$  atoms with rice Os3BGlu7  $\beta$ -glucosidase (2RGL), with which it shares 63% sequence identity. The other RMSD values are 0.481 Å over 379 C $\alpha$  residues with Os3BGlu6 (3GNO, 52% sequence identity), and 0.522 Å over 391 C $\alpha$  residues with Os4BGlu12 (3PTK, 51% sequence identity).

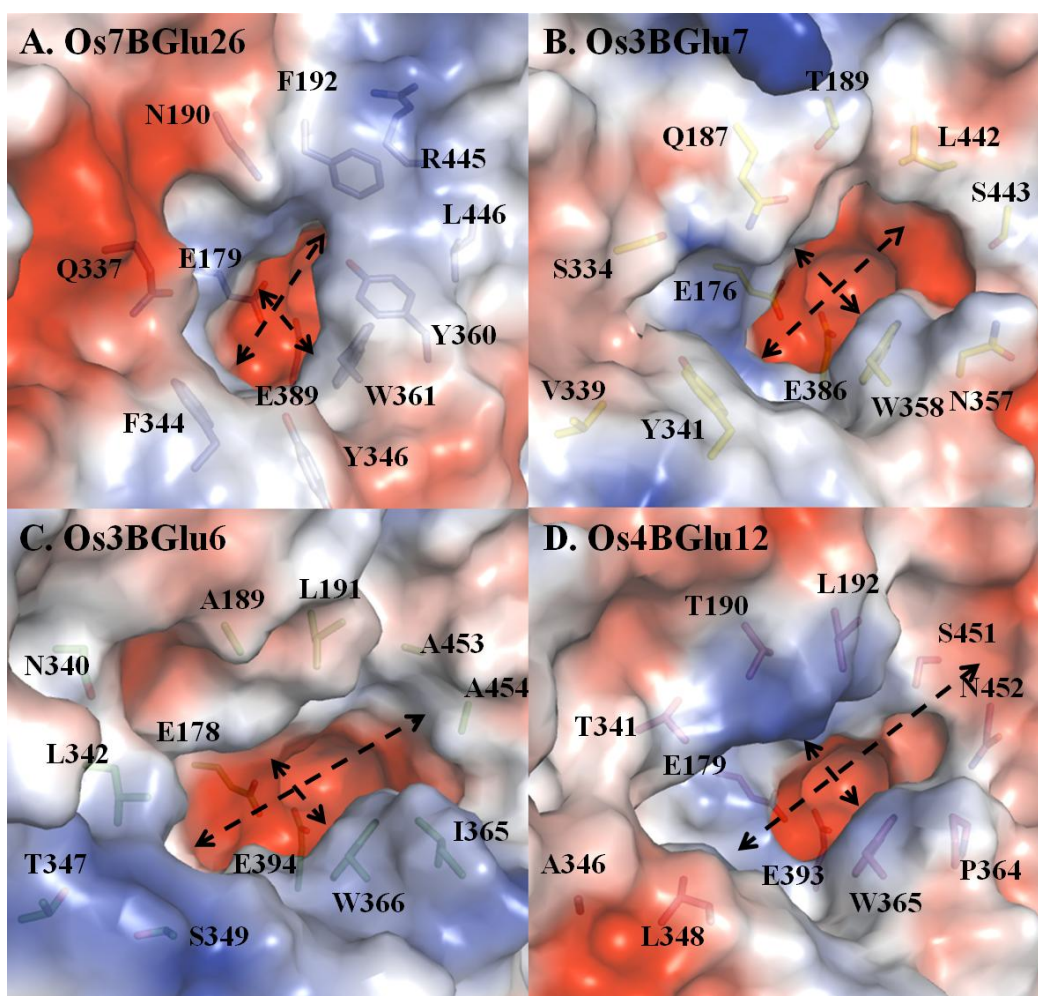


**Figure 4.8** Comparison of the active site clefts of the rice GH1 structures, Os7BGlu26, Os3BGlu7 (PDB code: 2RGL), Os3BGlu6 (PDB code: 3GNO) and Os4BGlu12 (PDB code: 3PTK). The dashed arrows indicate the width and breadth of the substrate binding cleft at the entrance to the active site, as described in the main text. *PyMol* was used to generate qualitative vacuum electrostatic charges to color the surfaces with red for negatively and blue for positively charged areas.

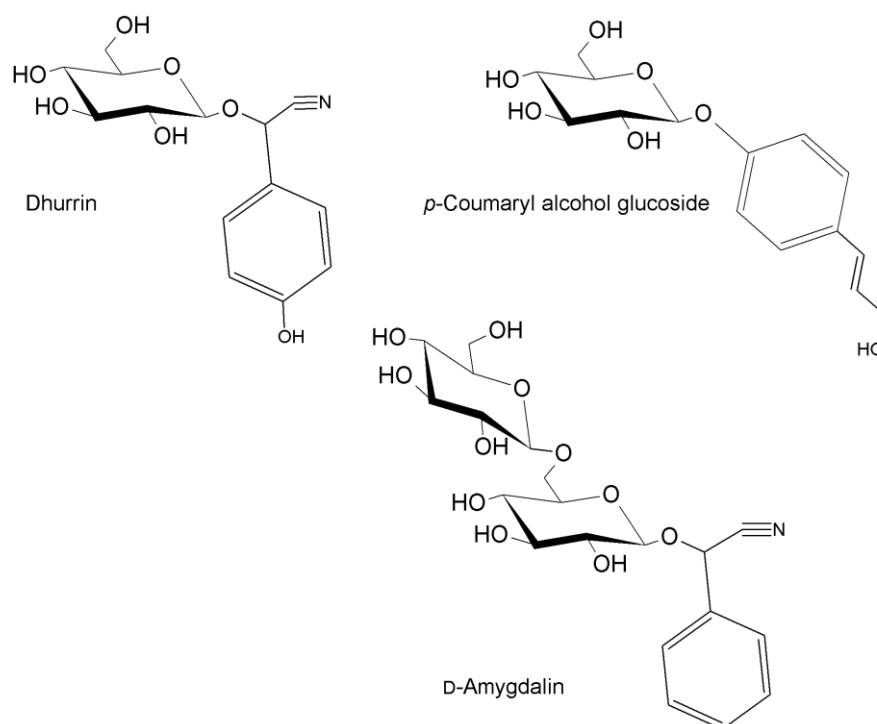


**Figure 4.9** Chemical structures of natural substrates hydrolyzed by Os7BGlu26.

#### 4.5 Os7BGlu26 in complex with the D-mannose hydrolysis product

To provide evidence for the interactions between Os7BGlu26 and D-mannosyl glycon, D-mannose was soaked in the Os7BGlu26 crystal. The resolution of this complex structure dataset was limited at 2.45 Å, which resulted in a calculated  $F_o - F_c$  OMIT map in which the mannose residue could be placed unambiguously (Figure 4.10A). The density clearly showed the presence of D-mannose in the  $\beta$ -anomeric configuration and the  ${}^1S_5$  conformation, indicating that Os7BGlu26 binds specifically to the  $\beta$ -anomer of D-mannose. The  $\beta$ -D-mannose hydrogen bonded to Q32, H133, Y134, N178, E179, E389, Y318, E443 and W444 (Figure 4.10B).

Previous structures of  $\beta$ -D-mannosidases from GH2 and GH26 include the Michaelis complex, transition state analogue and covalent intermediate complexes,

however this is the first report of a  $\beta$ -D-mannosidase product complex. Free D-mannose in the active site of Os7BGlu26 was distorted to the  ${}^1S_5$  skew boat, which is the same conformation as that reported for the Michaelis complexes of the enzymes hydrolyzing  $\beta$ -D-mannosides (Ducros *et al.*, 2002; Offen *et al.*, 2009). This result indicates that the conformation itinerary for the de-glycosylation step of a retaining  $\beta$ -mannosidase may be the reverse of the glycosylation step: the  ${}^oS_2$  skew boat in the covalent complex proceeds through a  $B_{2,5}$  boat near the transition state and to a  ${}^1S_5$  skew boat in the product complex. Superposition of the  $\beta$ -D-mannose complex and native structure showed that the position of the  $\beta$ -D-mannose was in essentially the same position as the glycerol and water molecules in the native Os7BGlu26 structure (Figure 4.10C). Nearly all of the residues in the -1 subsite were in the same positions in the two structures, with C $\delta$  of the catalytic nucleophile, E389, displaced by 0.4 Å. The superimposition of the Os7BGlu26/ $\beta$ -D-mannose complex structure with that of the Os3BGlu7 complex with cellopentaose (PDB entry 3F5K) showed that the  ${}^1S_5$  configured 1- $\beta$ -D-mannose orientation was similar to that of the  ${}^1S_3$  configured non-reducing terminal  $\beta$ -D-glucosyl ring of the cellopentaose in the -1 subsite. A HEPES molecule occupied the +1, +2, and +3 subsites defined for  $\beta$ -(1,4)-linked glucosyl residues in the Os3BGlu7 cellopentaose complex, apparently in multiple conformational states (Figure 4.10D). This structure indicates that the  $\beta$ -D-mannose hydrolysis product may be retained in the -1 subsite in a  ${}^1S_5$  conformation that suggests a conformational pathway of  ${}^oS_2$  to  $B_{2,5}$  to  ${}^1S_5$  for the deglycosylation step of Os7BGlu26  $\beta$ -D-mannoside hydrolysis, since the deglycosylation step in the retaining mechanism is essentially the reverse of the glycosylation step shown in Figure 2.12.

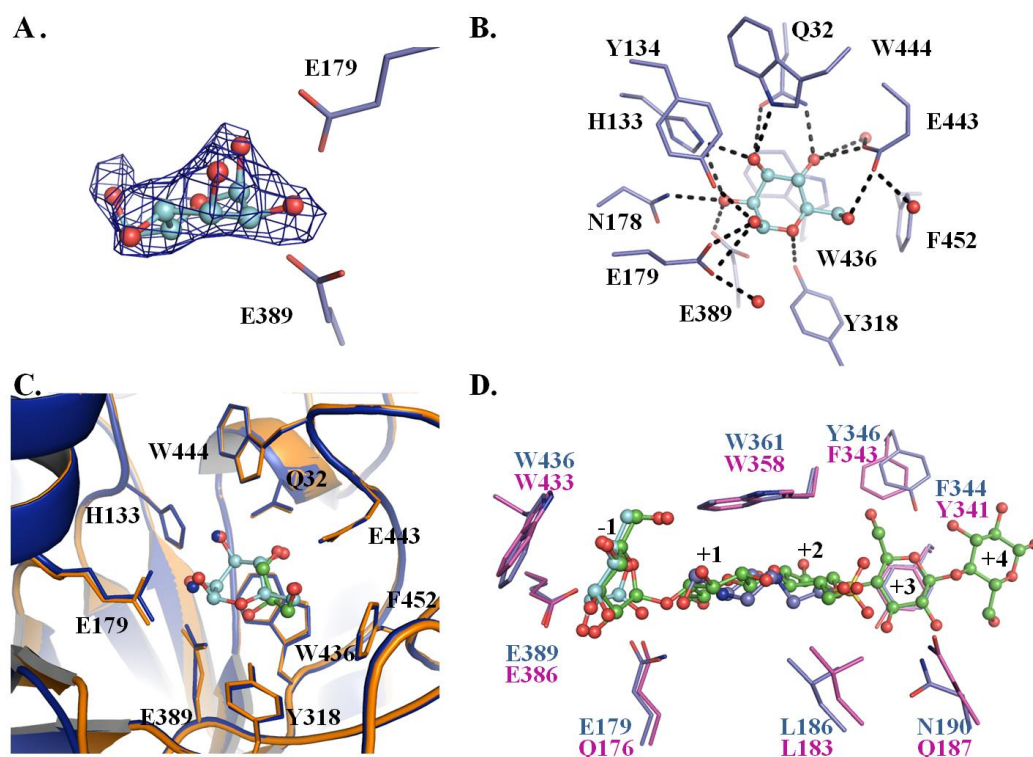


**Figure 4.10** The structure of rice Os7BGlu26 in complex with  $\beta$ -D-mannose. (A) An unbiased  $F_o - F_c$  (OMIT) map of  $\beta$ -D-mannose is represented as a blue mesh contoured at  $3\sigma$ . (B) Amino acid residues interacting with  $\beta$ -D-mannose in the active site. The contacts through hydrogen bonds between the protein and  $\beta$ -D-mannose are indicated by black dashed lines, while  $\beta$ -D-mannose is shown in cyan ball-and-stick representation. The superimposition of the Os7BGlu26/ $\beta$ -D-mannose complex (orange) over the native Os7BGlu26 structure (blue) is shown in (C). The superimposition of the Os7BGlu26/ $\beta$ -D-mannose complex (carbons in blue) with the cellopentaose/Os3BGlu7 E176Q complex (carbons in violet) is shown in (D).  $\beta$ -D-Mannoside, HEPES and cellopentaose are indicated in ball-and-stick representations with carbons in cyan, blue and green, respectively. The glucosyl residue-binding subsites observed in the cellopentaose complex are marked by -1, +1, +2, +3, and +4.

## 4.6 Docking studies of the Michaelis complex

To provide further evidence for the conformational itinerary in the glycosylation step of Os7BGlu26, 4NPGlc and 4NPMan were computationally docked in the active site of the Os7BGlu26 structure in the four starting conformations observed for pyranoside rings in glycoside hydrolase mechanisms (Volcadlo and Davies, 2008). The predicted binding energies for all the conformations tested are shown in Figure 4.11C. The binding energies for the 4NPGlc conformations are higher (more negative) than those calculated for 4NPMan (Figure 4.11). Therefore, the glucose derivative molecule binds more tightly to the enzymatic cavity than the mannose derivative. This is consistent with the lower  $K_m$  values observed for a  $\beta$ -D-glucoside ( $K_m$  0.124 mM) compared to a  $\beta$ -D-mannoside ( $K_m$  0.48 mM) (Table 3.3).

Both 4NPMan and 4NPGlc show similar trends of binding affinity with respect to the sugar conformation (Figure 4.11). However, whereas 4NPGlc binds preferentially to the enzyme in a  ${}^1S_3$  conformation (consistently with the experimental and theoretical evidence for a  ${}^1S_3$ - ${}^4H_3$ - ${}^4C_1$  catalytic conformational itinerary for  $\beta$ -glucosyl hydrolases), both  ${}^1S_3$  and  ${}^1S_5$  have a similar stability for 4NPMan. Together with the extensive support that the hydrolysis of  $\beta$ -mannosides follow a  ${}^1S_5$ - $B_{2,5}$ - ${}^0S_2$  itinerary, the results obtained suggests that the two substrates might follow a different conformational itinerary for catalysis ( ${}^1S_3$ - ${}^4H_3$ - ${}^4C_1$  for 4NPGlc and for  ${}^1S_5$ - $B_{2,5}$ - ${}^0S_2$  4NPMan). In fact, the  ${}^1S_5$  mannoside substrate was found more frequently than  ${}^1S_3$  glucoside substrate in the docking calculations, which may explain the 10-fold higher  $k_{cat}$  observed for the former.

Figure 4.11 shows the enzyme complexes with the  ${}^1S_5$   $\beta$ -D-mannoside (4NPMan) and the  ${}^1S_3$   $\beta$ -D-glucoside (4NPGlc). The substrate is nicely accommodated

in the binding cavity in each case. The mannose molecule forms hydrogen bonds with Q32, Y134, N178, E179, R181, Y318, E443 and W444 (Figure 3.11B) and the glucose molecule is hydrogen bonded to Q32, H133, N178, E179, E443 and W444 (Figure 4.11A). The catalytic residues (E179 and E389) are well oriented for catalysis in both complexes (the carboxylic acid hydrogen of E179 points towards the glycosidic oxygen and the nucleophile is within 3-3.5 Å distance from the anomeric carbon), in agreement with quantum chemical studies of glycosidic bond hydrolysis (Peterson *et al.*, 2010; Biarnés *et al.*, 2011).



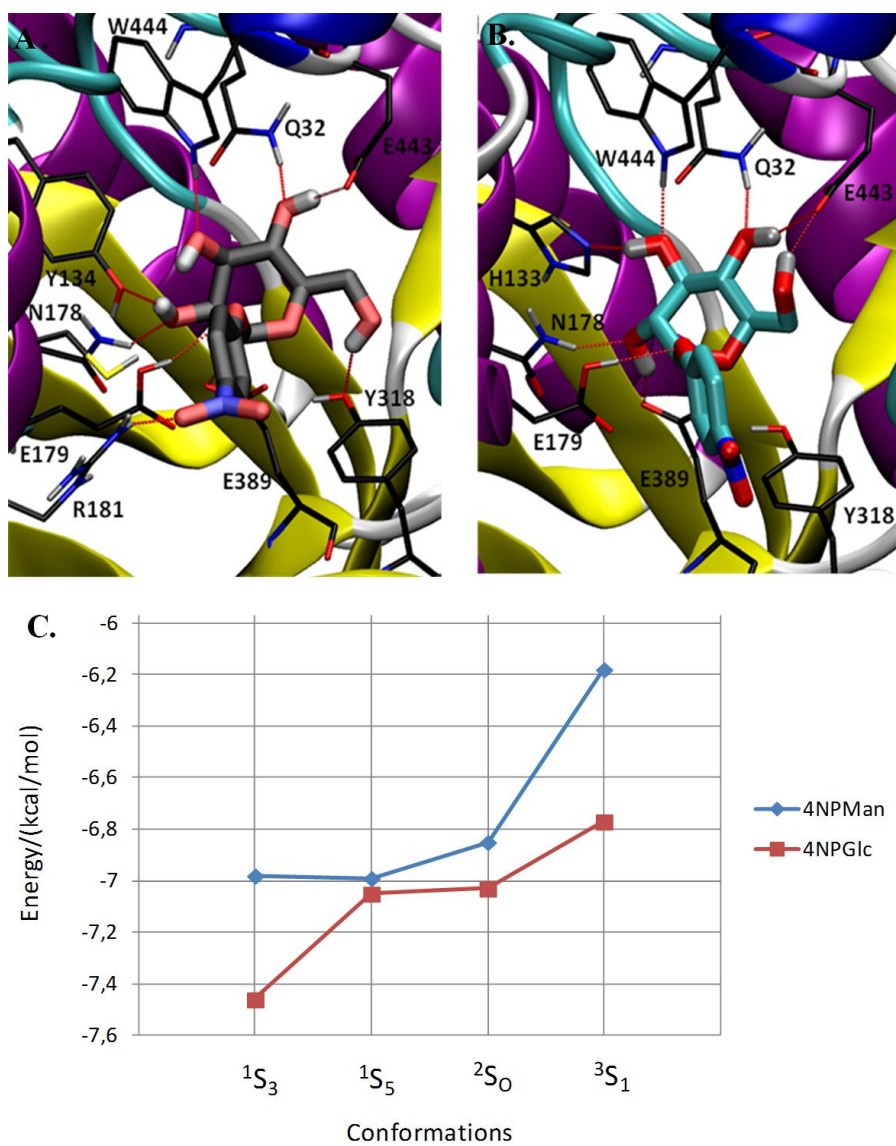


**Figure 4.11** Structures of Os7BGlu26 in complex with 4NPGlc (A) and 4NPMAN (B) obtained by computational docking. The distances between the carboxylic hydrogen atom of the catalytic acid/base residue (E179) and the glycosidic oxygen are 3.08 and 3.58 Å for the glucose and mannose molecules, respectively. The distances between the O $\epsilon$ 1 of the nucleophile (E389) and the anomeric carbons of glucose and mannose are both 3.0 Å. The binding energies of conformers of 4NPMAN and 4NPGlc in complex with Os7BGlu26 are shown in C.

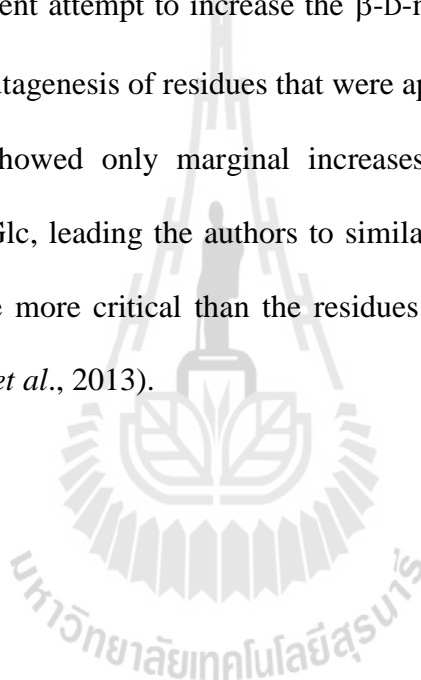
#### 4.7 Comparison of Os7BGlu26 with covalent intermediate complexes of other GH1 enzymes

To learn more about the residues effecting glycon specificity of Os7BGlu26, we endeavored to produce a covalent intermediate complex, as it was previously achieved for Os3BGlu7 (Chuenchor *et al.*, 2008). Attempts to soak the mechanism based inhibitors 2,4-dinitrophenyl 2-deoxy-2-fluoroglucoside (dNPG2F) and 2,4-dinitrophenyl 2-deoxy-2-fluoromannoside (dNPM2F) into the Os7BGlu26 crystals resulted in a release of 2,4-dinitrophenolate ion, as judged by a yellow chromophore. However, no glycon density was seen in the active site with either ligand. Pretreatment of Os7BGlu26 with dNPG2F or dNPM2F in sodium acetate buffer, pH 5.0, resulted in rapid hydrolysis with negligible inhibition of the enzyme at concentrations that strongly inhibited other rice GH1 enzymes (Figure 4.12). Although an  $^{\circ}S_2$  skew boat mannosyl covalent complex with a GH26  $\beta$ -D-mannanase has been reported (Ducros *et al.*, 2002), no such structure has been reported in the GH1 family. Therefore, the free Os7BGlu26 structure was superposed with the rice GH1 structures in complex with bound 2-deoxy-2-fluoroglucoside (G2F) moiety. This moiety occupies a low-energy  $^4C_1$  chair conformation and is covalently bound to the catalytic nucleophile residue (Figure 4.13). We conjectured that the glucoside and mannoside substrates are likely to bind in the same positions, and in the same orientations in enzymes that belong to the same family, although the conformations of these sugars may differ, as reported by Kuntothom and colleagues (2010).

The identities and placement of nearly all amino acid residues in direct contact with glycons in subsite -1 are conserved in the structures of rice GH1 isoenzymes, including the Os7BGlu26  $\beta$ -D-mannose complex structure and the complexes with

4NPGlc and 4NPMAN generated by molecular docking. The one exception is a tyrosine residue found in all characterized plant GH1 enzymes with  $\beta$ -D-mannosidase activity, *i.e.* Y134 of Os7BGlu26 that corresponds to Y131 of Os3BGlu7 (Figure 4.13A), to Y136 of barley HvBII, to Y136 of tomato LeMside and to Y137 of Arabidopsis AtBGLU44. This tyrosine residue is substituted by tryptophan in Os3BGlu6 (W133) and Os4BGlu12 (W134), which lack  $\beta$ -D-mannosidase activity (Figure 4.6 and 4.13B) (Seshadri *et al.*, 2009; Opassiri *et al.*, 2010), and most other plant  $\beta$ -D-glucosidases, including all others with known crystallographic structures, although a few others have Y, F or smaller residues in this position (Opassiri *et al.*, 2006). It is noteworthy that this tyrosine residue makes a very close contact through a hydrogen bond with the catalytic acid/base residue. Inspection of the superimposed structures revealed that the acid/base residues of Os3BGlu6 and Os4BGlu12 are displaced slightly from the positions of the acid/base residues in Os3BGlu7 and Os7BGlu26, to form contact through hydrogen bonds with T181 of Os3BGlu6 and T182 of Os4BGlu12 in the +1 subsite, whereas Os7BGlu26 and Os3BGlu7 have C182 and I179, respectively, in the corresponding positions. The equivalent residues from barley HvBII, tomato LeMside, and Arabidopsis AtBGLU44, V184, V184 and V185, respectively, do not have polar groups to form contact through hydrogen bonds to the catalytic acid/base residue. Although this position is not unique in plant GH1 enzymes, most of those with known structures have T in this position, including maize Glu1, sorghum Dhr1, wheat and rye hydroxaminic acid  $\beta$ -D-glucosidases, and *R. serpentina* strictosidine and raucafricine  $\beta$ -D-glucosidases. White clover cyanogenic  $\beta$ -D-glucosidase (ICBG) has G in this position, but its catalytic acid base maintains a position similar to those of Os3BGlu6, Os4BGlu12, and the other  $\beta$ -D-glucosidase

structures with T in this position. Aside from the two differences noted above, the -1 subsite architecture is similar in the four rice GH1 structures. Therefore, amino acid residues in other subsites or in the surrounding layers of residues outside catalytic sites might be important for the glycon specificity. Mutations of residues in the layers surrounding the active site residues have been shown to modulate  $\beta$ -D-fucosidase *versus*  $\beta$ -D-glucosidase activities in an insect GH1  $\beta$ -D-glucosidase (Mendoça and Marana, 2011). A recent attempt to increase the  $\beta$ -D-mannosidase activity of a plant  $\beta$ -D-glucosidase by mutagenesis of residues that were apparently close to the glycon in a homology model showed only marginal increases in the ratios of  $k_{cat}/K_m$  for 4NPMAN versus 4NPGlc, leading the authors to similarly speculate that the shape of the active site may be more critical than the residues that directly interact with the glycon (Ratananikom *et al.*, 2013).



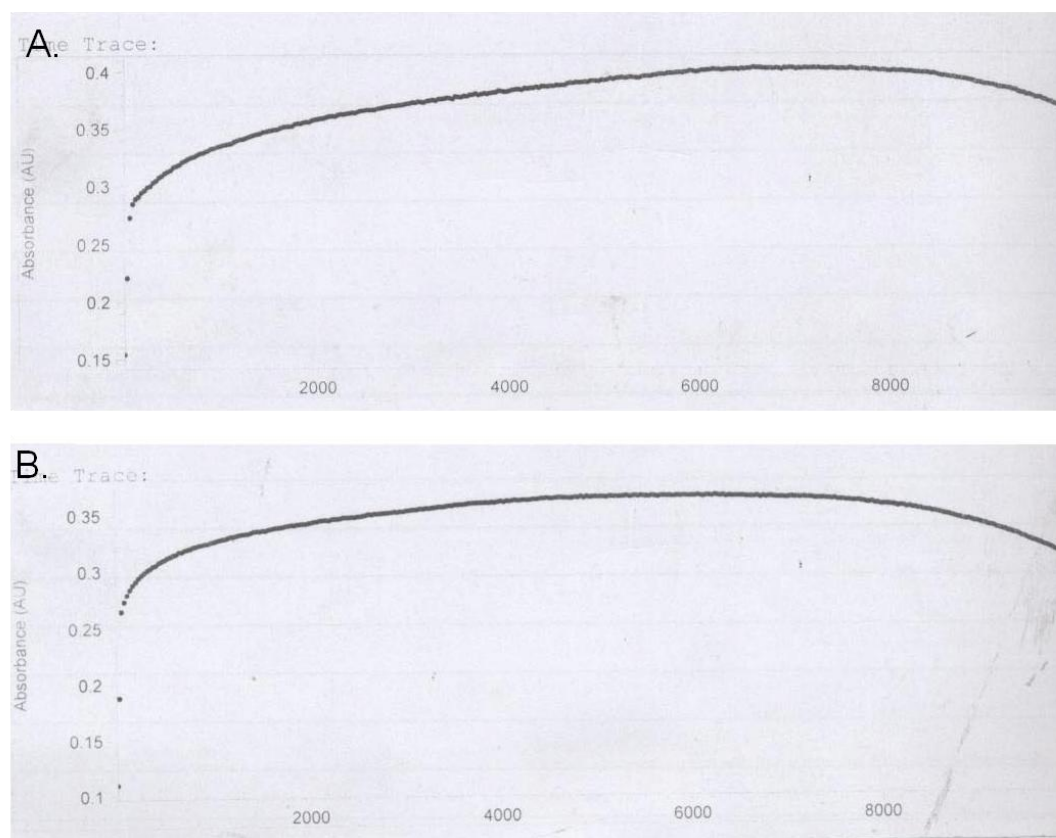


**Figure 4.12** DNP release from 2,4-dinitrophenyl 2-deoxy-2-fluoromannoside (dNPM2F)(A) and 2,4-dinitrophenyl 2-deoxy-2-fluoroglucoside (dNPG2F) (B) by the rice Os7BGlu26  $\beta$ -D-mannosidase.

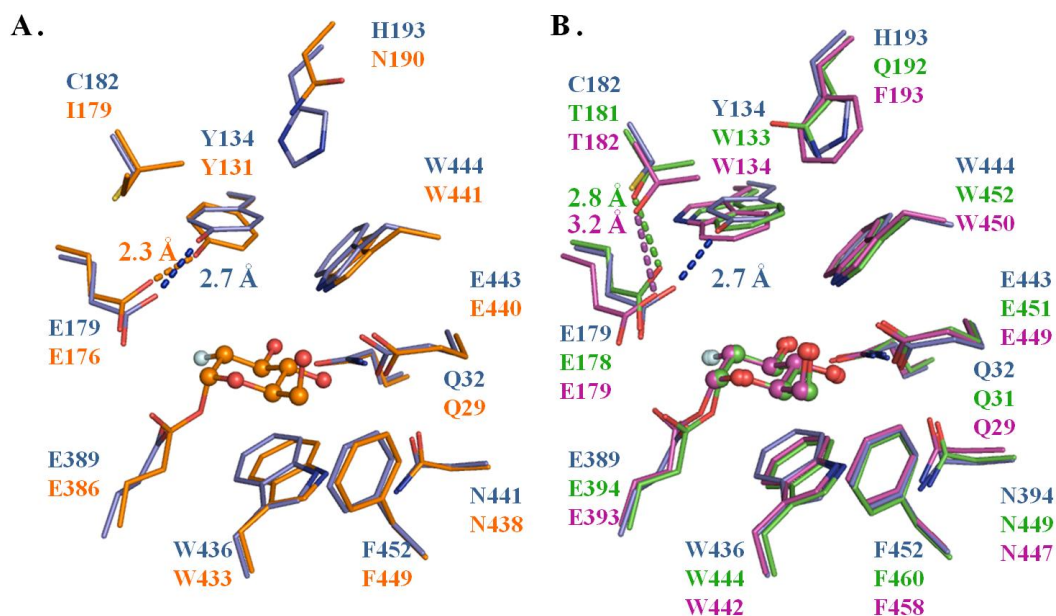


**Figure 4.13** Comparison of the active sites of the rice Os7BGlu26  $\beta$ -D-mannosidase and other rice GH1  $\beta$ -D-glucosidases with bound 2-deoxy-2-fluoroglucoside (G2F) moieties. (A) Superimposition of Os7BGlu26 with Os3BGlu7 (PDB code: 2RGM), both of which have significant  $\beta$ -D-mannosidase activity. (B) Superimposition of Os7BGlu26 with Os3BGlu6 (PDB code: 3GNR) and Os4BGlu12 (PDB code: 3PTM) which do not have significant  $\beta$ -D-mannosidase activity, in complex with G2F. The structures are shown in stick representations with carbons colored blue in Os7BGlu26, orange in Os3BGlu7, green in Os3BGlu6 and magenta in Os4BGlu12. The inhibitors are presented in ball-and-stick representations in the same colors as the corresponding protein.

#### 4.8 Kinetic studies of glycon specificity mutants of Os7BGlu26

To investigate function of the catalytic acid/base Glu179 and other key residues in the structure of Os7BGlu26 that were adjudged to play possible roles in Os7BGlu26 glycon-specificity (as described in Section 4.7), we mutated the E179 to Q (E179Q), Y134 to W (Y134W) and F (Y134F) and C182 to T (C182T) and A (C182A) residues. We have also evaluated the effects of the Y134W, Y134F, E179Q, C182T and Y134W/C182T mutations on hydrolysis of the  $\beta$ -D-glucoside and  $\beta$ -D-mannoside substrates in precise kinetic terms. The kinetic parameters and the Gibbs free energy changes for the Os7BGlu26 mutations are presented in Table 4.3.

The Os7BGlu26 catalytic acid/base mutant E179Q showed lower activity than wild-type, as indicated by the low  $k_{\text{cat}}/K_m$  for both 4NPMAN and 4NPGlc. However, this mutant affected  $\beta$ -D-mannosidase more than  $\beta$ -D-glucosidase activity, since its  $\Delta\Delta G$  with 4NPMAN was  $+9.0 \text{ kJ mol}^{-1}$ , whereas the  $\Delta\Delta G$  for 4NPGlc was  $+8.1 \text{ kJ mol}^{-1}$ . This change was driven by the 44-fold reduction in the  $k_{\text{cat}}$ , with a little change in  $K_m$  for 4NPMAN, although the  $K_m$  value increased 8-fold and  $k_{\text{cat}}$  decreased nearly 3-fold for 4NPGlc. It should be noted that GH1  $\beta$ -glucosidases with the mutation of the catalytic acid/base to Q have been shown to have relatively high activity for substrates with good leaving groups, such as 4NP or 2,4-dinitrophenolate, which have low  $pK_a$  and less need for protonation by the catalytic acid/base (Müllegger *et al.*, 2005; Chuenchor *et al.*, 2011). The use of acetate buffer, which can act as a substitute base or nucleophile, facilitates the deglycosylation step, so that this mutation has relatively mild effects in this assay. On the other hand mutation of E179 to A resulted in poor yields of soluble protein in this expression system, so this mutant could not be characterized.

The Os7BGlu26 Y134W mutant had a lesser effect on the  $\beta$ -mannosidase activity (Table 3.3), as characterized by a  $\Delta\Delta G$  of  $-0.9 \text{ kJ mol}^{-1}$ . However, it showed a nearly 6-fold increase in  $K_m$  to  $2.37 \text{ mM}$  that was compensated by a nearly 7-fold increase in  $k_{cat}$  to  $2.4 \text{ s}^{-1}$ . Since this mutant caused a nearly 4-fold decrease in  $K_m$  and a little change in  $k_{cat}$  for 4NPGlc, it appeared to improve binding of 4NPGlc and the transition state of the first covalent step of its hydrolysis (as judged by its  $\Delta\Delta G$  of  $-3.5 \text{ kJ mol}^{-1}$ ). It is of note that the  $k_{cat}/K_m$  values of the Os7BGlu26 Y134W mutant for 4NPGlc and 4NPMAN are nearly equal, although it will still hydrolyze 4NPMAN much faster than 4NPGlc at substrate concentrations above  $0.01 \text{ mM}$ . For Os7BGlu26 C182T, the  $K_m$  of this mutant was increased by approximately 25 to 30-fold for both substrates, but the  $k_{cat}$  increased 2.6-fold for 4NPGlc *versus* only 1.45-fold for 4NPMAN. For this reason, the  $\Delta\Delta G$  values were  $+7.1$  and  $+6.2 \text{ kJ mol}^{-1}$  for 4NPMAN and 4NPGlc, respectively. To verify whether these changes were due to the introduction of the hydrogen-bonding T or simply to removing the C sulfhydryl group, we also mutated C182 to A. The C182A mutation had minor effects on both 4NPMAN ( $\Delta\Delta G$  of  $+1.4 \text{ kJ mol}^{-1}$ ) and 4NPGlc ( $\Delta\Delta G$  of  $+0.8 \text{ kJ mol}^{-1}$ ), suggesting the major effect of the C182T mutation was from introduction of the T sidechain, which could hydrogen bond with the catalytic acid/base. The double mutant Os7BGlu26 Y134W/C182T had kinetic parameters and  $\Delta\Delta G$  similar to the single mutant C186T for 4NPGlc, and the  $K_m$  value for 4NPMAN was also similar to Os7BGlu26 C186T, but the  $k_{cat}$  was 40% lower in the double mutant. Hence, Y134W and C182T combined to give non-additive effects with 4NPMAN ( $\Delta\Delta G$  of  $+8.3 \text{ kJ mol}^{-1}$ ), which could be attributed to the fact that both mutated residues affect the position of the catalytic acid/base (Mildvan *et al.*, 1992; 2004). The results of our mutagenesis imply that the

hydrogen-bonding of neighboring residues to the catalytic acid/base have a significant effect on the relative hydrolytic rates of  $\beta$ -D-mannoside *versus*  $\beta$ -D-glucoside substrates.

To differentiate whether the effect of the Y134W mutation was due to the increase in size of the aromatic group or loss of the hydrogen bond from the hydroxyl group to the catalytic acid/base, Y134 was mutated to F instead of W in Os7BGlu26 Y134F. The Y134F mutant showed a similar  $K_m$  to the wild type enzyme for 4NPMan and a 1.4-fold increase in the  $K_m$  with 4NPGlc compared to the wild-type enzyme. Since the  $k_{cat}$  value was 4.4-fold that of wild-type for 4NPGlc, the  $k_{cat}/K_m$  of this mutant increased 3-fold to give a  $\Delta\Delta G$  of  $-2.9 \text{ kJ mol}^{-1}$ , which is a slightly smaller change than that observed in the Y134W mutant. However, the  $k_{cat}$  value for 4NPMan increased 36-fold and  $k_{cat}/K_m$  39-fold compared to the wild-type enzyme to give a  $\Delta\Delta G$  value of  $-9.2 \text{ kJ mol}^{-1}$  for 4NPMan. Thus, the selectivity of this mutant for 4NPMan over 4NPGlc is improved more than 37-fold, in terms of the relative  $k_{cat}/K_m$  values, suggesting the smaller steric bulk of the aromatic residue is a critical factor in the preference for  $\beta$ -mannosidase over  $\beta$ -glucosidase substrates.

**Table 4.3** Kinetic parameters of wild type Os7BGlu26 and its mutants for 4NPMAN and 4NPGlc substrates.

	substrate	$K_m$ (mM)	$k_{cat}$ (s <sup>-1</sup> )	$k_{cat}/K_m$ (s <sup>-1</sup> mM <sup>-1</sup> )	Mutant/wild type $k_{cat}/K_m$ ratio	$\Delta\Delta G_{s^*mut}$ (kJ mol <sup>-1</sup> )
Wild type	4NPMAN	0.48 ± 0.003	0.35 ± 0.004	0.714		
	4NPGlc	0.124 ± 0.002	0.029 ± 0.0001	0.237		
E179Q	4NPMAN	0.40 ± 0.003	0.008 ± 0.0004	0.02	0.028	+9.0
	4NPGlc	1.07 ± 0.02	0.0102 ± 0.0004	0.0095	0.040	+8.1
Y134W	4NPMAN	2.37 ± 0.04	2.4 ± 0.09	1.01	1.4	-0.9
	4NPGlc	0.032 ± 0.002	0.0306 ± 0.0006	0.959	4.0	-3.5
C182T	4NPMAN	12.4 ± 0.8	0.51 ± 0.03	0.043	0.060	+7.1
	4NPGlc	3.7 ± 0.14	0.078 ± 0.005	0.021	0.089	+6.1
Y134W/C182T	4NPMAN	11.6 ± 1.7	0.30 ± 0.03	0.026	0.036	+8.3
	4NPGlc	2.95 ± 0.17	0.058 ± 0.005	0.0198	0.084	+6.3
Y134F	4NPMAN	0.45 ± 0.02	12.5 ± 0.6	27.7	39	-9.2
	4NPGlc	0.167 ± 0.009	0.127 ± 0.003	0.759	3.2	-2.9
C182A	4NPMAN	2.46 ± 0.23	1.02 ± 0.07	0.414	0.58	+1.4
	4NPGlc	1.39 ± 0.11	0.242 ± 0.016	0.174	0.73	+0.8

$$\Delta\Delta G_{s^*mut} = -RT[\ln(k_{cat}/K_m)_{mutant} - \ln(k_{cat}/K_m)_{wildtype}] \text{ (Fersht } et al., 1987).$$

## 4.9 Os7BGlu26 complex with dNPG2F

Although we did not succeed in producing a covalent complex by soaking native Os7BGlu26 with dNPG2F as reported in other rice GH1 structures (Chuenchor *et al.*, 2008, Seshadri *et al.*, 2009, Sansenya *et al.*, 2011), we obtained a complex structure of Os7BGlu26 E178Q with this ligand at 2.5 Å resolution. The statistical data are presented in Tables 4.4 and 4.5. Figure 4.14 shows the Os7BGlu26 complex with dNPG2F, in which 2 molecules of dNPG2F were found in the structure. One molecule is located in the +1 and +2 subsites and the other molecule is located at a position further out in the active site cleft. The electron density difference map ( $F_o - F_c$ ) of the ligand sites with the dNPG2F molecules omitted at 4  $\sigma$  is shown in Figure 4.15. Both pyranose rings of dNPG2F appeared to take relaxed  ${}^4C_1$  chair conformations. The hydrogen bonding between dNPG2F and protein is shown in Figure 4.16. The dNPG2F in the +1 and +2 subsites appears to hydrogen bond with surrounding amino acid residues, including Y134, E179, Y318, Y360, W361, E389 and W444, and water molecules, and to form a stacking interaction between W361 and the dNP ring, whereas the dNPG2F bound further out in the active site cleft apparently only hydrogen bonds with N190, D202 and R445. Thus, the dNPG2F molecule further out in the cleft shows fewer interactions than the one in the +1 and +2 subsites, suggesting this external site represents a weaker binding or nonspecific site. In contrast, the structure of the Os4BGlu12 complex with dNPG2F represented a Michaelis complex structure, in which the 2-fluoroglucoside part of this inhibitor was found in the -1 subsite and the 2,4-dinitrophenyl ring in the +1 subsite (Sansenya *et al.*, 2011).

**Table 4.4** Data-collection statistics of complexes of Os7BGlu26 with dNPG2F and Os7BGlu26 E179Q with G2F.

Values in parentheses are for the outer shell.

	Os7BGlu26/dNPG2F	E179Q Os7BGlu26/G2F
PDB code		
Wavelength (Å)	1.00	1.00
Resolution range (Å)	30 - 2.50 (2.59 - 2.50)	30 - 2.50 (2.59 - 2.50)
Completeness (%)	98.6 (96.2)	99.3 (96.4)
Average redundancy per shell	5.8 (5.4)	4.2 (3.1)
$R_{\text{merge}}^{\dagger}$ (%)	13.0 (52.6)	12.6 (47.8)
$\{I/\sigma(I)\}$	12.4 (3.1)	10.4 (2.2)
Space group	$P2_12_12_1$	$P2_12_12_1$
Unit cell parameters (Å)	$a = 70.5, b = 73.3, c = 133.1$	$a = 68.1, b = 73.4, c = 133.5$
No. of unique reflections	24,234	23,543
No. of observed reflections	141,600	97,971
No. of molecules per ASU	1	1

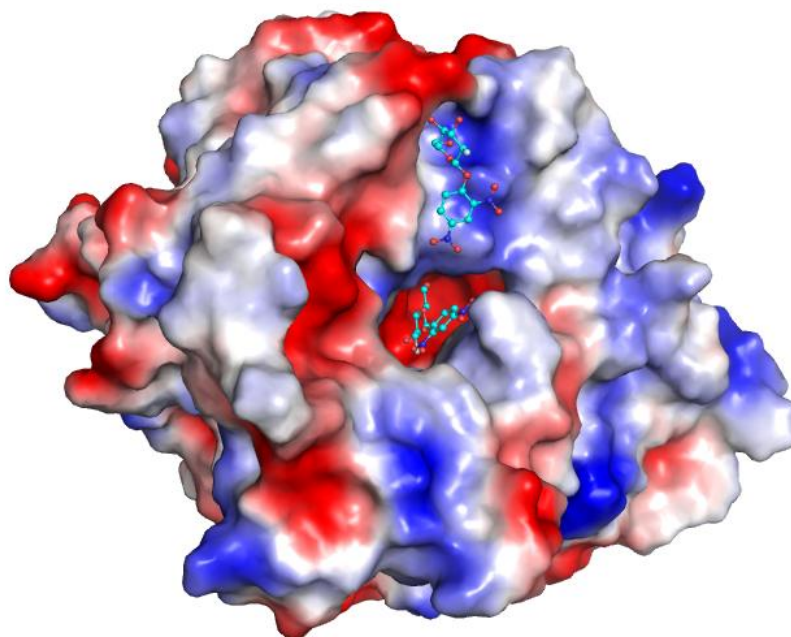
$$\dagger R_{\text{merge}} = \frac{\sum_{\text{hkl}} \sum_i |I_i(\text{hkl}) - \{I(\text{hkl})\}|}{\sum_{\text{hkl}} \sum_i I_i(\text{hkl})}$$

**Table 4.5** Refinement statistics of complexes of Os7BGlu26 with dNPG2F and Os7BGlu26 E179Q with G2F.

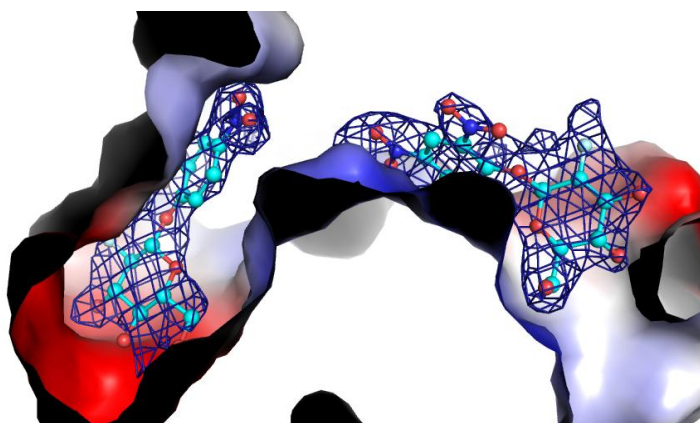
Values in parentheses are for the outer shell.

	Os7BGlu26/dNPG2F	E179Q Os7BGlu26/G2F
PDB code		
$R_{\text{factor}}$ (%)	17.4	15.8
$R_{\text{free}}^{\dagger\dagger}$ (%)	22.4	20.3
No. of protein atoms	3955	3955
No. of water molecules	244	213
No. of ligand atoms	48	11
No. of non solvent hetero atoms	24	30
r.m.s.d. bonds (Å)	0.011	0.011
r.m.s.d. angles (°)	1.146	1.305
Mean $B$ -factor		
- Protein	26.6	21.9
- non solvent hetero atom	45.8	42.5
- solvent	32.1	26.8
- ligand	35.4(dNPG2F)	23.3(G2F)
Ramachandran plot (%)		
Most favored	88.0	89.0
Allowed region	11.8	11.0
Outlier region	0.2	0.0

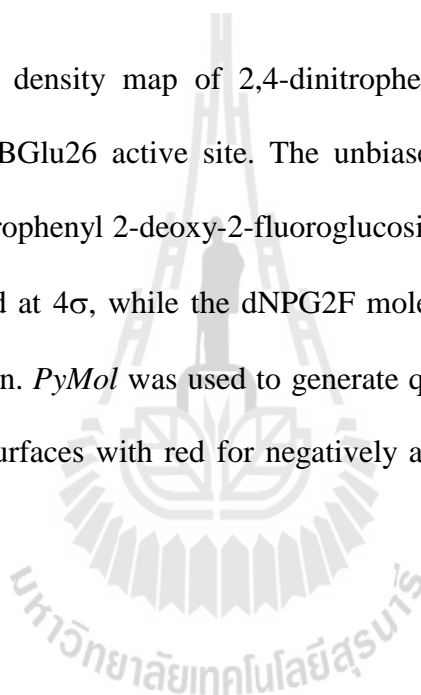
$R_{\text{free}}^{\dagger\dagger}$  represents the residual factor calculated from 5% of the data that was not used in the refinement.



**Figure 4.14** The electrostatic surface structure of rice Os7BGlu26 in complex with 2,4-dinitrophenyl 2-deoxy-2-fluoroglucoside (dNPG2F). The ligand molecules are shown in cyan ball-and-stick representation. *PyMol* was used to generate qualitative vacuum electrostatic charges to color the surfaces with red for negatively and blue for positively charged areas.



**Figure 4.15** Electron density map of 2,4-dinitrophenyl 2-deoxy-2-fluoroglucoside molecules in the Os7BGlu26 active site. The unbiased  $F_o - F_c$  ( OMIT) map of 2 molecules of 2,4-dinitrophenyl 2-deoxy-2-fluoroglucoside (dNPG2F) is represented as a blue mesh contoured at  $4\sigma$ , while the dNPG2F molecules are shown in cyan ball-and-stick representation. *PyMol* was used to generate qualitative vacuum electrostatic charges to color the surfaces with red for negatively and blue for positively charged areas.



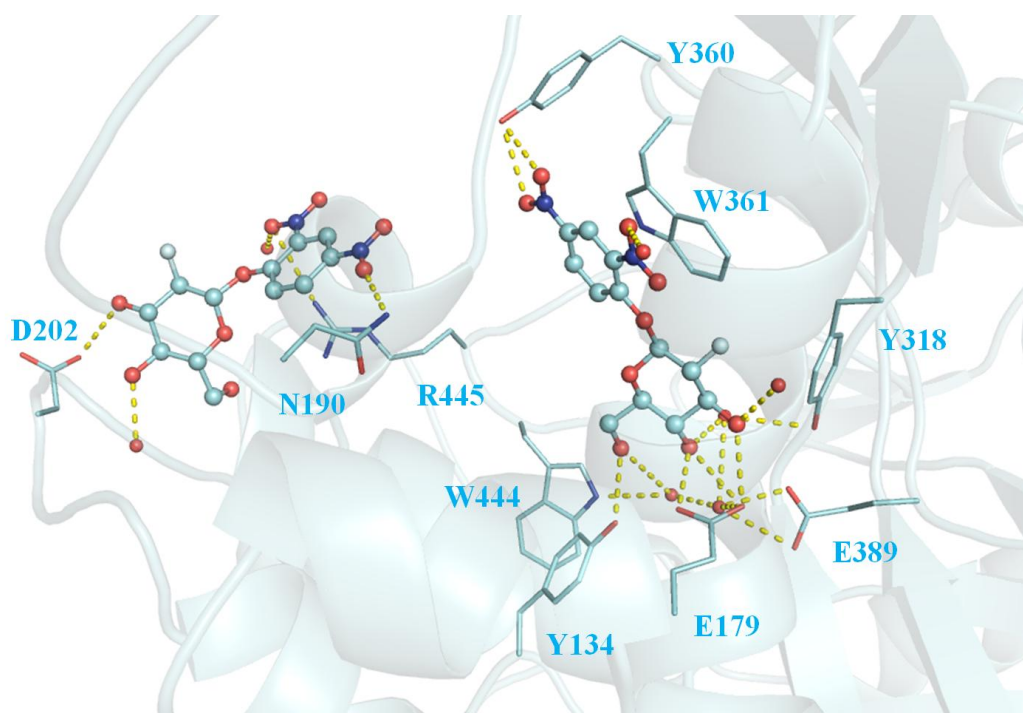


**Figure 4.16** Amino acid residues interacting with 2,4-dinitrophenyl 2-deoxy-2-fluoroglucosides (dNPG2F). The contacts through hydrogen bonds between the protein, dNPG2F and waters are indicated by yellow dashed lines, while the Os7BGlu26 and dNPG2F molecules are shown in cyan cartoon and ball-and-stick representations, respectively.

#### **4.10 Characterization of Os7BGlu26 E179Q acid/base mutant activity and its rescue**

Since the wildtype Os7BGlu26 appeared to rapidly hydrolyze dNPG2F and dNPM2F, in order to determine the structure of Os7BGlu26 complex with these covalent inhibitors and also with oligosaccharides, we utilized the E179Q Os7BGlu26 acid/base mutant enzyme described in Section 4.7. Before the structural studies, it was necessary to characterize the activity and rescue of this mutant. The mutant enzyme showed lower  $\beta$ -mannosidase activity than wild type enzyme in acetate buffer, MES buffer and universal buffer (UB). The  $\beta$ -mannosidase activity was rescued by adding azide in these buffers. A slight increase in activity was achieved in MES buffer by addition of KF, whereas ascorbate, formate and TFA did not rescue the mutant activity (Figure 4.17). As reported by Wang *et al* (1995), small nucleophiles, such as azide, carboxylates and thiolates, rescue the enzyme activity of acid/base mutants of  $\beta$ -glycosidases. Although the ascorbate cannot rescue Os7BGlu26 E179Q activity, this molecule restored hydrolysis activity in the rice Os3BGlu7 in both MES buffer and UB (Chuenchor *et al.*, 2011). An increase in the rate of hydrolysis of 4NPMan by the E179Q mutant was found with increasing azide nucleophile concentrations, but inhibition appeared at high concentrations of azide. The highest increase in rate enhancement was found in the presence of 50-100 mM azide and then dropped significantly at 800 mM (Figure 4.18). The activity versus pH profile of Os7BGlu26 E179Q  $\beta$ -mannosidase for 4NPMan cleavage was determined at 30 °C in universal buffer (pH 3.0-9.0) with 50 mM sodium azide. The acid/base mutant enzyme activity increased from pH 3.0 to pH 5.0, then was stable until pH 9.0. In contrast, the wild type Os7BGlu26 exhibits a bell-shaped, pattern as normally observed for

enzymes requiring a catalytic acid and a deprotonated base or nucleophile (Figure 4.19).

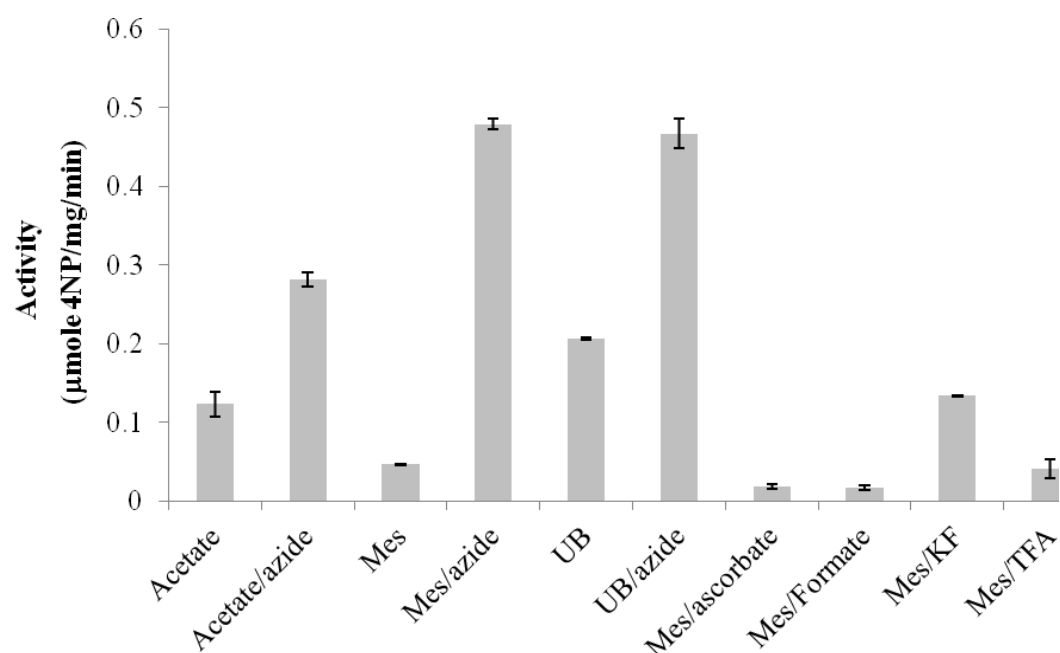


**Figure 4.17** The activities of the acid-base mutant forms of Os7BGlu26 in the presence and absence of nucleophiles.

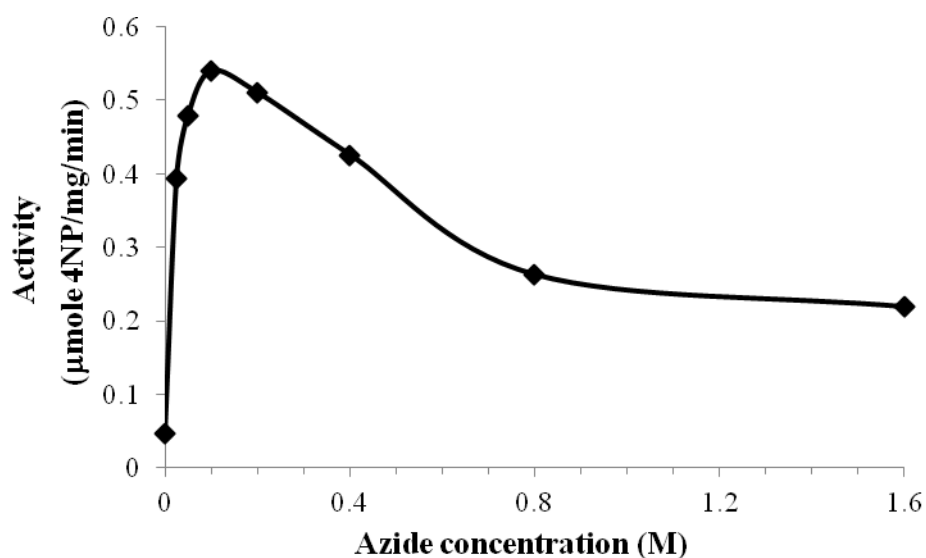


**Figure 4.18** The azide concentration dependence of 4NPM hydrolysis by the Os7BGlu26 E179Q mutant.

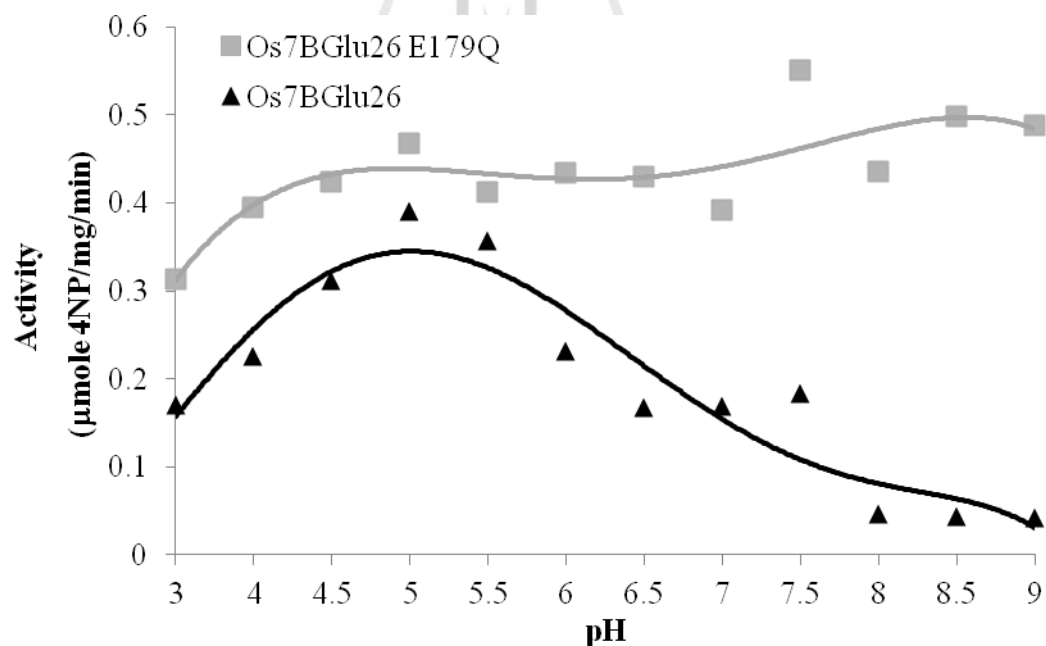


**Figure 4.19** Activity versus pH profiles of the Os7BGlu26 E179Q mutant and wild type Os7BGlu26 in universal buffer. For Os7BGlu26 E179Q, 50 mM azide was added to the reaction.

#### 4.11 The Os7BGlu26 E179Q covalent complex with G2F

To study the structure of the Os7BGlu26 covalent complex with a 2-fluoroglucosyl and fluoromannosyl moiety, the Os7BGlu26 E179Q mutant was soaked with the mechanism base inhibitors dNPG2F and dNPM2F, respectively. The E179Q acid/base mutant of Os7BGlu26 was crystallized by hanging drop vapor diffusion with seeding with a native Os7BGlu26 crystal seed stock and soaked with the inhibitors. The structure of Os7BGlu26 E179Q with G2F was solved at 2.50 Å resolution (Table 4.4), whereas the structure complexed with M2F was attempted, but not obtained. The refinement statistics for the G2F complex are reported in Table 4.5. Figure 4.20A shows the superimposition between the native Os7BGlu26 and E179Q mutant enzyme structures. Comparison of the amino acid residues in the glycon-binding site of the native and mutant structures shows that all of the amino acid residues of the mutant structure are in similar orientations as in the wild type enzyme, except E389, the catalytic nucleophile residue. The side chain of E389 in the mutant structure is flipped over and forms a covalent bond with G2F. The position of the nucleophilic residue is the major structural difference between the apo enzymes and covalent intermediate complexes of many GH1 enzymes. In the complex structures of the *P. polymyxa*, *S. solfataricus*, *T. maritima*, rice Os3BGlu6, rice Os3BGlu7 and human cytosolic  $\beta$ -glucosidases, the side-chain position of the nucleophilic residue has moved to covalently bond with the anomeric carbon of G2F. The ligand and sidechain-omitted electron density difference map of E389 covalently bonded with G2F is shown in Figure 4.20B as the weighted  $F_o - F_c$  electron density difference map contoured at 4  $\sigma$ . The G2F molecule was found in a  ${}^4C_1$  relaxed chair conformation, which is the conformation expected for the covalent intermediate according to the

conformational itinerary of glucoside hydrolysis shown in Figure 2.9. The superimposition of the Os7BGlu26 E179Q complex with G2F with similar complexes of Os3BGlu7 (PDB code: 2RGM), Os3BGlu6 (PDB code: 3GNR) and Os4BGlu12 (PDB code: 3PTM) is shown in Figure 4.20C. The positions of the G2F and acid/base residues from the 4 structures are similar, whereas only the nucleophilic residue of Os4BGlu12, E393, was positioned differently from the nucleophiles in the other G2F covalent complex structures.

The hydrogen bonding between the G2F and Os7BGlu26 protein is shown in Figure 4.21. The G2F molecule forms hydrogen bonds with 2 water molecules and several amino acid residues in the -1 subsite. E443 has 3 hydrogen bonds with G2F (O $\epsilon$ 2 with O4 and O6 of G2F and O $\epsilon$ 1 with O4 of G2F), whereas Q32 forms 2 hydrogen bonds (O $\epsilon$ 1 and N $\delta$ 2 with O3 and O4 of G2F, respectively) and the N $\epsilon$ 2 of H133 and N $\epsilon$ 1 of W444 show hydrogen bonding interactions to O3 of G2F. The N178 O $\delta$ 1 and N316 N $\delta$ 2 are hydrogen bonded with a water molecule that interacts with the O $\epsilon$ 2 atom of E389, which is covalently bonded with G2F. Another water molecule interacts with O5 and O6 of the G2F molecule. The native glucoside in a covalent complex with a GH1 enzyme (Os4BGlu12) was reported to show a position and orientation similar to G2F in its complex with the wildtype enzyme (Hua *et al.*, 2013). Based on that analysis and the orientation of the G2F moiety, the O2 of the glucosyl moiety might hydrogen bond with N $\epsilon$ 2 of H133, N $\delta$ 2 of N178 and the nearby water molecule.

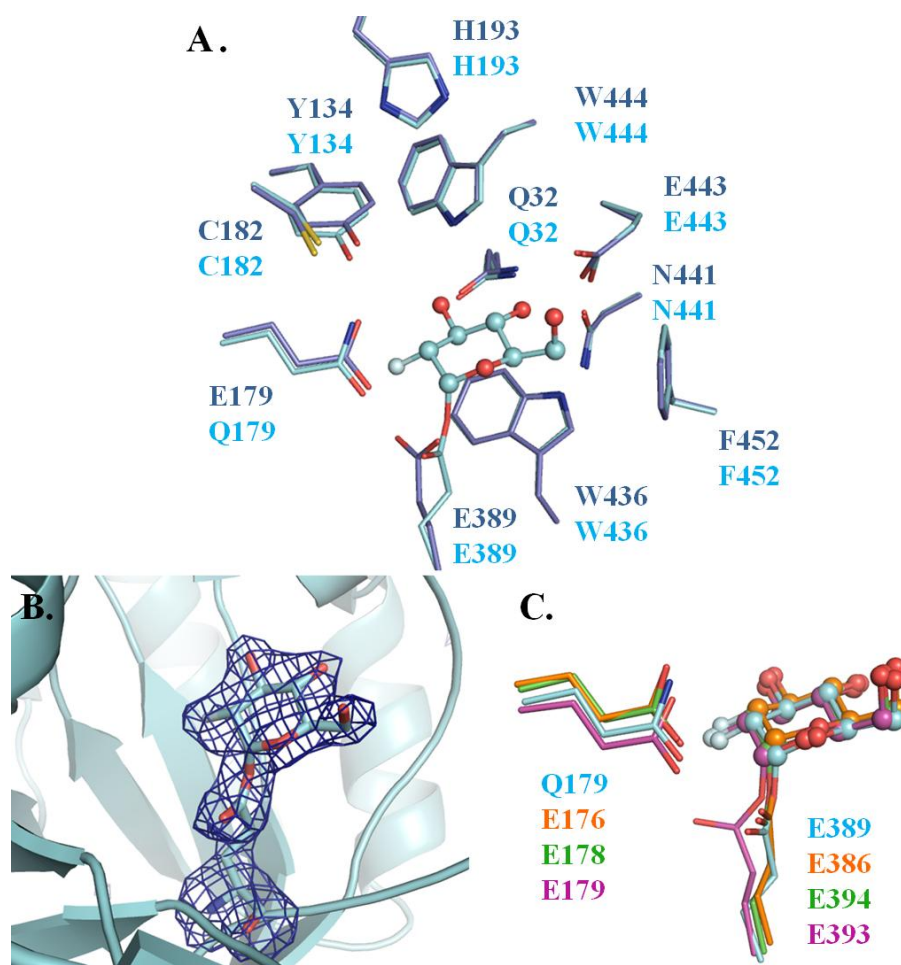


**Figure 4.20** The structure of rice Os7BGlu26 E179Q in a covalent complex with a 2-deoxy-2-fluoroglucoside (G2F) moiety. (A) Superimposition of Os7BGlu26 E179Q with native Os7BGlu26 (PDB code: 4JHO). (B) An unbiased  $F_o - F_c$  (OMIT) map of E389 covalently bonded with G2F is represented as a blue mesh contoured at  $+4\sigma$ . (C) Superimposition of Os7BGlu26 with Os3BGlu7 (PDB code: 2RGM), Os3BGlu6 (PDB code: 3GNR) and Os4BGlu12 (PDB code: 3PTM) in complexes with G2F. The structures are shown in stick representations with carbons colored cyan in Os7BGlu26 E179Q, blue in Os7BGlu26, orange in Os3BGlu7, green in Os3BGlu6 and magenta in Os4BGlu12. The inhibitors are presented in ball-and-stick representations in the same colors as the corresponding protein.

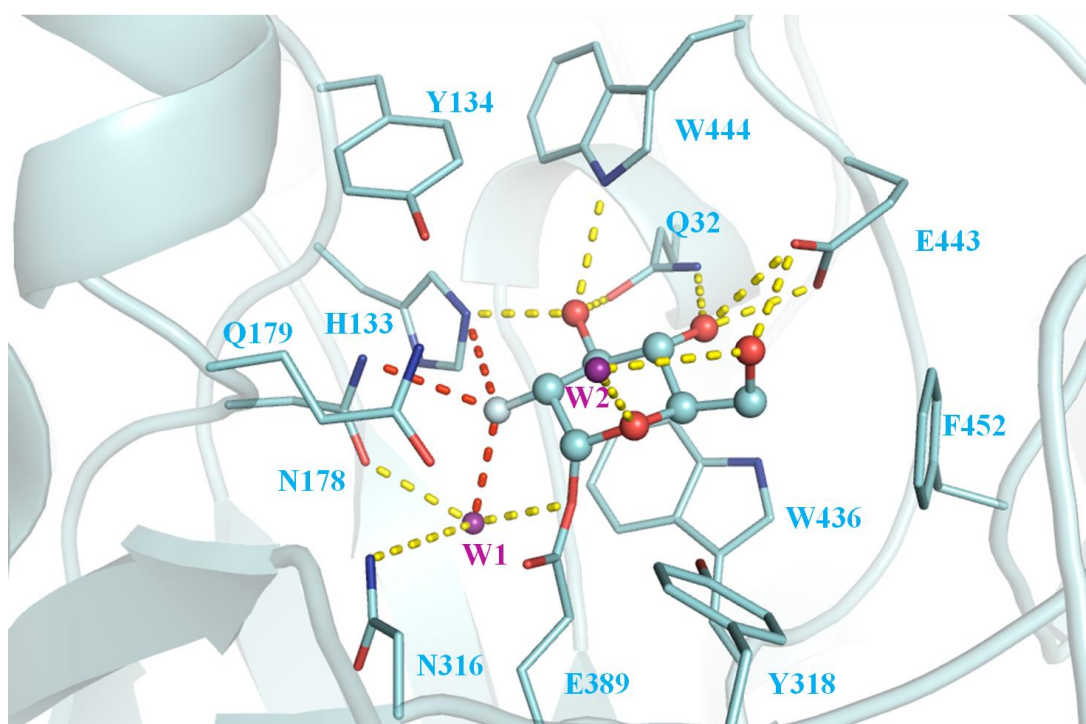


**Figure 4.21** Hydrogen bonding in the active site of the structure of rice Os7BGlu26 E179Q in complex with 2-deoxy-2-fluoroglucoside (G2F). The contacts through hydrogen bonds between the protein, G2F and waters are indicated by yellow dashed lines. The possible H-bonds from a 2 hydroxyl group are indicated as red dashed lines. The amino acid residue structures are shown in stick representations with carbons colored cyan in Os7BGlu26 E179Q. The G2F is presented in ball-and-stick representations in the same colors as the protein. The water molecules are presented as purple spheres.

#### 4.12 Os7BGlu26 complexes with putative transition state analogues

To understand the conformational pathway of mannoside and glucoside hydrolysis in plant GH1 enzymes and whether it affects the relative  $\beta$ -D-mannosidase versus  $\beta$ -D-glucosidase activities of these enzymes, we studied the binding interaction between Os7BGlu26 and putative transition state analogue inhibitors. Kinetic inhibition studies were performed to predict whether the candidate inhibitors are really transition state analogues, in addition to soaking crystals with them. Strong inhibition was observed with phenethyl-glucoimidazole > glucoimidazole > isofagomine > mannoimidazole > nojirimycin for Os7BGlu26 and rHvBII  $\beta$ -mannosidases and Os3BGlu7  $\beta$ -glucosidase (Table 3.6). In contrast, glucotetrazole, 1-deoxynojirincin and 1-deoxymannojojirimycin did not inhibit these enzymes under the conditions tested (data not shown). To assess the transition state mimicry of the inhibitors, the time dependence of the inhibition was investigated by measurement of the 4NPMan hydrolysis by Os7BGlu26 preincubated with or without putative transition state inhibitors 10 min or 2 h. The comparison of the reaction progress curves showed that more inhibition was observed after 2 h pre-incubation than 10 min preincubation with mannoimidazole, glucoimidazole and isofagomine. This indicates that the 3 putative transition state inhibitors exhibit slow onset inhibition to this enzyme, which has been observed for transition state analogues in other studies (Figure 3.22) (Lohse *et al.*, 2000).

**Table 4.6** Kinetics of inhibition of GH1 Os7BGlu26, Os3BGlu7 and rHvBII by putative transition state analogues.

	<b>Os7BGlu26</b>		<b>Os3BGlu7</b>		<b>rHvBII</b>	
	$K_i$ (M)	$\Delta G$ (kJ mol <sup>-1</sup> )	$K_i$ (M)	$\Delta G$ (kJ mol <sup>-1</sup> )	$K_i$ (M)	$\Delta G$ (kJ mol <sup>-1</sup> )
Mannoimidazole	$13.2 \times 10^{-6}$	-28.3	$3.8 \times 10^{-6}$	-31.4	$10.6 \times 10^{-6}$	-28.9
Glucoimidazole	$54.2 \times 10^{-9}$	-42.2	$8.0 \times 10^{-9}$	-47.0	$56.8 \times 10^{-9}$	-42.0
Phenethyl-Glucoimidazole	$18.0 \times 10^{-9}$	-44.93	$6.2 \times 10^{-9}$	-47.61	$16.5 \times 10^{-9}$	-45.2
Isofagomine	$2.97 \times 10^{-6}$	-32.06	$0.58 \times 10^{-6}$	-36.18	$0.10 \times 10^{-6}$	-40.6
Nojirimycin	$>100 \times 10^{-6}$	$>-23.2$	$17.3 \times 10^{-6}$	-27.63	$5.05 \times 10^{-6}$	-30.7

$\Delta G = -RT \ln[K_i]$

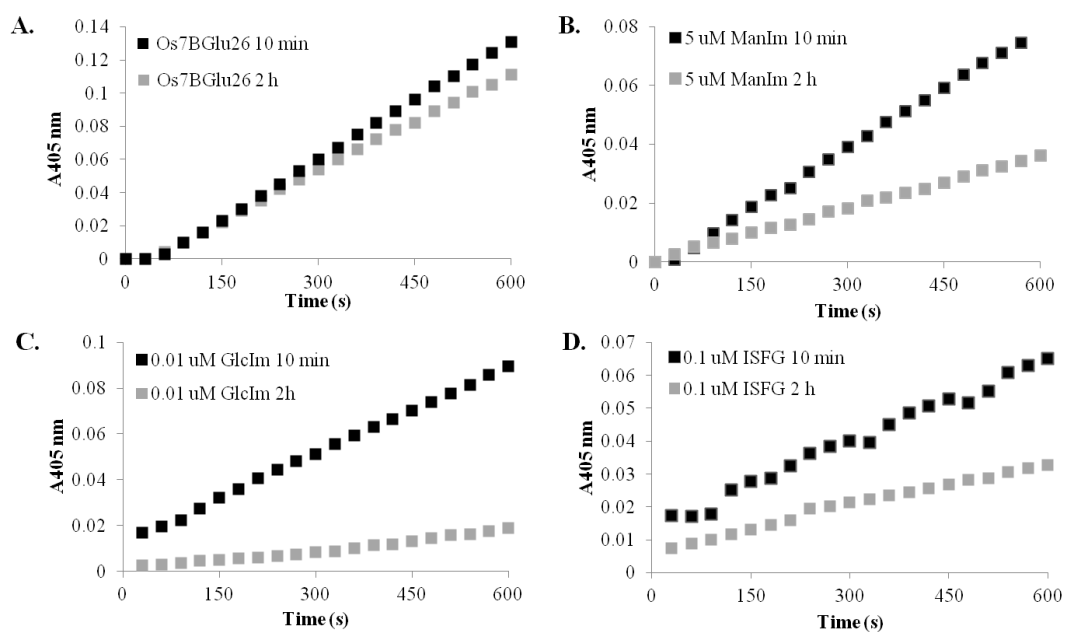


**Figure 4.22** The slow onset inhibition of Os7BGlu26 with putative transition state mimic inhibitors. Reaction progress curves after 10 min and 2 h preincubation without inhibitor (A), and with mannoimidazole (B), glucoimidazole (C) and isofagomine (D) are shown. The released 4NP was monitored at 405 nm.

The Os7BGlu26 protein was crystallized, crystals soaked with the putative transition state analogue inhibitors mannoimidazole, glucoimidazole and isofagomine and X-ray diffraction datasets were collected with resolutions of 2.00, 2.55 and 2.30 Å, respectively (Table 4.7). All of these complex structures show interactions between amino acid residues in the -1 subsite with different conformations of inhibitors (Figure 4.23).

The crystal structure of mannoimidazole showed a distorted ring between a  ${}^1S_5$  skew boat and a  $B_{2,5}$  boat, which is proposed to be the transition state conformation of mannosides (Palcic, 2008), and this inhibitor had a competitive  $K_i$  constant of  $13.2 \times 10^{-6}$  M. Until now, no report for mannoimidazole structure in a GH1 enzyme has been published, but a mannoimidazole complex has only been reported from the GH2 enzyme *Bacteroides thetaiotaomicron*  $\beta$ -mannosidase BtMan2A, in which mannoimidazole was also in the  $B_{2,5}$  conformation (Tailford *et al.*, 2008). The result suggests that the conformational transition of mannoside hydrolysis in GH1 proceeds similarly to that in the  $\beta$ -mannosidase from GH2.

In its complex with Os7BGlu26, glucoimidazole had distortion to a  ${}^4E$  envelope conformation, which is close to the  ${}^4H_3$  half chair transition state proposed for glucosides. This shape has been observed in complex structures of a GH1 myrosinase (Burmiester *et al.*, 2000) and  $\beta$ -glycosidase from *Thermotoga maritima* (TmGH1) (Gloster *et al.*, 2006). Glucoimidazole had a competitive  $K_i$  constant of  $54.2 \times 10^{-9}$  M. These results strongly suggest that Os7BGlu26 hydrolyzes  $\beta$ -D-mannosides and  $\beta$ -D-glucosides via different distortions. The crystal structure of the Os7BGlu26 complex with isofagomine showed the pyranose ring close to the  ${}^4C_1$  chair form, which is the relaxed state conformation of glycosides and corresponds to the shape of this inhibitor

in a similar complex with a GH1  $\beta$ -glucosidase from *Thermotoga maritima* (Zechel *et al.*, 2003), and this inhibitor had a competitive  $K_i$  constant of  $2.97 \times 10^{-6}$  M.

The hydrogen bond interactions between Os7BGlu26 and the putative transition state analog inhibitors are shown in Figure 4.24. The complex of this enzyme with mannoimidazole showed more apparent hydrogen bonding than glucoimidazole and isofagomine, respectively. Mannoimidazole and glucoimidazole show H-bonding with Q32, H133, Q178, E179, Y318, E389, E443 and W444, whereas isofagomine binds the same residues, except for Q178 and Y318. Although, isofagomine shows less bonding interactions, it displayed stronger inhibition than mannoimidazole. Due to lack of a hydroxyl group in the position corresponding to the 2-hydroxyl in an aldopyranose sugar in the structure of isofagomine, it cannot make the interactions specific to this group in other inhibitors. It is possible that the relatively weak binding of the mannoimidazole is due to the energy used distorting the mannopyranoside to the  $B_{2,5}$  conformation and/or the slight displacements of active site amino acid sidechains that allow it to make all of the same interactions as the glucopyranose in the  ${}^4H_3$  conformation.

**Table 4.7** Data-collection statistics of Os7BGlu26 complexes with mannoimidazole (MIM), glucoimidazole (GIM) and isofagomine (ISFG).

Values in parentheses are for the outer shell.

	Os7BGlu26/MIM	Os7BGlu26/GIM	Os7BGlu26/ISFG
PDB code			
Wavelength (Å)	1.00	1.00	1.00
Resolution range (Å)	30 - 2.00 (2.07 - 2.00)	30 - 2.55 (2.64 - 2.55)	30 - 2.30 (2.38 - 2.30)
Completeness (%)	99.9 (99.9)	99.9 (100)	99.9 (99.7)
Average redundancy per shell	5.5 (5.6)	6.3 (6.4)	5.6 (5.5)
$R_{\text{merge}}^{\dagger}$ (%)	7.4 (49.0)	11.5 (49.7)	11.3 (48.0)
$\{I/\sigma(I)\}$	20.7 (3.7)	16.0 (4.0)	14.8 (4.2)
Space group	$P2_12_12_1$	$P2_12_12_1$	$P2_12_12_1$
Unit cell parameters (Å)	$a = 68.1,$ $b = 71.9,$ $c = 135.9$	$a = 68.1,$ $b = 73.2,$ $c = 134.1$	$a = 68.5,$ $b = 72.1,$ $c = 135.1$
No. of unique reflections	45769	22658	30667
No. of observed reflections	251764	143742	172973
No. of molecules per ASU	1	1	1

$$\dagger R_{\text{merge}} = \frac{\sum_{\text{hkl}} \sum_i |I_i(\text{hkl}) - \{I(\text{hkl})\}|}{\sum_{\text{hkl}} \sum_i I_i(\text{hkl})}$$

**Table 4.8** Refinement statistics of Os7BGlu26 complexes with mannoimidazole (MIM), glucoimidazole (GIM) and isofagomine (ISFG).

Values in parentheses are for the outer shell.

	Os7BGlu26/MIM	Os7BGlu26/GIM	Os7BGlu26/ISFG
PDB code			
$R_{\text{factor}}$ (%)	18.8	17.5	16.9
$R_{\text{free}}^{\dagger\dagger}$ (%)	22.6	21.3	21.2
No. of protein atoms	3955	3955	3955
No. of water molecules	323	119	233
No. of ligand atoms	14	14	10
No. of non solvent hetero atoms	35	47	39
r.m.s.d. bonds (Å)	0.009	0.011	0.010
r.m.s.d. angles (°)	1.199	1.288	1.260
Mean $B$ -factor			
- Protein	22.6	20.4	21.7
- non solvent hetero atom	53.0	48.4	51.5
- solvent	35.6	23.7	27.8
- ligand	17.2(MIM)	18.7(GIM)	28.3(ISFG)
Ramachandran plot (%)			
Most favored	88.9	88.5	88.7
Allowed region	11.1	11.3	11.3
Outlier region	0.0	0.2	0.0

$R_{\text{free}}^{\dagger\dagger}$  represents the residual factor calculated from approximately 5% of the data that was not used in the refinement.

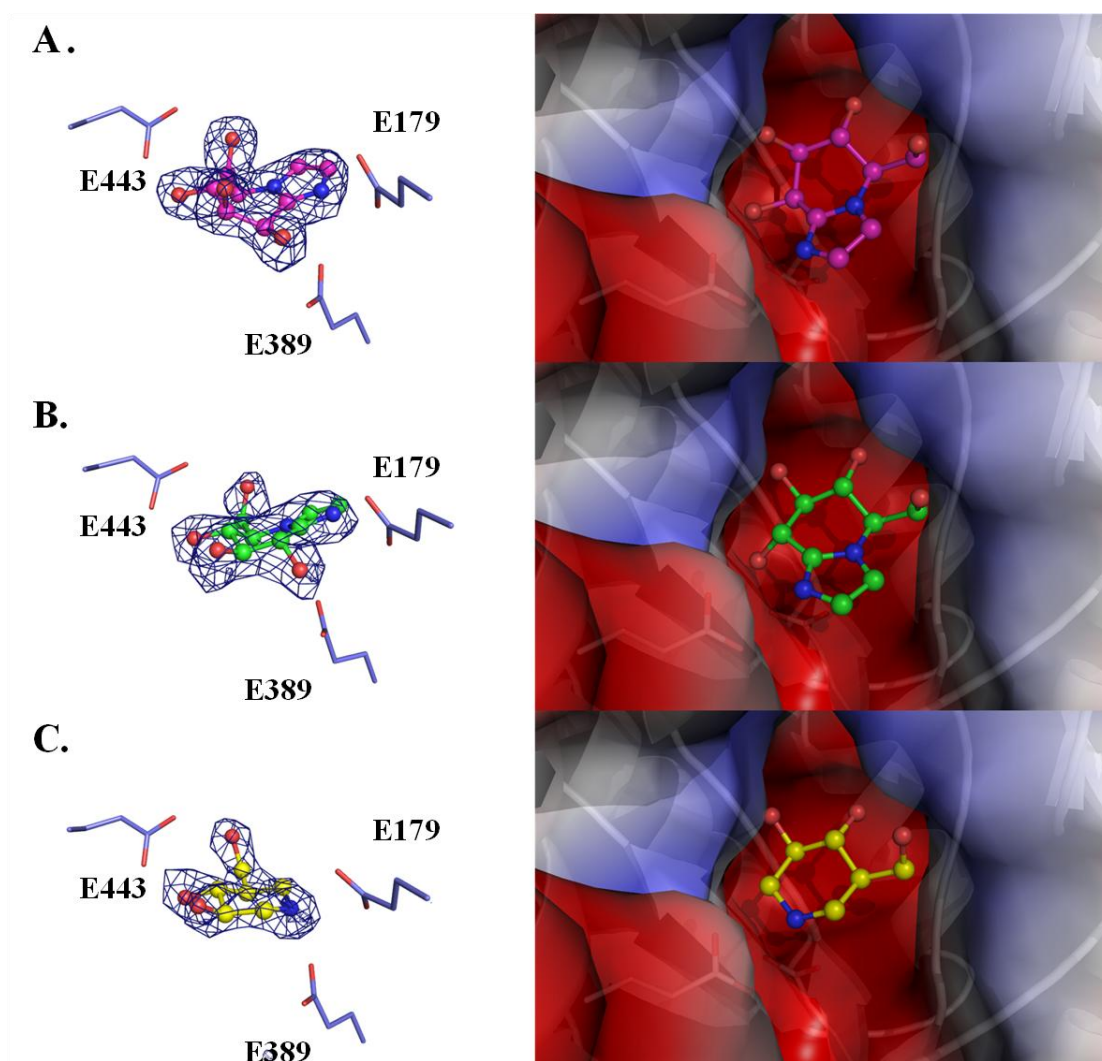


**Figure 4.23** The structures of rice Os7BGlu26 in complexes with mannoimidazole (A), glucoimidazole (B) and isofagomine (C). The unbiased weighted  $F_o - F_c$  (OMIT) electron density difference maps of the putative transition state mimic inhibitors are represented as a blue mesh contoured at  $+4\sigma$  (left panels). The inhibitors are shown located in the -1 subsite, which is represented as an electrostatic surface in the right panels. The amino acid side chain structures are shown in stick representations with carbons colored blue in Os7BGlu26. The inhibitors are presented in ball-and-stick representations, with carbons colored magenta in mannoimidazole, green in glucoimidazole and yellow in isofagomine.

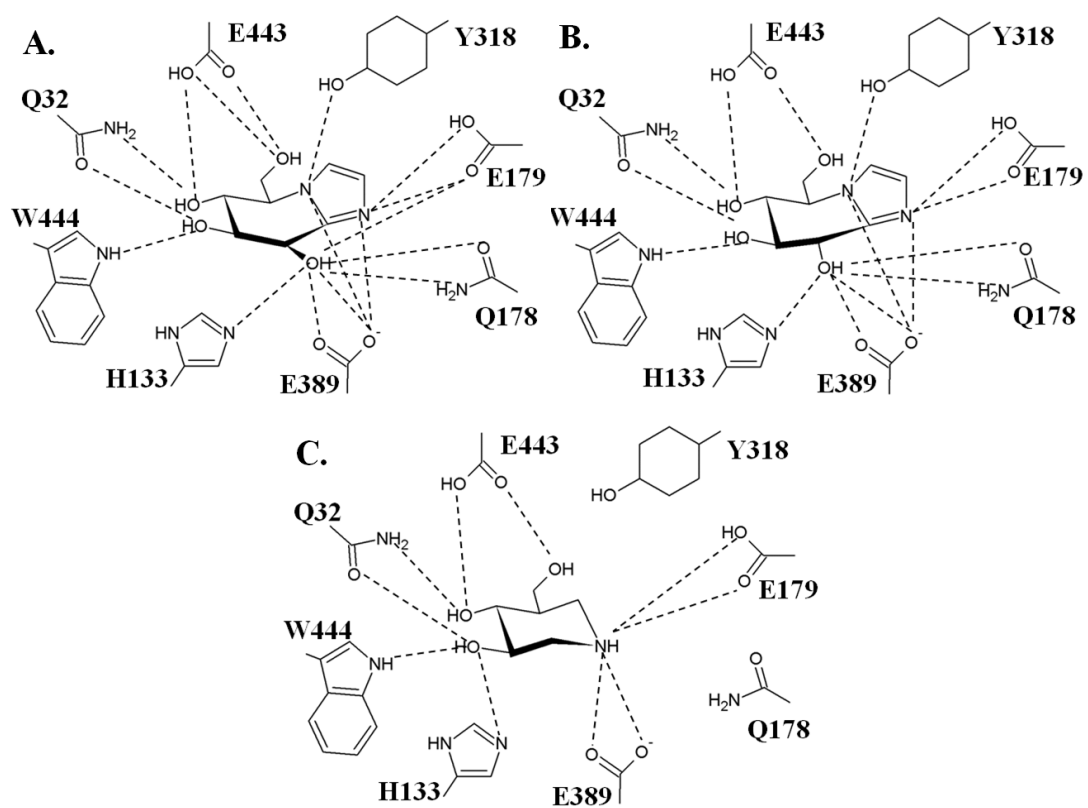


**Figure 4.24** Polar interactions of rice Os7BGlu26 with putative transition state mimics. Shown are: mannoimidazole (A), glucoimidazole (B) and isofagomine (C).

## CHAPTER V

### CONCLUSION

In summary, determination of the structure of a plant GH1  $\beta$ -D-mannosidase Os7BGlu26 and structural investigations of the residues interacting with the glucoside or mannoside substrates and putative transition state analogues indicated that the shape of the active site and interactions with surrounding residues are critical for glycon specificity.

Initially, the expression system had to be improved to allow production of sufficient quality and quantity of protein. The Os7BGlu26 was expressed in *E. coli* strain Rosetta-gami(DE3). In this system the highest expression of Os7BGlu26 was achieved by 24 h induction time with 0.3 mM IPTG at 20 °C, which gave protein of sufficient purity for structural and functional studies.

The protein produced was used for structural studies and the residues that appeared to differ in the structures of proteins with and without significant beta-mannosidase activities were mutated to investigate their significance. Crystallization of the Os7BGlu26 with and without mannose was accomplished in the conditions 0.58 M K<sub>2</sub>Na tartrate, 0.1 M Na HEPES, pH 7.25, by hanging drop vapor diffusion. The structure of Os7BGlu26 at a resolution of 2.20 Å and the structure of its complex with mannose at a resolution of 2.45 Å were obtained from isomorphous crystals in the  $P2_12_12_1$  space group. The  $(\beta/\alpha)_8$  barrel structure is similar to other GH1 family structures, but with a narrower active site cleft. A HEPES molecule from the crystallization buffer was found in the substrate binding cleft at the +1, +2 and +3

subsites and HEPES showed a non-competitive inhibition constant  $K_i$  of 81.4 mM. The Os7BGlu26 structure with D-mannose corresponds to a product complex, with  $\beta$ -D-mannose in the  ${}^1S_5$  skew boat conformation, which is the same conformation as that reported for the Michaelis complexes of the enzymes hydrolyzing  $\beta$ -D-mannosides. This result indicates that the conformation itinerary of mannoside during the deglycosylation step may be the reverse of the conformation itinerary of the glycosylation step. Docking of the  ${}^1S_3$ ,  ${}^1S_5$ ,  ${}^2S_0$ , and  ${}^3S_1$  pyranose ring conformations of 4NPMAN and 4NPGlc substrates into the active site of Os7BGlu26 indicated lowest energies in  ${}^1S_5$  and  ${}^1S_3$  skew boat conformations.

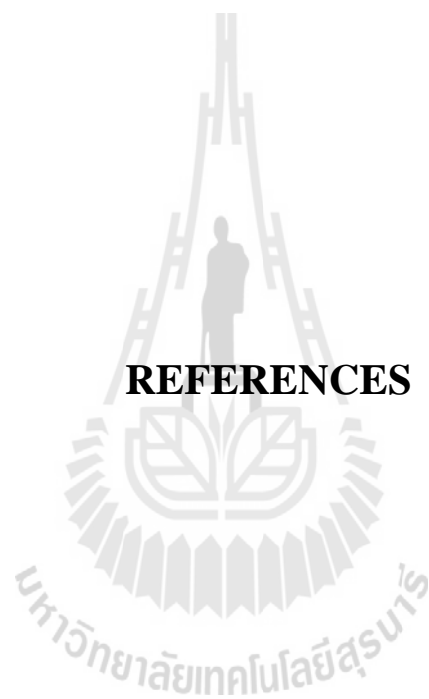
The Os7BGlu26 catalytic acid/base mutant E179Q showed lower activity than wild-type for both 4NPMAN and 4NPGlc, but the mutation affected  $\beta$ -D-mannosidase more than  $\beta$ -D-glucosidase activity. Mutation of Tyr134 to Trp in Os7BGlu26 resulted in a lower ratio of  $k_{cat}/K_m$  for 4NPMAN to that for 4NPGlc, while Tyr134 mutation to Phe increased this ratio 13-fold. In the case of the Os7BGlu26 C182T mutation, the  $K_m$  of this mutant was increased by approximately 25 to 30-fold for both substrates. The mutations described here had differential effects on the  $k_{cat}/K_m$  values of 4NPMAN *versus* 4NPGlc, indicating the residues interacting with the catalytic acid/base play a role in determining which of these is hydrolyzed more rapidly.

The determination of the structure of Os7BGlu26 complex with dNPG2F at 2.5 Å resolution shows the 2 molecules of dNPG2F were found in the structure. One molecule is located in the +1 and +2 subsites, whereas another molecule is located in the putative substrate binding cleft. This result implied that this enzyme might have an unusual substrate binding cleft, but further investigation is needed to confirm the function of this cleft. The Os7BGlu26 E179Q activity was rescued by adding azide in

50 mM MES buffer, pH 5.0. The crystals of this mutant enzyme were grown by the hanging drop technique with microseeding using native Os7BGlu26 crystal seeds. The structure of E179Q Os7BGlu26 covalent complex with G2F was found to have the G2F covalently bound in the  ${}^4C_1$  conformation. We still lack of the data of this enzyme covalently bound with M2F.

The structures of the complexes and enzyme inhibition kinetics of binding of putative transition state analogues were determined. Strong inhibition was observed with phenethylglucoimidazole > isofagomine > glucoimidazole > mannoimidazole > nojirimycin for Os7BGlu26, rHvBII  $\beta$ -mannosidases and Os3BGlu7  $\beta$ -glucosidase. The crystal structures of Os7BGlu26 in complexes with isofagomine, mannoimidazole and glucoimidazole indicated that D-mannosides and D-glucosides have different distortions during hydrolysis in Os7BGlu26. The shapes observed were according to those expected for each sugar, in that  $\beta$ -D-glucopyranosyl rings are thought to undergo a conformational change via a  ${}^4H_3$  half-chair near or at the transition state, whereas  $\beta$ -D-mannopyranosyl ring are thought to undergo a conformational change via a  $B_{2,5}$  boat.

Future structural studies of binding of substrates, such as cello- or manno-oligosaccharide of Os7BGlu26 by soaking the E179Q Os7BGlu26 crystals with these oligosaccharide will be useful to further illuminate the interactions that differentiate  $\beta$ -D-mannosidase and  $\beta$ -D-glucosidase activities in GH1.



## **REFERENCES**

## REFERENCES

- Ardèvol, A., Biarnés X., Planas, A., and Rovira, C. (2010) The conformational free-energy landscape of  $\beta$ -D-mannopyranose: evidence for a  ${}^1S_5 \rightarrow B_{2,5} \rightarrow {}^0S_2$  catalytic itinerary in  $\beta$ -mannosidases. **J. Am. Chem. Soc.** 132: 16058-16065.
- Barrett, T., Suresh, C. G., Tolley, S. P., Dodson, E. J., and Hughes, M. A. (1995) The crystal structure of a cyanogenic beta-glucosidase from white clover, a family 1 glycosyl hydrolase. **Structure** 3: 951-960.
- Biarnés, X., Ardèvol, A., Planas, A., Rovira, C., Laio, A., and Parrinello, M. (2007) The conformational free energy landscape of beta-D-glucopyranose. Implications for substrate preactivation in beta-glucoside hydrolases. **J. Am. Chem. Soc.** 129: 10686-10693.
- Biarnés, X., Ardèvol, A., Iglesias-Fernández, J., Planas, A., and Rovira, C. (2011) Catalytic itinerary in 1,3-1,4- $\beta$ -glucanase unraveled by QM/MM metadynamics. Charge is not yet fully developed at the oxocarbenium ion-like transition state. **J. Am. Chem. Soc.** 133: 20301-20309.
- Burmeister, W. P., Cottaz, S., Rollin, P., Vasella, A., and Henrissat, B. (2000) High resolution X-ray crystallography shows that ascorbate is a cofactor for myrosinase and substitutes for the function of the catalytic base. **J. Biol. Chem.** 275: 39385-39393.

- Cantarel, B. L., Coutinho, P. M., Rancurel, C., Bernard, T., Lombard, V., and Henrissat, B. (2009) The Carbohydrate-Active EnZymes database (CAZy): an expert resource for glycogenomics. **Nucleic Acids Res.** 37: 233-238.
- Chen, V. B., Arendall, W. B., Headd, J. J., Keedy, D. A., Immormino, R. M., Kapral, G. P., Murray, L. W., Richardson, J. S., and Richardson, D. C. (2010) MolProbity: all-atom structure validation for macromolecular crystallography. **Acta Cryst. D.** 66: 12-21.
- Chuenchor, W., Pengthaisong, S., Robinson, R.C., Yuvaniyama, J., Oonanant, W., Bevan, D. R., Esen, A., Chen, C.-J., Opassiri, R., Svasti, J., and Ketudat Cairns, J. R. (2008) Structural insights into rice BGlu1  $\beta$ -glucosidase oligosaccharide hydrolysis and transglycosylation. **J. Mol. Biol.** 377: 1200-1215.
- Chuenchor, W., Pengthaisong, S., Robinson, R. C., Yuvaniyama, J., Svasti, J., and Ketudat Cairns, J. R. (2011) The structural basis of oligosaccharide binding by rice BGlu1 beta-glucosidase. **J. Struct. Biol.** 173: 169-179.
- Cremer, D., and Pople, J. A. (1975) A general definition of ring puckering coordinates. **J. Am. Chem. Soc.** 97: 1354-1358.
- Czjzek, M., Cicek, M., Zamboni, V., Bevan, D. R., Henrissat, B., and Esen, A. (2000) The mechanism of substrate (aglycone) specificity in beta -glucosidases is revealed by crystal structures of mutant maize beta-glucosidase-DIMBOA, -DIMBOAGlc, and -dhurrin complexes. **Proc. Natl. Acad. Sci. U.S.A.** 97: 13555-13560.

- Davies, G. J., Mackenzie, L., Varrot, A., Dauter, M., Brzozowski, A. M., Schülein, M., and Withers, S. G. (1998) Snapshots along an enzymatic reaction coordinate: analysis of a retaining beta-glycoside hydrolase. **Biochemistry** 37: 11707-11713.
- Davies, G. J., Ducros, V.M.-A., Varrot, A., and Zechel, D. L. (2003) Mapping the conformational itinerary of  $\beta$ -glycosidases by X-ray crystallography. **Biochem. Soc. Trans.** 31: 523-527.
- Davies, G. J., Planas, A., and Rovira, C. (2012) Conformational analyses of the reaction coordinate of glycosidases. **Acc. Chem. Res.** 45: 308-316.
- Dias, F. M., Vincent, F., Pell, G., Prates, J. A., Centeno, M. S., Tailford, L. E., Ferreira, L. M., Fontes, C. M., Davies, G. J., and Gilbert, H. J. (2004) Insights into the molecular determinants of substrate specificity in glycoside hydrolase family 5 revealed by the crystal structure and kinetics of *Cellvibrio mixtus* mannosidase 5A. **J. Biol. Chem.** 279: 25517-25526.
- Dixon, M. (1953) The determination of enzyme inhibitor constants. **Biochem. J.** 55: 170-171.
- Ducros, V. M., Zechel, D. L., Murshudov, G. N., Gilbert, H. J., Szabo, L., Stoll, D., Withers, S. G., and Davies, G. J. (2002) Substrate distortion by a beta-mannanase: snapshots of the Michaelis and covalent-intermediate complexes suggest a B<sub>(2,5)</sub> conformation for the transition state. **Angew. Chem. Int. Ed. Engl.** 41: 2824-2827.
- Emsley, P., and Cowtan, K. (2004) Coot-model-building tools for molecular graphics. **Acta Cryst. D.** 60: 2126-2132.

- Fersht, A. R., Leatherbarrow, R. J., and Wells, T. N. (1987) Structure-activity relationships in engineered proteins: analysis of use of binding energy by linear free energy relationships. **Biochemistry** 26: 6030-6038.
- Gloster, T. M., Roberts, S., Perugino, G., Rossi, M., Moracci, M., Panday, N., Terinek, M., Vasella, A., and Davies, G. J. (2006) Structural, kinetic, and thermodynamic analysis of glucoimidazole-derived glycosidase inhibitors. **Biochemistry** 45: 11879-11884.
- Gloster, T. M., Moracci, M., Stick, R. V., Zechel, D., Vasella, A., and Davies, G. J. (2007) Glycosidase inhibition: an assessment of the binding of 18 putative transition-state mimics. **J. Am. Chem. Soc.** 129: 2345-2354.
- Gloster, T. M., and Davies, G. J. (2010) Glycosidase inhibition: assessing mimicry of the transition state. **Org. Biomol. Chem.** 45: 302-320.
- Gouet, P., Robert, X., and Courcelle, E. (2003) ESPript/ENDscript: extracting and rendering sequence and 3D information from atomic structures of proteins. **Nucleic Acids Res.** 31: 3320-3323.
- Escamilla-Treviño, L. L., Chen, W., Card, M. L., Shih, M. C., Cheng, C. L., and Poulton, J. E. (2006) *Arabidopsis thaliana* beta-glucosidases BGLU45 and BGLU46 hydrolyse monolignol glucosides. **Phytochemistry** 67: 1651-1660.
- Henrissat, B. (1991) A classification of glycosyl hydrolase based on amino acid sequence similarities. **Biochem. J.** 280: 309-316.
- Henrissat, B., Callebaut, I., Fabrega, S., Lehn, P., Mornon, J. P., and Davies, G. (1995) Conserved catalytic machinery and the prediction of a common fold for several families of glycosyl hydrolases. **Proc. Natl. Acad. Sci. U.S.A.** 92: 7090-7094.

- Hommalai, G., Withers, S. G., Chuenchor, W., and Ketudat Cairns, J. R., and Svasti, J. (2007) Enzymatic synthesis of cello-oligosaccharides by mutated rice  $\beta$ -glucosidases. **Glycobiology** 17: 744-753.
- Hrmova, M., Harvey, A. J., Wang, J., Shirley, N. J., Jones, G. P., Stone, B. A., Høj, P. B., and Fincher, G. B. (1996) Barley beta-D-glucan exohydrolases with beta-D-glucosidase activity. Purification, characterization, and determination of primary structure from a cDNA clone. **J. Biol. Chem.** 271: 5277-5286.
- Hrmova, M., MacGregor, E. A., Biely, P., Stewart, R. J., and Fincher, G. B. (1998) Substrate binding and catalytic mechanism of a barley  $\beta$ -D-glucosidase (1,4)- $\beta$ -D-glucan exohydrolase. **J. Biol. Chem.** 273: 11134-11143.
- Hrmova, M., and Fincher, G. B. (2001) Structure-function relationships of beta-D-glucan endo- and exohydrolases from higher plants. **Plant Mol. Biol.** 47: 73-91.
- Hrmova, M., De Gori, R., Smith, B. J., Vasella, A., Varghese, J. N., and Fincher, G. B. (2004) Three-dimensional structure of the barley beta-D-glucan glucohydrolase in complex with a transition state mimic. **J. Biol. Chem.** 279: 4970-4980.
- Hrmova, M., Streltsov, V. A., Smith, B. J., Vasella, A., Varghese, J. N., and Fincher, G. B. (2005) Structural rationale for low-nanomolar binding of transition state mimics to a family GH3 beta-D-glucan glucohydrolase from barley. **Biochemistry** 44: 16529-16539.

- Hrmova, M., Burton, R. A., Biely, P., Lahnstein, J., and Fincher, G. B. (2006) Hydrolysis of (1,4)-beta-D-mannans in barley (*Hordeum vulgare* L.) is mediated by the concerted action of (1,4)-beta-D-mannan endohydrolase and beta-D-mannosidase. **Biochem. J.** 399: 77-90.
- Jeng, W. Y., Wang, N. C., Lin, M. H., Lin, C. T., Liaw, Y. C., Chang, W. J., Liu, C. I., Liang, P. H., and Wang, A. H. (2011) Structural and functional analysis of three  $\beta$ -glucosidases from bacterium *Clostridium cellulovorans*, fungus *Trichoderma reesei* and termite *Neotermes koshunensis*. **J. Struct. Biol.** 173: 46-56.
- Jenkins, J., Lo Leggio, L., Harris, G., and Pickersgill, R. (1995) Beta-glucosidase, beta-galactosidase, family A cellulases, family F xylanases and two barley glycanases form a superfamily of enzymes with 8-fold beta/alpha architecture and with two conserved glutamates near the carboxy-terminal ends of beta-strands four and seven. **FEBS Lett.** 362: 281-285.
- Ketudat Cairns, J. R., and Esen, A. (2010)  $\beta$ -Glucosidases. **Cell Mol. Life Sci.** 67: 3389-3405.
- Koshland, Jr. D. E., (1953) Stereochemistry and mechanism of enzymatic reaction. **Biol. Rev.** 28: 416-436.
- Kuntothom, T., Luang, S., Harvey, A. J., Fincher, G. B., Opassiri, R., Hrmova, M., and Ketudat Cairns, J. R. (2009) Rice family GH1 glycoside hydrolases with  $\beta$ -D-glucosidase and  $\beta$ -D-mannosidase activity. **Arch. Biochem. Biophys.** 491: 85-95.

- Kuntothom, T., Raab, M., Tvaroska, I., Fort, S., Pengthaisong, S., Cañada, J., Calle, L., Jiménez-Barbero, J., Ketudat Cairns, J. R., and Hrmova, M. (2010) Binding of  $\beta$ -D-glucosides and  $\beta$ -D-mannosides by rice and barley  $\beta$ -D-glycosidases with distinct substrate specificities. **Biochemistry** 49: 8779-8793.
- Laemmli, U. K. (1970) Cleavage of structural proteins during the assembly of the head of bacteriophage T4. **Nature** 227: 680-685.
- Laskowski, R. A., MacArthur, M. W., Moss, D. S., and Thornton, J. M. (1993) PROCHECK: a program to check the stereochemical quality of protein structures. **J. Appl. Cryst.** 26: 283-291.
- Ly, H. D., and Withers, S. G. (1999) Mutagenesis of glycosidases. **Annu. Rev. Biochem.** 68: 487-522.
- Leah, R., Kigel, J., Svendsen, I., and Mundy, J. (1995) Biochemical and molecular characterization of a barley seed beta-glucosidase. **J. Biol. Chem.** 270: 15789-15797.
- Lohse, A., Hardlei, T., Jensen, A., Plesner, I. W., and Bols, M. (2000) Investigation of the slow inhibition of almond beta-glucosidase and yeast isomaltase by 1-azasugar inhibitors: evidence for the 'direct binding' model. **Biochem. J.** 349: 211-215.
- MacLeod, A. M., Tull, D., Rupitz, K., Warren, R. A., and Withers, S. G. (1996) Mechanistic consequences of mutation of active site carboxylates in a retaining beta-1,4-glycanase from *Cellulomonas fimi*. **Biochemistry** 35: 13165-13172.
- Matthews, B. W. (1968) Solvent content of protein crystals. **J. Mol. Biol.** 33: 491-497.

- McCleary, B. V., and Matheson, N. K. (1975) Galactomannan structure and  $\beta$ -mannanase and  $\beta$ -mannosidase activity in germinating legume seeds. **Phytochemistry** 14: 1187-1194.
- Mendoça, L. M. F., and Marana, S. R. (2011) Single mutations outside the active site affect the substrate specificity in a  $\beta$ -glycosidase. **Biochim. Biophys. Acta** 1814: 1616-1623.
- McCarter, J., and Withers, S. G. (1994) Mechanisms of enzymatic glycoside hydrolysis. **Curr. Opin. Struct. Biol.** 4: 885-892.
- Mildvan, A. S., Weber, D. J., and Kuliopuos, A. (1992) Quantitative interpretations of double mutaitons of enzymes. **Arch. Biochem. Biophys.** 294: 327-340.
- Mildvan, A. S. (2004) Inverse thinking and double mutants of enzymes. **Biochemistry** 43: 14517-14520.
- Mo, B., and Bewley, J. D. (2002) Beta-mannosidase (EC 3.2.1.25) activity during and following germination of tomato (*Lycopersicon esculentum* Mill.) seeds. Purification, cloning and characterization. **Planta** 215: 141-152.
- Morris, G. M., Goodsell, D. S., Halliday, R. S., Huey, R., Hart, W. E., Belew, R. K., and Olson, A. J. (1998) Automated docking using a Lamarckian genetic algorithm and an empirical binding free energy function. **J. Comput. Chem.** 19: 1639-1662.
- Murshudov, G. N., Lebedev, A., Vagin, A. A., Wilson, K. S., and Dodson, E. J. (1999) Efficient anisotropic refinement of macromolecular structures using FFT. **Acta Cryst. D.** 55: 247-255.

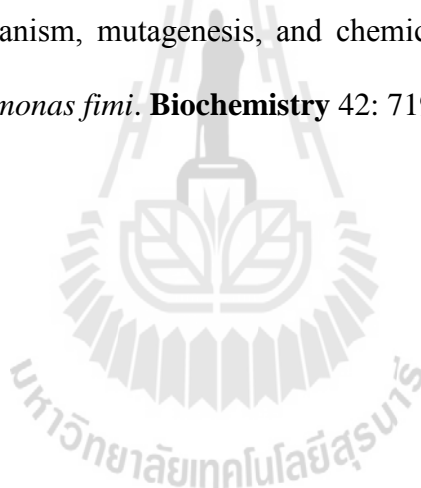
- Morant, A. V., Jørgensen, K., Jørgensen, C., Paquette, S. M., Sánchez-Pérez, R., Møller, B. L., and Bak, S. (2008) Beta-glucosidases as detonators of plant chemical defense. **Phytochemistry** 69: 1795-1813.
- Müllegger, J., Jahn, M., Chen, H. M., Warren, R. A. J., and Withers, S. G. (2005) Engineering of a thioglycoligase: randomized mutagenesis of the acid-base residue leads to the identification of improved catalysis. **Protein Eng. Des. Sel.** 18: 33-40.
- Offen, W. A., Zechel, D. L., Withers, S. G., Gilbert, H. J., and Davies, G. J. (2009) Structure of the Michaelis complex of beta-mannosidase, Man2A, provides insight into the conformational itinerary of mannoside hydrolysis. **Chem. Commun.** 18: 2484-2486.
- Opassiri, R., Ketudat Cairns, J. R., Akiyama, T., Wara-Aswapati, O., Svasti, J., and Esen, A. (2003) Characterization of a rice  $\beta$ -glucosidase genes highly expressed in flower and germinating shoot. **Plant Sci.** 165: 627-638.
- Opassiri, R., Hua, Y., Wara-Aswapati, O., Akiyama, T., Svasti, J., Esen, A., and Ketudat Cairns, J. R. (2004)  $\beta$ -Glucosidase, exo- $\beta$ -glucanase and pyridoxine transglucosylase activities of rice BGlu1. **Biochem. J.** 379: 125-131.
- Opassiri, R., Pomthong, B., Onkoksoong, T., Akiyama, T., Esen, A., and Ketudat Cairns, J. R. (2006) Analysis of rice glycosyl hydrolase family 1 and expression of Os4BGlu12 beta-glucosidase. **BMC Plant Biol.** 6: 33.
- Opassiri, R., Pomthong, B., Akiyama, T., Nakphaichit, M., Onkoksoong, T., Ketudat Cairns, M., and Ketudat Cairns, J. R. (2007) A stress-induced rice (*Oryza sativa* L.) beta-glucosidase represents a new subfamily of glycosyl hydrolase family 5 containing a fascin-like domain. **Biochem. J.** 408: 241-249.

- Opassiri, R., Maneesan, J., Akiyama, T., Pomthong, B., Jin, S., Kimura, A., and Ketudat Cairns, J. R. (2010) Rice Os4BGlu12 is a wound-induced  $\beta$ -glucosidase that hydrolyzes cell wall- $\beta$ -glucan-derived oligosaccharides and glycosides. **Plant Sci.** 179: 273-280.
- Otwinowski, Z., and Minor, W. (1997) Processing of X-ray diffraction data collected in oscillation mode. **Methods Enzymol.** 276: 307-326.
- Ouellette, B. F. F., and Bewley, J. D. (1986)  $\beta$ -Mannoside mannohydrolase and the mobilization of the endosperm cell wall of lettuce seeds, cv. Grand Rapids. **Planta** 169: 333-338.
- Palcic, M. M. (2008) Beta-mannoside hydrolysis goes by boat. **Nat. Chem. Biol.** 4: 269-270.
- Petersen, L., Ardèvol, A., Rovira, C., and Reilly, P. J. (2010) Molecular mechanism of the glycosylation step catalyzed by Golgi alpha-mannosidase II: a QM/MM metadynamics investigation. **J. Am. Chem. Soc.** 132: 8291-8300.
- Ratanakikom, K., Choengpanya, K., Tongtubtim, N., Charoenrat, T., Withers, S. G., and Konsaeree, P. T. (2013) Mutational analysis in the glycone binding pocket of *Dalbergia cochinchinensis*  $\beta$ -glucosidase to increase catalytic efficiency toward mannosides. **Carbohyd. Res.** 373: 35-41.
- Rempel, B. P., and Withers, S. G. (2008) Covalent inhibitors of glycosidases and their applications in biochemistry and biology. **Glycobiology** 18: 570-586.
- Rye, C. S. and Withers, S.G. (2000) Glycosidase mechanisms. **Curr. Opin. Chem. Biol.** 5: 573-580.

- Sansanya, S., Opassiri, R., Kuaprasert, B., Chen, C. J., and Ketudat Cairns, J. R. (2011) The crystal structure of rice (*Oryza sativa* L.) Os4BGlu12, an oligosaccharide and tuberonic acid glucoside-hydrolyzing  $\beta$ -glucosidase with significant thioglucosylhydrolase activity. **Arch. Biochem. Biophys.** 510: 62-72.
- Sanz-Aparicio, J., Hermoso, J. A., Martinez-Ripoll, M., Lequerica, J. L., and Polaina, J. (1998) Crystal structure of  $\beta$ -glucosidase A from *Bacillus polymyxa*: insights into the catalytic activity in family 1 glycosyl hydrolases. **J. Mol. Biol.** 275: 491-502.
- Seshadri, S., Akiyama, T., Opassiri, R., Kuaprasert, B., and Ketudat Cairns, J. R. (2009) Structural and enzymatic characterization of Os3BGlu6, a rice  $\beta$ -glucosidase hydrolyzing hydrophobic glycosides and (1 $\rightarrow$ 3)- and (1 $\rightarrow$ 2)-linked disaccharides. **Plant Physiol.** 151: 47-58.
- Shaikh, F. A., and Withers, S. G. (2008) Teaching old enzymes new tricks: engineering and evolution of glycosidases and glycosyl transferases for improved glycosides synthesis. **Biochem. Cell Biol.** 86: 169-177.
- Sinnott, M. L. (1990) Catalytic mechanism of enzymatic glycosyl transfer. **Chem. Rev.** 90: 1171-1202.
- Tailford, L. E., Offen, W. A., Smith, N. L., Dumon, C., Morland, C., Gratien, J., Heck, M. P., Stick, R. V., Blériot, Y., Vasella, A., Gilbert H. J., and Davies, G. J. (2008) Structural and biochemical evidence for a boat-like transition state in  $\beta$ -mannosidases. **Nat. Chem. Biol.** 4: 306-312.
- Vagin, A., and Teplyakov, A. (1997) MOLREP: an automated program for molecular replacement. **J. Appl. Cryst.** 30: 1022-1025.

- Verdoucq, L., Morinière, J., Bevan, D. R., Esen, A., Vasella, A., Henrissat, B., and Czjzek, M. (2004) Structural determinants of substrate specificity in family 1 beta-glucosidases: novel insights from the crystal structure of sorghum dhurrinase-1, a plant beta-glucosidase with strict specificity, in complex with its natural substrate. **J. Biol. Chem.** 279: 31796-31803.
- Vocadlo, D. J., and Davies, G. J. (2008) Mechanistic insights into glycosidase chemistry. **Curr. Opin. Chem. Biol.** 12: 539-555.
- Wang, Q., Graham, R. W., Trimbur, D., Warren, R. A. J., and Withers, S. G. (1994) Changing enzymatic reaction mechanisms by mutagenesis: Conversion of a retaining glucosidase to an inverting enzyme. **J. Am. Chem. Soc.** 116: 11594-11595.
- Wang, Q., Trimbur, D., Graham, R., Warren, R. A. J., and Withers, S. G. (1995) Identification of the acid/base catalyst in *Agrobacterium faecalis*  $\beta$ -glucosidase by kinetic analysis of mutants. **Biochemistry** 34: 14554-14562.
- Wang, C. Y., Chiou, C. Y., Wang, H. L., Krishnamurthy, R., Venkatagiri, S., Tan, J., and Yeh, K. W. (2008) Carbohydrate mobilization and gene regulatory profile in the pseudobulb of *Oncidium* orchid during the flowering process. **Planta** 227: 1063-1077.
- Winn, M. D., Ballard, C. C., Cowtan, K. D., Dodson, E. J., Emsley, P., Evans, P. R., Keegan, R. M., Krissinel, E. B., Leslie, A. G., McCoy, A., McNicholas, S. J., Murshudov, G. N., Pannu, N. S., Potterton, E. A., Powell, H. R., Read, R. J., Vagin, A., and Wilson, K. S. (2011) Overview of the CCP4 suite and current developments. **Acta Cryst. D.** 67: 235-242.

- Xu, Z., Escamilla-Treviño, L., Zeng, L., Lalgondar, M., Bevan, D., Winkel, B., Mohamed, A., Cheng, C. L., Shih, M. C., Poulton, J., and Esen, A. (2004) Functional genomic analysis of *Arabidopsis thaliana* glycoside hydrolase family 1. **Plant Mol. Biol.** 55: 343-367.
- Zechel, D. L., and Withers, S. G. (2000) Glycosidase mechanisms: anatomy of a finely tuned catalyst. **Acc. Chem. Res.** 33: 11-18.
- Zechel, D. L., and Withers, S. G. (2001) Dissection of nucleophilic and acid-base catalysis in glycosidases. **Curr. Opin. Chem. Biol.** 5: 643-649.
- Zechel, D. L., Reid, S. P., Stoll, D., Nashiru, O., Warren, R. A. J., and Withers, S. G. (2003) Mechanism, mutagenesis, and chemical rescue of a  $\beta$ -mannosidase from *Cellulomonas fimi*. **Biochemistry** 42: 7195-7204.





# APPENDIX

## PUBLICATIONS

### 1. Publications from Ph.D. Thesis

**Tankrathok, A.**, Iglesias-Fernández, J., Luang, S., Robinson, R. C., Kimura, A., Rovira, C., Hrmova, M., and Ketudat Cairns, J. R. (2013) Structural analysis and insight into glycon specificity of the rice GH 1 Os7BGlu26  $\beta$ -D-mannosidase. **Acta Cryst. D.** 69: 2124-2135.

Ketudat Cairns, J. R., Pengthaisong, S., Luang, S., Sansenya, S., **Tankrathok, A.**, and Svasti, J. (2012) Protein-carbohydrate interactions leading to hydrolysis and transglycosylation in plant glycoside hydrolase family 1 enzymes. **J. Appl. Glycosci.** 59: 51-62.

### 2. Other international publication

**Tankrathok, A.**, Daduang, S., Pataramanon, R., Araki, T., and Thammasirirak, S. (2009) Purification process for the preparation and characterizations of hen egg white ovalbumin, lysozyme, ovotransferrin, and ovomucoid. **Prep. Biochem. Biotech.** 39: 380-399.

# CURRICULUM VITAE

**NAME** Mr.Anupong Tankrathok

**DATE OF BIRTH** July 22, 1983

**PLACE OF BIRTH** Nakhon Ratchasima

## EDUCATION

2008-2013 School of Biochemistry, Institute of Science, Suranaree University of Technology, Nakhon Ratchasima, Thailand

### **Ph.D. in Biochemistry**

2006 Department of Biochemistry, Faculty of Science, Khon Kaen University, Khon Kaen, Thailand

### **M.Sc. in Biochemistry**

2004 Department of Biochemistry, Faculty of Science, Khon Kaen University, Khon Kaen, Thailand

### **B.Sc. in Biochemistry**

## SCHOLARSHIP

2008-2011 The Strategic Scholarships for Frontier Research Network Ph.D. Program from the Thailand Commission on Higher Education